Title

The Rnf Complex is Vital for Metabolic Adaptation and Virulence in the Oral Pathogen Fusobacterium nucleatum

Author

Britton, Timmie Arthur

Publication Date

2024

UNIVERSITY OF CALIFORNIA

Los Angeles

The Rnf Complex is Vital for Metabolic Adaptation and Virulence in the Oral Pathogen *Fusobacterium nucleatum*

A dissertation submitted in partial satisfaction of the requirements for the degree Doctor of Philosophy in Molecular Biology

by

Timmie Arthur Britton

2024

ABSTRACT OF THE DISSERTATION

The Rnf Complex is Vital for Metabolic Adaptation and Virulence in the Oral Pathogen *Fusobacterium nucleatum*

by

Timmie Arthur Britton

Doctor of Philosophy in Molecular Biology

University of California, Los Angeles, 2024

Professor Hung Ton-That, Chair

Bacteria utilize a wide array of metabolic pathways to conserve energy from various substrates, powering many physiological processes including bacterial adhesion, motility, biofilm formation, polymicrobial interaction, and virulence. The Gram-negative oral anaerobe, *Fusobacterium nucleatum*, is an emergent pathogen implicated in a multitude of extra-oral disorders including colorectal cancer (CRC), breast cancer, adverse pregnancy outcomes, cardiovascular disease, and rheumatoid arthritis. *F. nucleatum* owes its ability to spread from the oral cavity and colonize a range of extra-oral tissues in large part to the expression of several outer membrane proteins (OMPs) that act as molecular adhesins. However, the mechanisms by which *F. nucleatum* metabolically adapts to changing extra-oral environments to maintain its virulence potential remain poorly understood. Informed by our Tn5 transposon mutagenesis

screens to identify additional *F. nucleatum* virulence factors involved in biofilm formation and polymicrobial interaction, we hereby describe in this dissertation the metabolic role of a conserved prokaryotic respiratory enzyme, the *Rhodobacter* nitrogen-fixation (Rnf) complex, and its impact on fusobacterial virulence.

The Rnf complex is a well-studied, six-subunit, ferredoxin:NAD^+ oxidoreductase that promotes microbial fitness via conserving energy from several metabolic niches, including those relying on autotrophic, heterotrophic, and/or syntrophic metabolism. Here, we show that genetic disruption of the fusobacterial Rnf complex, via in-frame deletion of subunit-encoding genes, causes pleotropic defects in polymicrobial interaction, biofilm formation, ATP biosynthesis, toxic hydrogen sulfide production, bacterial cell growth, and morphology. Targeted metabolomic screening demonstrates loss of Rnf causes global deficiencies in amino acid fermentation, negatively impacting fusobacterial virulence in a mouse model of preterm birth. This study establishes the fusobacterial Rnf enzyme as a metabolic conduit of *F. nucleatum* pathophysiology within and outside of the oral cavity.

F. nucleatum is an oncobacterium that promotes carcinogenesis of colorectal cancer, and the amyloid-forming adhesin FadA is integral to this process. Previous studies suggest that the highly conserved *Rhodobacter* nitrogen-fixation (Rnf) complex modulates the virulence potential of this pathobiont via metabolic signaling; however, a mechanism for this modulation remains unknown. Here, we show that genetic disruption of the Rnf complex, via *rnfC* deletion, significantly reduced the transcript level of *fadA*, relative to the wildtype. This was accompanied by near complete abolition of the precursor form of FadA (pFadA) and reduced surface assembly of FadA at the mature cell pole. Noticeably, *rnfC* deletion caused a severe defect in osmotic stress-induced amyloid formation that was rescued by ectopic expression of *rnfC*. Gene deletion analysis identified three response regulators – CarR, ArlR, and S1 – that modulate expression of pFadA, without affecting its transcript level, suggesting that these response regulators control expression

of factors that process FadA. Consistently, deletion of *rnfC*, *arlR*, and *s1* significantly reduced expression of the signal peptidase-encoding gene *lepB*, and CRISPR-induced depletion of *lepB* nearly abolished FadA expression. Importantly, while *rnfC* deletion did not affect the ability of mutant cells to adhere to cancer cells HCT116, *rnfC* deficiency significantly diminished fusobacterial invasion of HCT116. Consistent with the role of FadA in tumor formation, the *rnfC* mutant was markedly defective in promotion of spheroid tumors. Evidently, the Rnf complex modulates expression of FadA and formation of FadA-associated amyloids and tumors via regulation of LepB by multiple response regulators.

The dissertation of Timmie Arthur Britton is approved.

Robert Thompson Clubb

Elissa A. Hallem

Renate Lux

Megan Marie McEvoy

Hung Ton-That, Committee Chair

University of California, Los Angeles

2024

I dedicate this dissertation to my beloved cousin, who passed away at the early age of 26. His love, support, and commitment to spreading the Gospel message will not be forgotten. This one is for you cuzzo.

Table of Contents

List of Figures

List of Tables

Acknowledgements

Throughout life's endeavors we meet people who inspire us to rewrite the personal narrative we've grown accustomed to, who give us a newfound hope and willingness to pursue the opportunities and challenges set before us. Some of these individuals are only a part of our story for a season, but their words and actions have a lasting impact on how we move through this life. This section is a dedication to those whose selfless mentorship motivated me to shine my light and reach new academic heights. First and foremost, I give all thanks and praise to my Lord and Savior, Jesus Christ. The never-changing, unending love of my God has blessed me beyond measure, teaching me the importance of being steadfast in my faith. The Lord guided my decision to pursue a doctoral degree at UCLA, saved me and my fiancé in the Colorado wilderness as we journeyed over 2,000 miles from Minneapolis to Los Angeles in a car with a cracked engine mount, wiped away the tears and hopelessness I felt after losing so many in my family throughout graduate school, and gave me the conviction to forge a present and future built upon the sturdy foundation of faith. 2,000 years ago, the apostle Paul preached to the Romans in Corinth: "*Do not be conformed to this world, but be transformed by the renewal of your minds, so that you may prove what the will of God is, that which is good and acceptable and perfect*" (Romans 12:2). To this end, my mind is stronger than it ever has been and will continue to be strengthened through the power of the Holy Spirit.

Success is almost always spurred by people who recognize a talent and/or passion that may be hidden from you at the time. My parents, Carmen and Keith Britton, were the first to witness a deep interest I had in the sciences from an early age. They consistently watered and fertilized my scientific aspirations throughout my childhood, gifting me a microscope on Christmas Day, helping me with multiple science fair projects, and taking a mutual interest in educational programs. My father taught me of how not to be fearful of new experiences, but rather to embrace the unexpected. My mother showed me what it means to be steadfast in your dedication to a goal,

seeing it through to the very end. Most of all, she gave me the closest physical example I will ever have to God's love on Earth. Together, they raised a selfless son who took advantage of every opportunity that came his way, who expected setbacks and challenges, and who most of all believed in something greater than what the world showed me. Mom, Dad, I love you from the bottom of my heart.

In high school I was blessed to have multiple passionate instructors whom I would like to acknowledge for their faith in my academic potential. When my 9th grade physical science teacher, Mr. Molohon, placed our first exam on my desk, I was convinced I barely passed. However, when I flipped over the test I was absolutely shocked to see I got a nearly perfect score. Mr. Molohon asked me to stay after class, where he confidently exclaimed that I have a mind and talent for science, and to consider a career in it. He may not have known it, but in that moment he instilled in me a deep personal confidence, sparking a path of stellar academic performance in pursuit of scientific exploration that I am continuing to this day. Mr. Molohon still teaches 9th grade physical science at Champlin Park High School, placing hope in students like me. There are many who fertilized the roots of my dreams throughout high school that I cannot leave out. Mrs. Garofano, Mr. Grinage, Mrs. Manbeck, Mr. Baker-Raivo, thank you for continuing to educate and believe in my capabilities.

Next, I would like show my deep appreciation for my principal investigator (PI) and primary graduate mentor, Dr. Hung Ton-That. Professor Ton-That has taught me so many valuable research, career, and life skills throughout my graduate school tenure. His continued scientific excellence, high research standard, and leadership qualities were immediately noticeable upon first rotating in his lab in the Spring of 2020. Thanks to him, I am confident in my ability to write scientific manuscripts, create publishable figures, communicate my scientific findings in a logical and digestible manner, brainstorm research questions, identify the scientific tools necessary to address gaps in our field, and ultimately independently lead a research project. I truly look up to

Dr. Ton-That, not only as my scientific mentor, but also for how he carries himself outside the workplace. I will always be grateful for the lessons I have gleaned from him, and the immense impact he has had on my growth as a man, and scientist.

I would also like to acknowledge the time and effort put forth by members of my doctoral thesis committee. Drs. Robert Clubb, Elissa Hallem, Renate Lux, and Megan McEvoy have provided ample review, critique, and recommendation to advance my graduate research. Every time I presented my research aims, goals, and findings, these individuals made me feel supported and validated and I cannot thank them enough for their contributions. Prior to joining the Ton-That lab, I worked closely with Dr. Hallem as I rotated in her lab studying the sensory mechanisms of the skin-infecting nematode, *Strongyloides stercoralis*. She also served as the chair of my thesis committee prior to me passing the oral qualifying exam (OQE) in December of 2021. Shortly after, I was happy to see her become Home Area Director (HAD) for the Immunology, Microbiology, and Microbial Pathogenesis (IMMP) home area, which reflects her commitment to mentorship and creating an environment where graduate students feel safe and supported. The role of HAD for IMMP was previously held by Dr. Peter Bradley, who played a huge role in my decision to accept the admission offer from the UCLA Molecular Biology Interdepartmental Doctoral Program (MBIDP). He was, and still is, one of the most personable professors I have met in my academic journey, which includes time spent at the University of Minnesota-Twin Cities, Harvard University, and of course UCLA. I distinctly remember Dr. Bradley calling me at random before I had accepted the offer from MBIDP to answer any questions, doubts, or concerns I had about pursuing a graduate degree at UCLA. For example, when I expressed financial concern over the living expenses in Los Angeles, he suggested I apply for a summer transition program designed to provide a bridge to newly admitted doctoral students from underrepresented backgrounds whereby each student engaged in six weeks of intensive, paid research with a UCLA faculty member. I was grateful to conduct this research with Dr. Bradley, providing a runway for a

successful graduate career. In addition, he offered me the prestigious Dean award based on my academic merit, encouraged me to apply to the Eugene V. Cota-Robles diversity fellowship which I was awarded, and was forthright about the advantages and disadvantages of the MBIDP program. Dr. Bradley was a major reason for why I chose to attend UCLA over the University of North Carolina – Chapel Hill for my PhD work.

I want to give a special thank you to the members of the Ton-That lab. These close colleagues offered mental and research support that was instrumental in accomplishing my graduate work. In the beginning of my PhD, I worked closely with Dr. Yi-Wei Chen, who taught me several experiments that we later published in my first-author research article described in chapter 3. A close friend and colleague of mine, Dana Franklin, performed several mouse experiments in conjunction with Dr. Chen, which are also presented in chapter 3. Dr. Julie Chang constructed many bacterial strains that were used relentlessly in my research (chapter 4). Her constant intrigue in my work was much appreciated, and she challenged current hypotheses to better my proposed experiments. Dr. Aadil Bhat happily answered countless research questions almost daily and provided the framework for CRISPR machinery that I later used in chapter 4. A previous member of our lab, Kevin To, served as our lab assistant for the first half of my PhD. Together, we co-authored a protocol chapter now published in Methods in Molecular Biology (MiMB), presented in chapter 5. I want to thank Mr. To, not only for his research contributions on the development of the immunofluorescence protocol but also the timely ordering of required scientific materials. Dr. Chenggang Wu, a previous member of the Ton-That lab, provided the basis for my research, performing several experiments with transposon mutants that I used in chapter 3. I would also like to thank Dr. Asis Das for his careful review of all my manuscripts.

Lastly I would like to acknowledge my funding sources. This work was supported by the UCLA Eugene V. Cota-Robles Fellowship, the National Institute of Dental and Craniofacial Research of the National Institute of Health by the Ruth L. Kirschstein National Research Service

Award (T90DE030860), and National Institute of Dental and Craniofacial Research Diversity Supplement of the National Institute of Health by the Ruth L. Kirschstein National Research Service Award (R21DE032906-02S1).

Vita

Education

B.S., Microbiology, University of Minnesota, Twin Cities 2019

Publications

Britton TA, Guo H, Ji Y (2020). Interaction between two essential, conserved bacterial proteins YeaZ and glycoprotease as a potential antibacterial target in multi-drug-resistant *Staphylococcus aureus*. *Science Progress*. vol. 103,1 (2020): 36850419890521. doi:10.1177/0036850419890521. PMC10452758

Britton TA, Wu C, Chen YW, Franklin D, Chen Y, Camacho MI, Luong TT, Das A, and Ton-That H (2024). The respiratory enzyme complex Rnf is vital for metabolic adaptation and virulence in *Fusobacterium nucleatum*. *mBio*, 15(1):e0175123; doi: 10.1128/mbio.01751-23. PMC10790702

Kevin To*, Timmie Britton*, and Hung Ton-That (2024). Visualization of a Cell Wall Hydrolase Inhibitor in *Fusobacterium nucleatum* by Immunofluorescence Microscopy. *Methods in Molecular Biology*, 2727:27-33. doi: 10.1007/978-1-0716-3491-2_3. *Equal Contribution

Pasquarelli R, Quan J, Chang E, Yang V, Britton, T, Jihui S, Wohlschlegel J, Bradley P. (2024) Characterization and functional analysis of Toxoplasma Golgi-associated proteins identified by proximity labelling. *mBio*. 2024 Sep 30:e0238024. doi: 10.1128/mbio.02380-24.

Britton TA, Chen YW, Wu C, Lee JH, Das A, and Ton-That H (2024). The Rnf Complex modulates FadA-mediated amyloid formation and tumor development in *Fusobacterium nucleatum*. ***TBD***

Presentations

Britton TA, Wu C, Ton-That H. The respiratory enzyme complex Rnf is vital for metabolic adaptation and virulence in *Fusobacterium nucleatum*. Gordon Research Conference on Microbial Adhesion and Signal Transduction, Newport RI, **July 2023**.

Britton TA, Wu C, Ton-That H. The respiratory enzyme complex Rnf is vital for metabolic adaptation and virulence in *Fusobacterium nucleatum*. UCLA School of Dentistry Research and Clinical Excellence Day, UCLA, **February 2024.**

Honors and Awards

2024 UCLA School of Dentistry Research and Clinical Excellence Day Awardee

2022 – 2024 T90/R90 Ruth L. Kirschstein National Research Service Award T90DE030860

2022 UCLA Society for the Advancement of Chicanos/Hispanics and Native Americans in Science (SACNAS) Travel Scholarship

2020 Ruth L. Kirschstein National Research Service Diversity Supplement XXXXXXXXXX

2019 – 2023 Eugene V. Cota-Robles Fellowship Recipient

2019 - 2020 UCLA Graduate Dean Scholar Awardee

2018 HHMI Exceptional Research Opportunities Program (EXROP) Scholar

2015 – 2019 Wallin Education Partners Scholar

Chapter 1 The Rnf complex is a prokaryotic respiratory enzyme that promotes metabolic versatility and bacterial virulence

1.1 Abstract

In 1993, researchers working with the purple non-sulfur bacterium *Rhodobacter capsulatus*, identified a six-subunit operon encoding an ancient membrane-bound bacterial respiratory enzyme proposed to have ferredoxin-NAD^+ oxidoreductase (fno) activity, later shown to be crucial for diazotrophic growth. This operon was named *rnf*, short for *Rhodobacter* nitrogen-fixation. Each gene in the *rnf* operon (*rnfABCDGE)* encodes a single membrane-bound subunit. Together, they form a respiratory complex that couples the reversible oxidation of ferredoxin (Fd^{2-}/Fd) with the formation of NADH and the establishment of an ion (Na^+/H^+)-motive force (IMF). The latter can be used for ATP biosynthesis or substrate transport. Since its discovery, the Rnf complex has been identified in hundreds of bacterial species and two archaeal genera, carrying out both "forward" (exergonic) and "reverse" (endergonic) redox reactions for energy conservation. This unique flavin-based respiratory enzyme functions as a versatile metabolic exchange center, coupling energy conservation from inorganic substrates in energy-poor environments while promoting bacterial resource sharing, the production of useful biofuels such as ethanol, bacterial gut colonization, and virulence. Given the Rnf complex is absent in eukaryotes, it may serve as an attractive target for drug development, and/or microbial engineering. Herein we describe the distribution, topology, evolutionary history, and functions of the Rnf complex, and highlight its instrumental role in microbial physiology and virulence.

1.2 Introduction

Independent of fermentative substrate level phosphorylation (SLP) that produces ATP, a second mechanism of energy conservation was proposed more than six decades ago, whereby the oxidation of an electron donor (e.g., NAD(P)H, $FADH_2$) powers the transport of cations (H^+/Na^+) through the cell membrane, generating an electrochemical ion gradient ($\Delta\mu_{ion}$) which can be used

for ADP phosphorylation (1). We now know this chemiosmotic hypothesis provides ~89% of the ATP used by respiring organisms to energize various cellular processes (2). Bacteria and Archaea also conserve energy by SLP and chemiosmosis, often without the aid of strong electron acceptors such as oxygen or nitrate, having evolved an eclectic pallet of oxidoreductases to bridge the redox spectrum. Nonetheless, the transfer of electrons across a chain of membrane-bound proteins is not the only means to energize the cell, rather decarboxylation (3) and methyl transfer (4) reactions are additional pathways to conserve energy for these domains of life (2). For this reason, Hess and colleagues have coined the term “ion-gradient-driven phosphorylation” (IGP) instead of “electron transport phosphorylation” to better highlight the ways in which these organisms survive, and indeed even thrive, in some of the most thermodynamically challenging microbial ecosystems on Earth (2).

Aerobic bacteria use an electron transport chain composed of complexes I-IV, similar to aerobically-respiring eukaryotes, which oxidize NADH (complex I) and $FADH_2$ (Complex II) and transfer electrons to the quinone-based electron-carrier, cytochrome c (complex III). Cytochrome c then reduces oxygen via a cytochrome c oxidase (complex IV) (5). Therefore, with NADH as donor ($E^{0'}$: -320mV) and O_2 as electron acceptor ($E^{0'}$: +800mV), enough energy is generated to produce 3 mol of ATP. In contrast, many strictly anaerobic bacteria lack even one of these membrane complexes, relying on other enzymes to energize the cell membrane (6).

In 1993, a gene cluster encoding a putative ferredoxin-NAD^+ oxidoreductase (fno) in the purple non-sulfur bacterium, *Rhodobacter capsulatus*, was found to be required for the reduction of nitrogenase enzymes which function to convert inorganic dinitrogen (N_2) into metabolically useful ammonia (NH_3) (7). These six genes (*rnfABCDGE*) were named corresponding to their discovered function in *Rhodobacter* nitrogen fixation. Corrections were later made leading to 7 genes, *rnfABCDGEH*, however *rnfH* is not present in most *rnf* operons and its function is unknown

(8). The Rnf complex garnered early interest for its strong similarity to a pre-discovered sodium-translocating NADH-ubiquinone oxidoreductase (Na^+-Nqr) (9), the latter of which is present in many pathogenic bacteria, including *Vibrio cholerae*, where it was shown to metabolically promote exotoxin production (10). Continued interest in the Rnf complex yielded insights into its broad functionality and distribution, now known to be one of the most abundant electron transport systems in prokaryotes, with over 154 organisms containing *rnf* operons (8). There are three recognized cluster orientations (Table 1). Rnf is present in oxygenic and non-oxygenic prokaryotes, with high abundance in anaerobic species. There is even evidence for its presence in two archaeal genera – *Methanosarcina* (11, 12) and *Methanococcoides* (8). The Rnf complex is also present in multiple phylogenic and trophic levels, including chemolithoautotrophs, photolithoautotrophs, and chemoorganoheterotrophs (8).

Table 1. Distribution of *rnf* clusters

rnfABCDGE	***rnfCDGEAB***	***rnfBCDGEA***
Escherichia coli	*Clostridium tetani*	*Bacteroides vulgatus*
Vibrio fischeri MJ11	*Acetobacterium woodii*	*Chlorobium limicola*
Vibrio cholerae	*Clostridium kluyveri*	*Chlorobium luteolum*
Klebsiella pneumoniae	*Clostridium difficile*	*Parabacteroides spp.*
Haemophilus influenzae	*Clostridium botulinum*	*Prosthecochloris aestuarii*
Haemophilus ducreyi	*Clostridium phytofermentans*	*Porphyromonas uenonis*
Shigella dysenteriae	*Clostridium thermocellum*	
Pseudomonas stutzeri	*Clostridium novyi*	
Photobacterium profundum	*Clostridium beijerinckii*	
Azotobacter vinelandii	*Fusobacterium nucleatum*	
*Citrobacter spp.**	*Alkaliphilus oremlandii*	
*Erwinia spp.**	*Alkaliphilus metalliredigens*	
*Marinobacter spp.**	*Thermanaerobacter pseudethanolicus*	
*Shewanella spp.**	*Ruminococcus torques*	
*Serratia spp.**	*Ruminococcus obeum*	
*Alteromonas spp.**		

*Endonuclease III (*nth*) downstream *rnfE*

1.3 Topology and biochemical properties of the Rnf complex

The Rnf complex functions as one large 185 kDa protein complex that oxidizes reduced ferredoxin and transports those electrons to the electron acceptor NAD^+, generating energy for the

translocation of ions (H^+/Na^+) outside the inner membrane into the periplasm or extracellular milieu depending on Gram type. In general, the cofactors and topology of Rnf subunits are largely conserved. The first purified Rnf complexes were described in review papers from *Clostridium tetanomorphum* and *Fusobacterium nucleatum*, and shown to have 6 subunits (13, 14). It is believed each gene encodes a single Rnf subunit (8).

1.3.1 RnfC and RnfB

RnfC is the largest subunit of the complex, with a molecular weight of 48.7 kDa. It is also predicted to be the only soluble subunit (8). Cysteine motifs (C-XX-C-XX-C-XXX-C-P), typical for the coordination of iron-sulfur (FeS) clusters, are also present in RnfC. The RnfC subunit is proposed to bind NADH on the cytoplasmic face of the membrane. RnfB is a 36.6 kDa subunit located on the cytoplasmic-facing side of the membrane, like RnfC. RnfB contains the binding site for the low-potential electron acceptor, ferredoxin, and also harbors FeS clusters for electron transfer (8).

1.3.2 RnfD and RnfG

Integral membrane proteins, RnfD and RnfG, both contain FMN cofactors important for facilitating electron transport, and have molecular weights of 35 kDa and 22.8 kDa, respectively. RnfD has 6-9 proposed transmembrane alpha-helices, while RnfG has only one. An investigation into RnfG residues critical for flavin cofactor binding in *V. cholerae* found that there is a conserved S(T)GAT motif in the C-terminus, and that the last threonine ($RnfG^{T175}$) binds FMN as shown by mutational studies and SDS-PAGE fluorescent analysis (15). For RnfD, the last threonine ($RnfD^{T187}$) of a partially conserved TMAT motif found also in *Escherichia coli*, *Idiomarina loihiensis*, *Thermogota maritima*, and *R. capsulatus*, is responsible for binding flavin cofactors. RnfD also contains many conserved acidic residues, several of which correspond to residues in the homologous Nqr subunit, NqrB, known to be involved in sodium ion translocation (16). However, NqrB binds ubiquinone, otherwise known as coenzyme Q (CoQ), while RnfD does not. It is speculated from

the topologies and sequences of these subunits that the bulky residues of RnfD in transmembrane helix III were exchanged for smaller glycine residues in NqrB, as these residues are involved in the formation of a ubiquinone binding pocket (17).

1.3.3 RnfA and RnfE

RnfA contains at least six acidic residues predicted to be ligands for cations. Most notably the highly conserved $RnfA^{E109}$ residue, which is homologous to $NqrE^{E95}$, known to be one of the key amino acids important in sodium ion uptake. RnfE also has several acidic residues conserved in the homologous subunit, NqrD, shown to be important for Na^+ transport (16). Both RnfA and RnfE are membrane integral proteins with molecular masses of ~ 21 kDa. Neither subunit contains FMN or FeS clusters, further strengthening the hypothesis that these subunits, along with RnfD, are important for ion translocation and not electron transfer.

1.4 Evolutionary history of Rnf and related oxidoreductases

1.4.1 The Rnf complex is an early ancestor of the Nqr complex

When *rnf* genes in *R. capsulatus* were first sequenced, there was striking homology to a known sodium-dependent NADH-ubiquinone oxidoreductase (Na^+-Nqr) first described in *Vibrio alginolyticus* as a primary sodium pump for flagellar rotation (9). The Nqr complex is slightly larger than the Rnf complex, with a molecular weight of ~200 kDa consisting of six subunits (A-F) encoded in the *nqr* operon (8). Physiologically, it is very similar to the Rnf complex, with three membrane-integral proteins, NqrB, NqrD, and NqrE, with strong homology to RnfD, RnfE, and RnfA, respectively. These Nqr subunits also have similar acidic residues as their corresponding Rnf homologs, reinforcing the hypothesis they are important in the translocation of ions across the membrane (16). Likewise, the RnfD and RnfG homologs, NqrB and NqrC, respectively, both contain FMN cofactors hypothesized to be crucial for electron transport. Despite their similarities, there are some noteworthy differences between the two respiratory complexes. Rnf mediates electron transfer between Fd^{2-}/Fd and NAD^+/NADH, while Nqr between NAD^+/NADH and

ubiquinone (CoQ)/ubiquinol ($CoQH_2$). With respect to redox potential, Rnf is located “upstream” of the Nqr complex, with a redox range from -500 mV (Fd^{2-}/Fd) to -320 mV (NAD^+/NADH), whereas Nqr has a redox range from -320 mV (NAD^+/NADH) to +90 mV ($CoQ/CoQH_2$). As such, Rnf is able to conserve energy from substrates with a lower redox potential, commonly found in anoxic conditions, in contrast to the Nqr complex. However, given the broader redox range of the Nqr complex, over twice the ATP is produced following NADH oxidation coupled to ubiquinone reduction, compared to Rnf. In addition, there are no subunits of Nqr with sequence homology to the ferredoxin-binding RnfB subunit (17). While NqrA has homology to the NADH-binding RnfC subunit, it lacks any putative cofactor or substrate binding sites, suggesting another Nqr subunit is responsible for NADH-binding and reduction.

Intriguingly, phylogenic data suggest Rnf originated in the Chlorobi/Bacteroides (C/B) phyla. Chlorobi are ancient marine photoautotrophs that evolved after the rise of oxygen-producing cyanobacteria, spawning the “Great Oxygen Catastrophe” around 2.4 billion years ago. These green sulfur bacteria (GSB) oxidize sulfur and use a non-cyclic electron transport complex, likely Rnf, for anoxygenic photosynthesis (18). Phylogenetic evidence suggests the Nqr complex originated from a gene duplication and neofunctionalization event of the Rnf complex in which the acquisition of an aromatic monooxygenase containing a transmembrane domain from RnfB fusion became the NADH-binding NqrF subunit. The current distribution of the Nqr complex into Chlamydiae, Planctomyces, Delta (δ)-, Alpha (α)-, Beta (β)-, and Gamma (γ) – Proteobacteria can be explained by at least two ancestral horizonal gene transfer (HGT) events. Overall however, the distribution of the Rnf complex is still greater than that of Nqr, being found in almost every phyla Nqr is found plus members of Firmicutes, Fusobacteria, Spirochaetes, Tenericutes, Thermotogae, and Methanosarcinales (17). In contrast, the Nqr operon is only found in bacteria. Na^+-Nqr is strongly associated with aerobic respiratory metabolism of pathogenic bacteria including *V. cholerae*, *Vibrio harveyi*, *Klebsiella pneumoniae*, and *H. influenzae*. Evidence

indicates this complex plays critical roles in virulence and the survival of cells in their host environments (17). It has therefore been long speculated, given Na^+-Nqr originated from the Rnf complex, that the Rnf complex also functions in bacterial virulence.

1.4.2 Ech and complex I: two evolutionarily related membrane oxidoreductases

The energy converting hydrogenase (Ech) is a member of a large family of [NiFe]-hydrogenases found in Bacteria and Archaea that use ferredoxin ($E^{0'}$: -500 mV) to reduce protons to molecular hydrogen (H_2) ($E^{0'}$: -421 mV). By far, the most studied Ech is from the methanogen, *Methanosarcina barkeri*, which grows chemolithoautotrophically off H_2 and CO_2 forming methane (CH_4). Understanding the phylogenetic relationship between Ech and other membrane-bound electron transport chains in Bacteria and Archaea reveals interesting lines of evolution that result in different solutions to the same thermodynamic problem (8). The Ech complex from *M. barkeri* is composed of six-subunits (A-F). EchA and EchB are the only membrane-integral proteins and appear to have no cofactor binding sites, unlike EchCDEF, which all face the cytoplasm, contain FeS clusters, and catalyze the oxidation of ferredoxin to reduce molecular hydrogen (19). This exergonic "forward" reaction is coupled to the translocation of cations outside the membrane. The Ech complex is an ancestor to complex I, the latter of which is present in the inner mitochondrial membrane of eukaryotic cells and the cytoplasmic membrane of some aerobic bacteria, catalyzing the exergonic oxidation of NADH ($E^{0'}$: -320 mV) coupled to the reduction of quinone ($E^{0'}$: +700 mV), generating an IMF (5). Interestingly, in many circumstances, the Ech complex uses an ion gradient for reverse electron flow to power endergonic reduction of ferredoxin from molecular hydrogen. Fd^{2-} can then go to power other flavin-based reactions, similar to the reversibility of the Rnf complex. While the Ech complex is homologous to complex I, Rnf is homologous to Nqr. Ech and Rnf are both reversible, flavin-based oxidoreductases while complex I and Nqr are both quinone-based oxidoreductases. However, neither Ech and Rnf nor complex I

and Nqr are homologous. Evidently, evolutionary pressure has created two independent solutions to safeguard energy conservation across a wide range of redox potentials (8).

1.5 Functions of the Rnf complex

1.5.1 Nitrogen fixation

Since its literary debut in the nitrogen-fixing bacterium, *R. capsulatus* (7), *rnf* clusters have been uncovered in several diazotrophs, including *Pseudomonas stutzeri* (20), *Azotobacter vinelandii* (21), and *Clostridium ljungdahlii* (22). Nitrogen fixation is the process of reducing inorganic dinitrogen (N_2) using low-potential electrons from ferredoxin (Fd) or flavodoxin (Fld) to generate useful ammonia (NH_3). N_2-fixation emerged in an anaerobic bacterial background due to the oxygen-sensitivity of the nitrogenase enzyme. However, we now know nitrogenases have evolved to operate in multiple genomic and metabolic backgrounds including aerobes and facultative anaerobes (23). Nitrogenases are widely distributed in bacteria but only present in one archaeal phylum, Euryarchaeota, which includes methanogens. Nitrogenases have not been identified in Eukarya.

There are at least 6 ferredoxin-reducing complexes involved in N_2-fixation: pyruvate-ferredoxin oxidoreductase (PFOR), [NiFe]-hydrogenases (like Ech), [FeFe]-hydrogenases, Fix, ferredoxin-NADP$^+$ oxidoreductases (FNR), and Rnf. Anaerobic purple sulfur and non-sulfur (*R. capsulatus*) bacteria utilize their photosystems to reduce NADP$^+$/NAD$^+$ supplied by the oxidation of inorganic (sulfide or H_2) or organic (fructose) compounds. Here, the Rnf complex uses the Na^+-potential and NADH generated by the photosynthetic apparatus during the day to drive reverse electron flow to reduce ferredoxin, which then serves as a donor to reduce nitrogenase enzymes (Nif) for diazotrophic growth at night (8). Given the oxygen sensitivity of nitrogenases, some diazotrophs have evolved to fix nitrogen at night, when oxygenic photosynthesis ceases (23). Therefore, Rnf provides a necessary metabolic adaptation, supplying these photosynthetic

organisms with reducing power to produce energy without sunlight. A similar mechanism applies to the nitrogen-fixing bacteria *P. stutzeri* (24) and *C. ljungdahlii* (22). Indeed, an *rnf* mutant in *C. ljungdahlii* was unable to grow without the presence of ammonia (22). In *A. vinelandii*, the Rnf complex was found to participate in transcriptional and/or post-translational maturation of nitrogenase (21). Therefore, it is evident that for this organism, Rnf regulates the expression of nitrogenases rather than its redox state.

1.5.2 Growth from low-energy substrates

Prior to 2008, there were minimal findings regarding how the Rnf complex functioned in bacterial metabolism. That year, the Rnf complex was found to function in the electron-bifurcating bacterium *Clostridium klyuveri* (25). Electron-bifurcation (EB) is now regarded as the third mechanism of energy conservation, along with substrate-level phosphorylation (SLP) and chemiosmosis. EB is defined as the splitting of electrons from a hydride donor into low- and high-potential electrons which go to reduce low- and high-potential electron acceptors, respectively. The reaction can also proceed in reverse, known as electron confurcation, whereby a lower- and higher-energy electron pair is combined into one ultra-high-energy electron. There are two types of electron bifurcation, quinone-based (QBEB) and flavin-based (FBEB). QBEB has been well-studied in aerobes, phototrophs, and respiring Bacteria & Archaea for over 40 years, however FBEB was only recently discovered in *C. kluyveri* in 2008, and to date is only found in strict anaerobes (25, 26). Electron donors for FBEB can be formate, NAD(P)H, or H_2 while the electron acceptor can be Fd/Fld (low-potential), NAD^+, pyruvate, CoM-S-S-CoB, menaquinone, caffeyl-CoA, crotonyl-CoA, or ubiquinone (high-potential). Fd^{2-} can be sent to the Rnf complex for energy conservation, go to reduce nitrogen to ammonia, protons to hydrogen, CO_2 to CO, or carbohydrates to alcohols. *C. kluyveri*, *Clostridium difficile*, *F. nucleatum*, *A. woodii*, *A. vinelandii*, and *M. acetivorans* are all known to encode *rnf* and electron-bifurcating enzymes.

Clostridium kluyveri

C. kluyveri is a strict anaerobe with the unique ability to ferment ethanol and acetate. Ethanol is first oxidized to acetyl-CoA by the concerted actions of alcohol dehydrogenase (Adh) and acetaldehyde dehydrogenase (Ald), forming NADH (Fig. 1). Acetyl-CoA can then be converted into acetate via the phosphotransferase and acetate kinase (Pta-Ack) pathway, or reduced to crotonyl-CoA, an intermediate in butyrate synthesis. A cytoplasmic butyryl-CoA dehydrogenase (Bcd) in concert with an electron-transferring (EtfAB) complex uses NADH generated during ethanol oxidation as an electron donor to bifurcate electrons and reduce the high-potential acceptor, crotonyl-CoA, forming butyryl-CoA (leading to butyrate formation), and the low-potential acceptor, ferredoxin. Fd^{2-} is believed to be used by the Rnf complex to generate a proton gradient which is used for ATP biosynthesis while also regenerating NADH pools (8, 25, 26) (Fig. 1). A similar mechanism is proposed for *C. difficile* (27), *C. tetani* (28, 29), *Clostridium sporogenes* (30), and *F. nucleatum* (31).

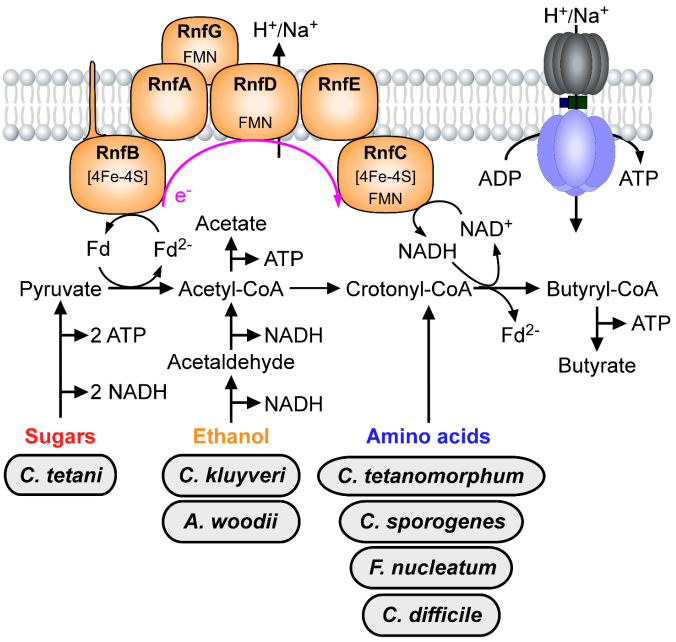

Figure 1. Model of Rnf-mediated acetate and butyrate formation. Biosynthesis of short-chain fatty acids (acetate and butyrate) from various metabolic substrates utilizing the Rnf complex (orange) to conserve energy in the form of an ion (H^+/Na^+)-motive force, which is used for ATP biosynthesis.

Acetobacterium woodii

In 2009, *rnf* genes were discovered in the acetogen, *Acetobacterium woodii*, using inverted membrane vesicles to verify fno activity, which was shown to be dependent on sodium (32). *A. woodii* is a strictly anaerobic bacterium whose main source of energy comes from the autotrophic

fixation of CO_2 into acetate via the Wood-Ljungdahlii Pathway (WLP) (Fig. 2). Acetogens are widely distributed, being found in soils, extreme environments such as hypersaline water, and the digestive tract of humans, termites, and ruminants. The acetate generated can be used for metabolism by the microbial host or the surrounding community (33, 34). The pathway is broken into two branches – "Eastern" (methyl) and "Western" (carbonyl). The "Eastern" branch is simply folate-mediated one-carbon metabolism present in all domains of life, whereby CO_2 is reduced to formate via formate dehydrogenase, and subsequently bound to tetrahydrofolate (THF), yielding formyl-THF (Fig. 2). Following the dehydration of formyl-THF, methylene-THF is reduced into methyl-THF, often using H_2, NADH, or Fd^{2-} as electron donors (Fig. 2) (34). The "Western" branch is unique to acetogens, sulfate reducers, and methanogens (Fig. 2). Here, CO_2 is reduced to carbon monoxide (CO) by ferredoxin, catalyzed by a carbon monoxide dehydrogenase (CODH) which is central to the pathway. An acetyl-CoA synthase (ACS) subsequently combines CO with the methyl group of methyl-THF, producing acetyl-CoA. Acetyl-CoA can be used for cellular carbon or converted to acetate by the concerted actions of Pta and Ack (34).

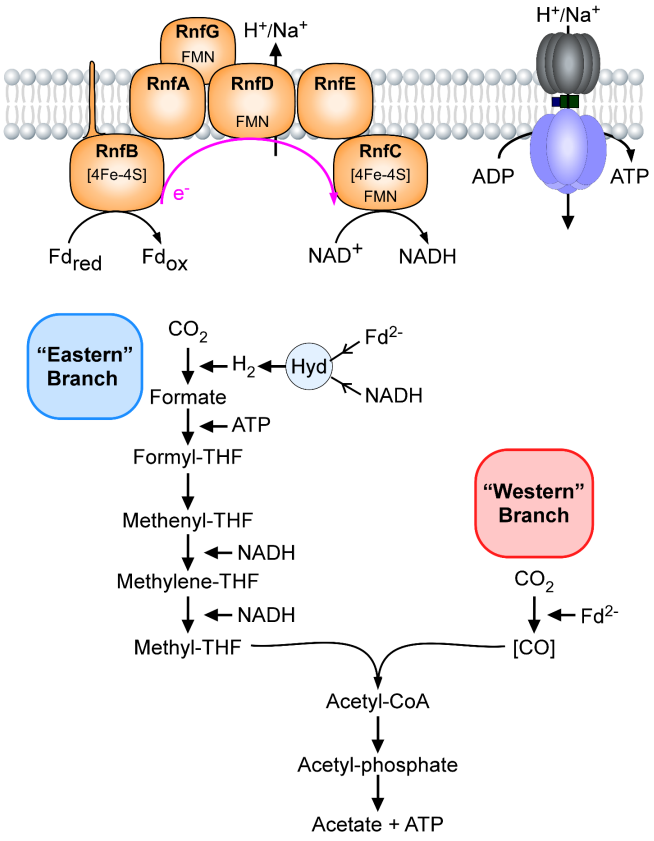

Figure 2. Rnf-modulated acetogenesis via the Wood-Ljungdahlii pathway in *A. woodii*. The Rnf complex (orange) provides reducing power (Fd^{2-}/NADH) for carbon dioxide fixation into carbon monoxide ("Western" Branch) or formate via an electron-confurcating hydrogenase (Hyd) ("Eastern" Branch), while simultaneously conserving energy via an ion (H^+/Na^+)-motive force. Convergence of "Eastern" and "Western" pathways produces acetate and ATP.

As evident, reducing power is critical for acetogenesis. Atmospheric H_2 can be used as a sole energy source, or H_2 can be bifurcated to accomplish the endergonic formation of NADH and Fd^{2-} (35). Both NADH and Fd^{2-} can now power the "Eastern" and "Western" branches of the WLP, and remaining Fd^{2-} can enter the Rnf complex, conserving additional energy through NADH production and a Na^+-motive force. The reversibility of Rnf provides additional metabolic flexibility, allowing *A. woodii* to grow off lactate and ethanol. Ethanol is a common oxidative substrate in anaerobic bacteria despite its high redox potential ($E^{0'}$ = - 190 mV), and therefore relatively low reducing power. This presents a thermodynamic barrier to "uphill" NAD^+ reduction (35). As we saw with ethanol oxidation in *C. kluyveri*, ethanol is converted into acetyl-CoA by Adh and Ald (Fig. 1). For *A. woodii*, this process produces 4 mol of NADH for every 2 mol of ethanol. Half of the NADH generated in ethanol oxidation to acetyl-CoA goes to reduce folate intermediates in the "Eastern" branch of the WLP. Another 1.5 mol of NADH goes to the Rnf complex to generate 1.5 mol of Fd^{2-} from reverse electron flow powered by a Na^+ gradient generated from ATP hydrolysis. The last 0.5 mol of NADH, along with 0.5 mol of Fd^{2-}, now go to the electron-bifurcating hydrogenase, which functions in reverse to confurcate electrons, producing H_2. Molecular hydrogen can then be used to reduce CO_2 to formate in the "Eastern" branch of the WLP. The last molecule of Fd^{2-} goes to reduce CO_2 to CO in the "Western" branch (36, 37) (Fig. 2). In short, the Rnf complex allows *A. woodii* to adapt and thrive off substrates with low energy such as ethanol or carbon dioxide in the absence of energy-rich sugars, producing acetate and conserving energy in the form of an ion gradient for downstream ATP biosynthesis. *A. woodii* also uses Rnf in reverse to provide Fd^{2-} for lactate oxidation into pyruvate (38).

Clostridium ljungdahlii and *Clostridium ultunse*

The Rnf complex is found in numerous *Clostridia* species. The acetogens *C. ljungdahlii* and *Clostridium ultunse* both use the Rnf complex likely to provide Fd^{2-} for the reduction of intermediates in the WLP as in *A. woodii* (Fig. 2). *C. ljungdhalii* specifically can grow both

autotrophically (nitrogen-fixation or acetogenesis) or heterotrophically. However, transcriptome analysis of *rnf* mutants under autotrophic (H_2 + CO_2) and heterotrophic (fructose) growth conditions showed *rnf* expression is upregulated when grown on H_2 + CO_2 compared to fructose, suggesting Rnf is critical for autotrophic growth in *C. ljungdahlii*, similar to *A. woodii* (6).

Clostridium tetani and *Clostridium tetanomorphum*

Clostridium tetani is the causative agent of tetanus. *C. tetani* oxidizes sugars into pyruvate by the Embden-Meyerhof-Parnas (EMP) pathway. Pyruvate is then oxidized by PFOR to acetyl-CoA, while also yielding Fd^{2-}, which enters the Rnf complex to produce NADH and an ion (Na^+/H^+)-motive force (Fig. 1). NADH generated in the EMP pathway or through the Rnf complex can be used to reduce acetyl-CoA into crotonyl-CoA and subsequently form butyrate and ATP. Interestingly, *C. tetani* does not encode an F_1F_0 ATP synthase but rather a V-type ATPase. It's proposed that the ion gradient generated by Rnf electron transfer is used by symporters for the uptake of sugars and amino acids (8, 28, 29). *Clostridium tetanomorphum* is an obligate, anaerobic, glutamate-fermenting bacterium. Like *C. tetani*, butyrate formation is proposed to be catalyzed by the reduction of butyryl-CoA with NADH produced from the Rnf complex while the Na^+-motive force is also thought to drive the transport of sugars and amino acids (Fig. 1). *C. tetanomorphum* also has a V-type ATPase which, in addition to the Rnf complex, likely contributes to the ion-gradient (6, 14).

Clostridium thermocellum

Clostridium thermocellum is a thermophilic anaerobe that produces lactate, acetate, and ethanol from the fermentation of cellulose. This bacterium is of interest as a candidate for consolidated bioprocessing (CBP), defined as the deconstruction of lignocellulose into useful biofuels (39). *C. thermocellum* uses mixed-acid fermentation pathways in which glucose and cellodextrins (glucose polymers from cellulose breakdown) are used to make pyruvate via the EMP pathway.

Pyruvate is converted into acetyl-CoA via the pyruvate formate lyase (PFL), producing formate, or catalyzed by PFOR which produces CO_2 and Fd^{2-}. Acetyl-CoA can then be oxidized into acetate by Pta-Ack pathway or reduced to ethanol by Adh and Ald (Fig. 1). NADH produced from the Rnf complex as a result of pyruvate oxidation was shown to be crucial for the reduction of acetyl-CoA into ethanol. Fd^{2-} can also be used to make H_2 through the Ech complex or combined with NADH to confurcate electrons into molecular hydrogen (H_2) for continued formate reduction into acetate via the WLP, as discussed in *A. woodii* (Fig. 2) (39).

1.5.3 Syntrophy and methanogenesis

Syntrophus aciditrophicus and *Syntrophobacter fumaroxidans*

Metabolic interspecies interactions in syntrophic bacteria offer an additional glimpse into how the Rnf complex enables growth in marginal energy economies (40). Here, Rnf fills Fd^{2-} pools for the reduction of metabolites important for growth and interspecies electron transfer. *Syntrophobacter fumaroxidans* and *Syntrophus aciditrophicus* are two syntrophic species in which the Rnf complex is most well understood. *S. aciditrophicus* is a rod-shaped, Gram-negative bacterium that degrades fatty acids, benzoate, crotonate, and cyclohexane, while *S. fumaroxidans* primarily degrades propionate as its sole carbon source. Both species require coculture with hydrogen/formate-utilizing methanogens (*Methanospirillum* spp.) for growth (40). These methanogens use hydrogen and formate to fix CO_2 into methane. The degradation of organic compounds, such as benzoate or propionate, by *S. fumaroxidans* and *S. aciditrophicus* is thermodynamically unfavorable unless hydrogen and formate are maintained at low concentrations by methanogens (41).

The metabolism of *S. aciditrophicus* is quite complex. As mentioned, it can oxidize benzoate, fatty acids, and a host of other organic compounds. Benzoate is converted to benzoyl-CoA catalyzed by an ATP-dependent enzyme, enabling the subsequent reduction of benzoyl-

CoA's aromatic ring. However, *S. aciditrophicus* does not encode such an enzyme. It is thought an ion gradient (possibly generated by Rnf) powers the reduction of the benzoyl-CoA aromatic ring in this species (40). The Rnf complex clearly comes into play further in the benzoate metabolic cascade in which reverse electron flow powered by a H^+/Na^+-motive force and NADH from earlier redox reactions produces Fd^{2-}, which can fuel the unfavorable reduction of acetyl-CoA to pyruvate, which enters the reverse TCA cycle for energy conservation. Fd^{2-} can also be used for formate or H_2 production via formate dehydrogenase and hydrogenase complexes, respectively. *S. aciditrophicus* encodes formate-oxalate antiporters. Thus, it appears the Rnf complex may directly function in interspecies metabolic trade by providing reduced ferredoxin for the production of H_2 and formate for methanogenesis in exchange for useful intermediates (i.e. oxalate) (40). It is not known if *S. aciditrophicus* can synthesize oxalate. If not, this would explain the presence of such an antiporter in order to keep formate concentrations within *S. aciditrophicus* low relative to the extracellular milieu. The remaining H_2 produced could also be used for ATP biosynthesis. The Rnf complex is proposed to function in the same manner through reverse electron transport in *S. fumaroxidans* following propionate degradation (41). The conserved function of the Rnf complex in several syntrophic communities highlights its importance in maintaining microbial fitness in metabolically-limited environments in which resource sharing is key to microbial success (40).

Methanosarcina acetivorans

As previously shown, acetate is a very common microbial substrate for energy conservation. There are only two genera (*Methanosarcina* and *Methanosaeta*) of acetate-utilizing/methane-producing Archaea, of which *Methanosarcina* species are the most well-studied. *Methanosarcina* produce and consume H_2 to drive the generation of a proton gradient and ATP biosynthesis. However, *Methanosarcina acetivorans* is unable to utilize H_2 as an electron donor, unlike closely-related species (*Methanosarcina barkeri*, *Methanosarcina mazei*). Instead, *M. acetivorans* relies on acetate oxidation into methane via a complex metabolic route whereby incoming acetate is

converted to acetyl-CoA through the functions of Ack and Pta (Fig. 3). Acetyl-CoA then serves as a substrate for a CODH/ACS complex (Cdh), which cleaves carbon-carbon (C-C) and carbon-sulfur (C-S) bonds of acetyl-CoA, yielding coenzyme A (CoA). Cdh also transfers a methyl group to tetrahydrosarcinapterin (H_4SPT) yielding methyltetrahydrosarcinapterin (CH_3-H_4SPT), and oxidizes a carbonyl group to CO_2, reducing ferredoxin in the process (Fig. 3). A membrane transferase (Mtr) complex transfers coenzyme M (CoM) to CH_3-H_4SPT coupled to the generation of a Na^+-motive force. A methyl-coenzyme M reductase (Mcr) reduces the methyl group of the resulting molecule, CH_3-S-CoM, to methane (CH_4). The product of the CH_3-S-CoM demethylation reaction, a heterodisulfide CoM-S-S-CoB, is then reduced by a membrane-bound heterodisulfide reductase (Hdr-DE). Fd^{2-} generated earlier in the oxidation of the carbonyl group of acetate by Cdh goes into the *M. acetivorans* Rnf complex. However, instead of NAD^+, cytochrome c (Cyt c) is the electron acceptor which is coupled to the generation of a Na^+-motive force. Cytochrome c sends electrons to a membrane-bound methanophenazine (MP) whose reduction is coupled to the generation of a proton gradient. Reduced MP (MPH_2) donates electrons to the Hdr-DE for reduction of CoM-S-S-CoB, completing the metabolic pathway (12, 42).

In summary, the oxidation of acetate in *M. acetivorans* generates a dual Na^+/H^+ gradient which can drive ATP synthesis by an ATP synthase that accepts both ions. It is clear the Rnf complex differs from those studied in bacteria as cytochrome c is the electron acceptor versus NAD^+. Also, the *rnf* operon in *M. acetivorans* contains 8 genes instead of 6, with the addition of cytochrome c and a hypothetical membrane-integral protein. The latter protein does not have any cofactor binding sites, and is therefore proposed to stabilize Cyt C. The RnfC subunit of *M.*

acetivorans also lacks an NADH binding pocket, yet still has an FeS cluster, indicating it likely mediates electron transfer to cytochrome c (12).

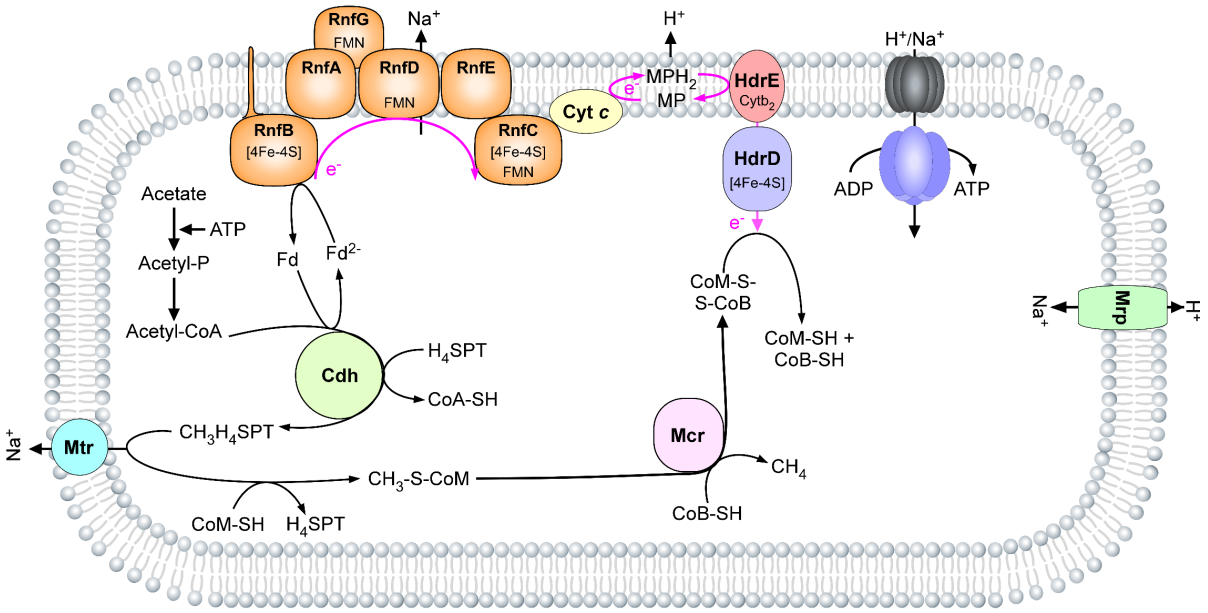

Figure 3. Model of Rnf-mediated methanogenesis in *Methanosarcina acetivorans.* Following acetate reduction into acetyl-CoA, acetyl-CoA is oxidized by the carbon monoxide dehydrogenase/acetyl-CoA synthase complex (Cdh) which generates methyltetrahydrosarcinapterin (CH_3H_4SPT) and reduced ferredoxin (Fd^{2-}), the latter of which enters the Rnf complex and conserves energy via an ion (H^+/Na^+)-motive force in conjunction with a heterodisulfide reductase (HdrDE). CH_3H_4SPT is oxidized by a methyltransferase (Mtr) that generates a sodium ion (Na^+) potential, and covalently attaches coenzyme-M, generating CH_3-S-CoM. The latter is oxidized by a methyl-coenzyme M reductase (Mcr) to produce methane (CH_4) and a heterodisulfide coenzyme (CoM-S-S-CoB) which gets reduced by HdrDE powered by Rnf. *M. acetivorans* also encodes a multisubunit sodium/proton antiporter (Mrp).

1.5.4 Bacterial physiology and virulence

Vibrio cholerae and *Vibrio alginolyticus*

The Rnf complex is found in dozens of pathogenic bacteria including *F. nucleatum*, *C. difficile*, *C. tetani*, *Salmonella enterica*, *Yersinia pestis*, *H. influenzae*, and more (8). However, there are few known examples of how this electron-transport complex regulates bacterial virulence. As mentioned, the Rnf homolog – Nqr, is commonly associated with aerobic respiratory metabolism in pathogenic species. For example, *V. cholerae* encodes both Rnf and Nqr, the latter of which was shown to modulate levels of ToxT, a global regulator of virulence genes (43, 44). How the Rnf complex comes into play is unknown. As shown, Rnf is instrumental in energy conservation by functioning as a versatile metabolic exchange center to provide cellular reducing power. It is

speculated *V. cholerae* Rnf could function as a sensory hub to regulate expression of virulence factors much like Nqr, however further research is needed (44). Cytoplasmic membranes containing *V. cholerae* Rnf were able to catalyze fno activity independent of Na^+, arguing *V. cholerae* Rnf is proton-dependent (6). The Nqr complex also mediates aminoglycoside resistance in *Vibrio alginolyticus* via a cAMP/CRP-dependent manner. Indeed, genetic disruption of *nqr* results in reduced L-alanine, reducing expression of Atp and Mnh antiporters required for aminoglycoside resistance (45).

Escherichia coli

In 2003, a reducing system for the *E. coli* transcriptional regulator, SoxR, involved in mounting oxidative stress responses, was identified as the Rnf complex and termed Rsx for reducer of SoxR, encoded as an operon (*rsxABCDGE*) (46). Aerobic oxidation of the 2Fe-2S center of SoxR results in the increase of the downstream regulator, SoxS, activating the *E. coli* stress regulon (47, 48). As oxidative stress diminishes, SoxR should no longer be activated. Inactivation of SoxR is accomplished through the reduction of the 2Fe-2S center by the Rsx reducing system in complex with thiamine biosynthesis proteins, ApbE and RseC, which share sequence similarity with RnfF, a subunit located outside the *rnfABCDEG* operon in *R. capsulatus* with unknown function (8, 46, 47).

Clostridium difficile* and *Clostridium sporogenes

As discussed, Rnf provides reducing power for autotrophic growth from inorganic compounds (7, 21, 22), the conservation of energy from low-energy substrates such as ethanol (37), lactate (38), and caffeate (49), acetogenesis (32, 36), methanogenesis (11, 12), biofuel production (39), and bacterial resource sharing (40, 41). While the establishment of a sodium-motive force by the sister Nqr complex is known to affect the expression of *toxT*, a master regulator of virulence genes in *V. cholerae* (43, 44), there are very few reports directly linking the Rnf complex to bacterial

virulence. Recent efforts to characterize the function of the Rnf complex in anaerobic, butyrate-producing *Clostridia* spp., revealed an important role in amino acid Stickland metabolism leading to butyrate (27, 30, 50). The Stickland reaction couples the oxidation of one amino acid to the reduction of another. The oxidative branch generates energy by SLP, while the reductive branch was originally believed to provide redox balance yet is now known to also produce energy via flavin-based electron transfer involving Rnf. Here, Rnf provides necessary reducing power in the form of NADH (Fig. 1A). The concerted actions of an electron transferring flavoprotein (EtfAB) in association with a butyryl-CoA dehydrogenase (Bcd) catalyzes the bifurcation of electrons from NADH, in which the pair is split into high- and low-potential electrons, which go to reduce the fermentative intermediate and butyrate precursor, crotonyl-CoA, and ferredoxin, respectively (Fig. 1A). Reduced ferredoxin can then go through Rnf to conserve additional energy via an ion-motive force, while also refilling NADH pools. Recently, genetic disruption of *rnf* expression attenuated ATP production and the colonization of the mouse gut by *Clostridium sporogenes* (30), highlighting the importance of Rnf-mediated energy conservation on host-microbe interactions.

Fusobacterium nucleatum

Recent attempts to characterize the function of Rnf in the oral opportunistic pathogen, *Fusobacterium nucleatum*, which contains high genomic and metabolic similarity to many *Clostridia* spp., including the gut pathogen *C. difficile*, demonstrated reductive Stickland metabolism leading to butyrate is likely coupled to an IMF for ATP biosynthesis using the Rnf enzyme. *F. nucleatum* is a Gram-negative anaerobic bacterium that plays important roles in dental plaque accumulation due to an inherent capacity to interact with several microbial species (51-55). Unfortunately, *F. nucleatum* is well known to spread to extra-oral sites, including the colon and placenta where it drives colorectal carcinogenesis (56-58) and adverse pregnancy outcomes (59, 60). Surprisingly however, genetic disruption of the *rnf* operon through deletion of *rnfC* in *F. nucleatum* negatively impacted many fusobacterial virulence traits, including but not limited to

biofilm formation (31, 60), polymicrobial interaction (31, 61), and toxic hydrogen sulfide production (31), which together reduced the ability of *F. nucleatum* to induce pre-term birth in a mouse model of infection (31). It is believed that the *F. nucleatum* Rnf complex metabolically mediates the expression of important enzymes and outer membrane adhesins required for several fusobacterial virulence traits, maintaining metabolic versatility as it spreads to extra-oral sites within the human body. Given the close functional and genetic similarity between fusobacterial Rnf and those of important gut commensals (*C. sporogenes*) and pathogens (*C. difficile*), further investigation into the role of Rnf in gut dysbiosis and/or homeostasis is warranted.

1.6 Conclusion

In this introduction, we discuss the distribution, topology, evolutionary history, and functions of the Rnf complex, an ancient flavin-based oxidoreductase. Rnf is highly conserved in prokaryotes, with strong selection in anaerobic organisms facing the thermodynamic edge of microbial life. This is due in large part to the reversibility of the system, endowing cells the metabolic flexibility to adapt to changes in redox states. As a result, Rnf can provide reducing power for the autotrophic fixation of inorganic substrates (N_2, CO_2), conserve energy from low-energy (ethanol) and high energy (sugars, amino acids) metabolites, and regulate oxidative stress responses. Rnf may also serve as an ideal candidate for metabolic engineering to generate useful biofuels from sugars, as discussed in *C. thermocellum*, which would reduce energy production costs, high infrastructure demands, and most importantly the consumption of environmentally harmful fossil fuels. Given the strong homology to the Nqr complex, which has been shown to regulate virulence gene expression in the cholera-causing agent, *V. cholerae*, and the recent evidence associating Rnf metabolism with the virulence of notable opportunistic pathogens (*C. difficile, F. nucleatum*), further examination of the mechanisms by which respiratory enzymes modulate bacterial pathophysiology is warranted. Coupled with its absence in eukaryotic species, Rnf may serve as an ideal target for drug screening.

1.7 References

1. **Mitchell P.** 1961. Coupling of phosphorylation to electron and hydrogen transfer by a chemi-osmotic type of mechanism. Nature 191:144-8.
2. **Muller V, Hess V.** 2017. The Minimum Biological Energy Quantum. Front Microbiol 8:2019.
3. **Buckel W, Semmler R.** 1982. A biotin-dependent sodium pump: glutaconyl-CoA decarboxylase from Acidaminococcus fermentans. FEBS Lett 148:35-8.
4. **Muller V, et al.** 1988. Electron-transport-driven sodium extrusion during methanogenesis from formaldehyde and molecular hydrogen by Methanosarcina barkeri. Eur J Biochem 178:519-25.
5. **Nolfi-Donegan D, et al.** 2020. Mitochondrial electron transport chain: Oxidative phosphorylation, oxidant production, and methods of measurement. Redox Biol 37:101674.
6. **Hess V, et al.** 2016. Occurrence of ferredoxin:NAD(+) oxidoreductase activity and its ion specificity in several Gram-positive and Gram-negative bacteria. PeerJ 4:e1515.
7. **Schmehl M, et al.** 1993. Identification of a new class of nitrogen fixation genes in Rhodobacter capsulatus: a putative membrane complex involved in electron transport to nitrogenase. Mol Gen Genet 241:602-15.
8. **Biegel E, et al.** 2011. Biochemistry, evolution and physiological function of the Rnf complex, a novel ion-motive electron transport complex in prokaryotes. Cell Mol Life Sci 68:613-34.
9. **Tokuda H, Unemoto T.** 1981. A respiration-dependent primary sodium extrusion system functioning at alkaline pH in the marine bacterium Vibrio alginolyticus. Biochem Biophys Res Commun 102:265-71.

10. **Hase CC, Mekalanos JJ.** 1999. Effects of changes in membrane sodium flux on virulence gene expression in Vibrio cholerae. Proc Natl Acad Sci U S A 96:3183-7.
11. **Schlegel K, et al.** 2012. Electron transport during aceticlastic methanogenesis by Methanosarcina acetivorans involves a sodium-translocating Rnf complex. FEBS J 279:4444-52.
12. **Suharti S, et al.** 2014. Characterization of the RnfB and RnfG subunits of the Rnf complex from the archaeon Methanosarcina acetivorans. PLoS One 9:e97966.
13. **Kim J, et al.** 2004. Dehydration of (R)-2-hydroxyacyl-CoA to enoyl-CoA in the fermentation of alpha-amino acids by anaerobic bacteria. FEMS Microbiol Rev 28:455-68.
14. **Boiangiu CD, et al.** 2005. Sodium ion pumps and hydrogen production in glutamate fermenting anaerobic bacteria. J Mol Microbiol Biotechnol 10:105-19.
15. **Backiel J, et al.** 2008. Covalent binding of flavins to RnfG and RnfD in the Rnf complex from Vibrio cholerae. Biochemistry 47:11273-84.
16. **Hreha TN, et al.** 2015. Complete Topology of the RNF Complex from Vibrio cholerae. Biochemistry 54:2443-2455.
17. **Reyes-Prieto A, et al.** 2014. Origin and evolution of the sodium -pumping NADH: ubiquinone oxidoreductase. PLoS One 9:e96696.
18. **Ward LM, Shih PM.** 2022. Phototrophy and carbon fixation in Chlorobi postdate the rise of oxygen. PLoS One 17:e0270187.
19. **Hedderich R.** 2004. Energy-converting [NiFe] hydrogenases from archaea and extremophiles: ancestors of complex I. J Bioenerg Biomembr 36:65-75.
20. **Desnoues N, et al.** 2003. Nitrogen fixation genetics and regulation in a Pseudomonas stutzeri strain associated with rice. Microbiology (Reading) 149:2251-2262.

21. **Curatti L, et al.** 2005. Genes required for rapid expression of nitrogenase activity in Azotobacter vinelandii. Proc Natl Acad Sci U S A 102:6291-6.

22. **Tremblay PL, et al.** 2012. The Rnf complex of Clostridium ljungdahlii is a proton-translocating ferredoxin:NAD+ oxidoreductase essential for autotrophic growth. mBio 4:e00406-12.

23. **Poudel S, et al.** 2018. Electron Transfer to Nitrogenase in Different Genomic and Metabolic Backgrounds. J Bacteriol 200.

24. **Chen S, et al.** 2021. Bioelectrochemical Fixation of Nitrogen to Extracellular Ammonium by Pseudomonas stutzeri. Appl Environ Microbiol 87:e0199820.

25. **Seedorf H, et al.** 2008. The genome of Clostridium kluyveri, a strict anaerobe with unique metabolic features. Proc Natl Acad Sci U S A 105:2128-33.

26. **Buckel W, Thauer RK.** 2018. Flavin-Based Electron Bifurcation, Ferredoxin, Flavodoxin, and Anaerobic Respiration With Protons (Ech) or NAD(+) (Rnf) as Electron Acceptors: A Historical Review. Front Microbiol 9:401.

27. **Neumann-Schaal M, et al.** 2019. Metabolism the Difficile Way: The Key to the Success of the Pathogen Clostridioides difficile. Front Microbiol 10:219.

28. **Bruggemann H, Gottschalk G.** 2004. Insights in metabolism and toxin production from the complete genome sequence of Clostridium tetani. Anaerobe 10:53-68.

29. **Bruggemann H, et al.** 2003. The genome sequence of Clostridium tetani, the causative agent of tetanus disease. Proc Natl Acad Sci U S A 100:1316-21.

30. **Liu Y, et al.** 2022. Clostridium sporogenes uses reductive Stickland metabolism in the gut to generate ATP and produce circulating metabolites. Nat Microbiol 7:695-706.

31. **Britton TA, et al.** 2024. The respiratory enzyme complex Rnf is vital for metabolic adaptation and virulence in Fusobacterium nucleatum. mBio 15:e0175123.

32. **Biegel E, et al.** 2009. Genetic, immunological and biochemical evidence for a Rnf complex in the acetogen Acetobacterium woodii. Environ Microbiol 11:1438-43.

33. **Ragsdale SW, Pierce E.** 2008. Acetogenesis and the Wood-Ljungdahl pathway of CO(2) fixation. Biochim Biophys Acta 1784:1873-98.

34. **Ragsdale SW.** 2008. Enzymology of the wood-Ljungdahl pathway of acetogenesis. Ann N Y Acad Sci 1125:129-36.

35. **Schuchmann K, Muller V.** 2012. A bacterial electron-bifurcating hydrogenase. J Biol Chem 287:31165-71.

36. **Westphal L, et al.** 2018. The Rnf Complex Is an Energy-Coupled Transhydrogenase Essential To Reversibly Link Cellular NADH and Ferredoxin Pools in the Acetogen Acetobacterium woodii. J Bacteriol 200.

37. **Bertsch J, et al.** 2016. A novel route for ethanol oxidation in the acetogenic bacterium Acetobacterium woodii: the acetaldehyde/ethanol dehydrogenase pathway. Environ Microbiol 18:2913-22.

38. **Weghoff MC, et al.** 2015. A novel mode of lactate metabolism in strictly anaerobic bacteria. Environ Microbiol 17:670-7.

39. **Lo J, et al.** 2017. Engineering electron metabolism to increase ethanol production in Clostridium thermocellum. Metab Eng 39:71-79.

40. **McInerney MJ, et al.** 2007. The genome of Syntrophus aciditrophicus: life at the thermodynamic limit of microbial growth. Proc Natl Acad Sci U S A 104:7600-5.

41. **Worm P, et al.** 2011. Growth- and substrate-dependent transcription of formate dehydrogenase and hydrogenase coding genes in Syntrophobacter fumaroxidans and Methanospirillum hungatei. Microbiology (Reading) 157:280-289.

42. **Jasso-Chavez R, et al.** 2013. MrpA functions in energy conversion during acetate-dependent growth of Methanosarcina acetivorans. J Bacteriol 195:3987-94.

43. **Minato Y, et al.** 2014. Inhibition of the sodium-translocating NADH-ubiquinone oxidoreductase [Na+-NQR] decreases cholera toxin production in Vibrio cholerae O1 at the late exponential growth phase. Microb Pathog 66:36-9.

44. **Hase CC, Barquera B.** 2001. Role of sodium bioenergetics in Vibrio cholerae. Biochim Biophys Acta 1505:169-78.

45. **Jiang M, et al.** 2020. Na(+)-NQR Confers Aminoglycoside Resistance via the Regulation of l-Alanine Metabolism. mBio 11.

46. **Koo MS, et al.** 2003. A reducing system of the superoxide sensor SoxR in Escherichia coli. EMBO J 22:2614-22.

47. **Lee KL, et al.** 2022. Characterization of components of a reducing system for SoxR in the cytoplasmic membrane of Escherichia coli. J Microbiol 60:387-394.

48. **Tsaneva IR, Weiss B.** 1990. soxR, a locus governing a superoxide response regulon in Escherichia coli K-12. J Bacteriol 172:4197-205.

49. **Biegel E, Muller V.** 2010. Bacterial Na+-translocating ferredoxin:NAD+ oxidoreductase. Proc Natl Acad Sci U S A 107:18138-42.

50. **Li F, et al.** 2008. Coupled ferredoxin and crotonyl coenzyme A (CoA) reduction with NADH catalyzed by the butyryl-CoA dehydrogenase/Etf complex from Clostridium kluyveri. J Bacteriol 190:843-50.

51. **Kolenbrander PE, Andersen RN.** 1989. Inhibition of coaggregation between Fusobacterium nucleatum and Porphyromonas (Bacteroides) gingivalis by lactose and related sugars. Infect Immun 57:3204-9.

52. **Lancy P, Jr., et al.** 1983. Corncob formation between Fusobacterium nucleatum and Streptococcus sanguis. Infect Immun 40:303-9.

53. **Coppenhagen-Glazer S, et al.** 2015. Fap2 of Fusobacterium nucleatum is a galactose-inhibitable adhesin involved in coaggregation, cell adhesion, and preterm birth. Infect Immun 83:1104-13.

54. **Wu T, et al.** 2015. Cellular Components Mediating Coadherence of Candida albicans and Fusobacterium nucleatum. J Dent Res 94:1432-8.

55. **Rickard AH, et al.** 2003. Bacterial coaggregation: an integral process in the development of multi-species biofilms. Trends Microbiol 11:94-100.

56. **Rubinstein MR, et al.** 2013. Fusobacterium nucleatum promotes colorectal carcinogenesis by modulating E-cadherin/beta-catenin signaling via its FadA adhesin. Cell Host Microbe 14:195-206.

57. **Abed J, et al.** 2016. Fap2 Mediates Fusobacterium nucleatum Colorectal Adenocarcinoma Enrichment by Binding to Tumor-Expressed Gal-GalNAc. Cell Host Microbe 20:215-25.

58. **Rubinstein MR, et al.** 2019. Fusobacterium nucleatum promotes colorectal cancer by inducing Wnt/beta-catenin modulator Annexin A1. EMBO Rep 20.

59. **Han YW, et al.** 2009. Uncultivated bacteria as etiologic agents of intra-amniotic inflammation leading to preterm birth. J Clin Microbiol 47:38-47.

60. **Wu C, et al.** 2018. Forward Genetic Dissection of Biofilm Development by Fusobacterium nucleatum: Novel Functions of Cell Division Proteins FtsX and EnvC. mBio 9.

61. **Wu C, et al.** 2021. Genetic and molecular determinants of polymicrobial interactions in Fusobacterium nucleatum. Proc Natl Acad Sci U S A 118.

Chapter 2

The respiratory enzyme complex Rnf is vital for metabolic adaptation and virulence in *Fusobacterium nucleatum*

Published in *mBio*

AMERICAN SOCIETY FOR MICROBIOLOGY | mBio

Check for updates

| Bacteriology | Research Article

The respiratory enzyme complex Rnf is vital for metabolic adaptation and virulence in *Fusobacterium nucleatum*

Timmie A. Britton,[1] Chenggang Wu,[2] Yi-Wei Chen,[3] Dana Franklin,[1] Yimin Chen,[3] Martha I. Camacho,[3] Truc T. Luong,[3] Asis Das,[4] Hung Ton-That[1,3,5]

AUTHOR AFFILIATIONS See affiliation list on p. 15.

ABSTRACT The Gram-negative oral pathobiont *Fusobacterium nucleatum* can traverse to extra-oral sites such as placenta and colon, promoting adverse pregnancy outcomes and colorectal cancer, respectively. How this anaerobe sustains many metabolically changing environments enabling its virulence potential remains unclear. Informed by our genome-wide transposon mutagenesis, we report here that the highly conserved *Rhodobacter* nitrogen-fixation (Rnf) complex, encoded by the *rnfCDGEAB* gene cluster, is key to fusobacterial metabolic adaptation and virulence. Genetic disruption of the Rnf complex via non-polar, in-frame deletion of *rnfC* (Δ*rnfC*) abrogates polymicrobial interaction (or coaggregation) associated with adhesin RadD and biofilm formation. The defect in coaggregation is not due to reduced cell surface of RadD, but rather an increased level of extracellular lysine, which binds RadD and inhibits coaggregation. Indeed, removal of extracellular lysine via washing Δ*rnfC* cells restores coaggregation, while addition of lysine inhibits this process. These phenotypes mirror that of a mutant (Δ*kamA*) that fails to metabolize extracellular lysine. Strikingly, the Δ*rnfC* mutant is defective in ATP production, cell growth, cell morphology, and expression of the enzyme MegL that produces hydrogen sulfide (H_2S) from cysteine. Targeted metabolic profiling demonstrated that catabolism of many amino acids, including histidine and lysine, is altered in Δ*rnfC* cells, thereby reducing production of ATP and metabolites including H_2S and butyrate. Most importantly, we show that the Δ*rnfC* mutant is severely attenuated in a mouse model of preterm birth. The indispensable function of Rnf complex in fusobacterial pathogenesis via modulation of bacterial metabolism makes it an attractive target for developing therapeutic intervention.

IMPORTANCE This paper illuminates the significant question of how the oral commensal *Fusobacterium nucleatum* adapts to the metabolically changing environments of several extra-oral sites such as placenta and colon to promote various diseases as an opportunistic pathogen. We demonstrate here that the highly conserved *Rhodobacter* nitrogen-fixation complex, commonly known as Rnf complex, is key to fusobacterial metabolic adaptation and virulence. Genetic disruption of this Rnf complex causes global defects in polymicrobial interaction, biofilm formation, cell growth and morphology, hydrogen sulfide production, and ATP synthesis. Targeted metabolomic profiling demonstrates that the loss of this respiratory enzyme significantly diminishes catabolism of numerous amino acids, which negatively impacts fusobacterial virulence as tested in a preterm birth model in mice.

KEYWORDS *Fusobacterium nucleatum*, Rnf complex, metabolism, hydrogen sulfide, coaggregation, preterm birth, virulence

A prominent member of the human oral microbiota that is known to harbor over 700 bacterial and fungal species (1, 2), the Gram-negative anaerobe *Fusobacterium*

Invited Editor Ozlem Yilmaz, Medical University of South Carolina, Charleston, South Carolina, USA

Editor Indranil Biswas, The University of Kansas Medical Center, Kansas City, Kansas, USA

Address correspondence to Hung Ton-That, htonthat@dentistry.ucla.edu.

The authors declare no conflict of interest.

See the funding table on p. 15.

Received 6 July 2023
Accepted 20 October 2023
Published 7 December 2023

nucleatum plays an integral role in oral biofilm development and dental plaque formation, by virtue of its inherent capacity to adhere to diverse microbial species, notably the *Actinomyces* spp., *Streptococcus* spp., *Porphyromonas gingivalis*, and *Candida albicans* (3–12). Beyond commensalism, *F. nucleatum* is also an opportunistic pathogen that can induce preterm birth, promote tumor growth and metastatic progression of breast cancer cells, proliferation and migration of pancreatic cancer cells, and colorectal cancer (CRC), and is noted for its ability to spread from the oral cavity and colonize many extra-oral sites, including placental, breast, pancreatic, and colorectal tissues (13–17). To date, a number of adhesins have been shown to mediate host-pathogen interactions. These include Fap2 and FadA, with the former aiding fusobacterial binding to tumor- and placenta-expressed Gal-GalNAc (18, 19), while the latter promoting placental colonization and CRC progression (17, 20–22). The other known adhesin RadD is a major fusobacterial virulence factor that not only mediates polymicrobial interaction (or coaggregation), a process that is inhibited by arginine and lysine (23, 24), but is also critical for adverse pregnancy outcomes in a mouse model of preterm birth (24).

Recently, a genome-wide Tn5 transposon mutagenesis screen for identifying additional coaggregation factors revealed that the genetic disruption of a lysine metabolic pathway (LMP), e.g., deletion of *kamA* and *kamD* genes, blocks coaggregation through the excess accumulation of extracellular lysine, which binds and inhibits RadD (24). The subsequent discovery that the *kamA* deletion mutant is significantly attenuated in inducing preterm birth in mice (24) led to the realization that amino acid metabolism might play a key role in fusobacterial virulence. Consistent with this, targeted genetic analyses showed that a mutant, Δ*megL*, defective in cysteine/methionine metabolism leading to decreased hydrogen sulfide (H_2S) production, is also attenuated in virulence in the mouse model of preterm birth (25). Yet another set of genes whose disruption by Tn5 insertional mutagenesis obliterated both coaggregation and biofilm development by fusobacteria encodes a putative respiratory enzyme commonly known as the Rnf (*Rhodobacter* nitrogen-fixation) complex (26).

Originally identified in *Rhodobacter capsulatus* (27), the Rnf complex is a highly conserved and evolutionarily ancient membrane-bound ferredoxin:NAD^+ oxidoreductase that is thought to couple reversible electron transfer from reduced ferredoxin (fd_{red}) to NAD^+ with the establishment of an ion-motive force, enabling substrate import and/or ATP biosynthesis (27–29). Found in over 150 bacterial genomes and 2 archaeal genomes, with high occurrence in anaerobes (28), the Rnf complex has been demonstrated to be a multifunctional respiratory enzyme that acts as a versatile metabolic exchange center for nitrogen fixation (27), carbon dioxide fixation (30), metabolism of low-energy substrates, such as ethanol and lactate (31–33), gene regulation to some extent (34, 35), and gut colonization in mice (36). Importantly, whether the Rnf complex contributes to bacterial virulence remains to be explored. Here, we show that *F. nucleatum* encodes a functional *rnf* locus, *rnfC-rnfD-rnfG-rnfE-rnfA-rnfB*, and that genetic disruption of the Rnf complex, via deletion of *rnfC* or *rnfD*, causes severe defects in many virulence traits of *F. nucleatum*, including coaggregation, biofilm formation, H_2S production, and ATP production, in addition to altering cell morphology and growth. Intriguingly, while the defect in coaggregation is mechanistically linked to a failure of lysine catabolism, leading to an increased level of extracellular lysine that inhibits RadD-mediated coaggregation, the defects in other traits are attributed to global reduction of amino acid metabolism as determined by targeted metabolomic analysis. Most significantly, the *rnfC* mutant is severely impaired in inducing preterm birth in mice. This study establishes that the Rnf complex is a central component in *F. nucleatum* metabolism that broadly impacts bacterial virulence.

RESULTS

Transposon mutagenesis reveals the involvement of the *F. nucleatum* Rnf complex in biofilm formation, coaggregation, and H_2S production

In our previous genome-wide screens that identified *F. nucleatum* mutants defective in biofilm formation and coaggregation, multiple subunit-encoding genes for the predicted Rnf complex were frequently targeted by Tn5 transposon insertion (24, 26) (Fig. 1A). To establish the potential multifunctional role of the Rnf complex, we further characterized these mutants in standard biofilm and coaggregation assays (24, 26). To cultivate

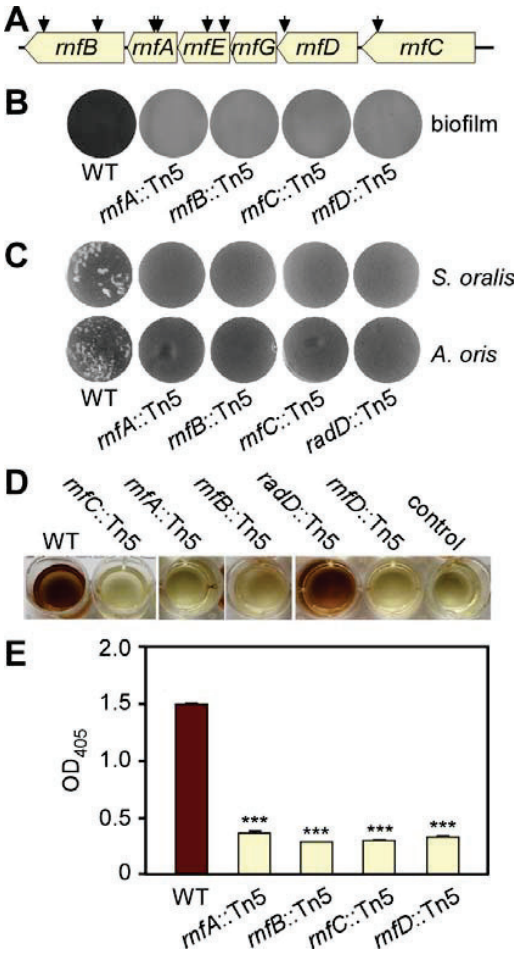

FIG 1 Transposon mutagenesis reveals the involvement of an Rnf complex in biofilm formation, coaggregation, and H_2S production. (A) Shown is the *rnf* gene locus in *F. nucleatum*, with arrows indicating the Tn5 insertion sites of previously identified Tn5 mutants (24, 26). (B) Monospecies biofilms of the wild-type (WT) and Tn5 *rnf* mutant strains were cultivated in multi-well plates, stained with 1% crystal violet, and imaged. (C) Indicated fusobacterial strains were examined for their adherence to *S. oralis* and *A. oris* by a coaggregation assay. A *radD*::Tn5 mutant was used as a negative control. (D–E) Production of H_2S from indicated strains was determined by the bismuth sulfide method (D) and quantified by absorbance measurement at 405 nm (E). Cell-free samples were used as a negative control. All results were obtained from three independent experiments performed in triplicate.

monospecies biofilms, normalized fusobacterial cultures of different strains were seeded into sterile multi-well plates, anaerobically cultured at 37°C for 48 h, and the resultant biofilms were then stained with crystal violet. Compared to the wild-type strain (ATCC 23726), each of the four tested mutant strains were defective in biofilm formation (Fig. 1B). To examine whether these mutants are also deficient in coaggregation, normalized, unwashed fusobacterial cells were mixed and incubated with *Streptococcus oralis* or *Actinomyces oris* in a standard assay, followed by imaging (see Materials and Methods). The tested Tn5 mutants also failed to co-aggregate with these two oral co-colonizers at a level similar to that of a *radD* mutant used as a negative control (Fig. 1C).

Unexpectedly, we noticed that all of the *rnf* mutants lacked the rotten egg odor characteristically produced by wild-type fusobacteria, suggestive of severe deficiency in hydrogen sulfide production by these mutants. Indeed, in a bismuth sulfide assay, in which bismuth trichloride reacts with H_2S to yield precipitation of brown bismuth sulfide, all *rnf*::Tn5 mutants showed a significantly reduced level of hydrogen sulfide relative to the wild-type strain (Fig. 1D and E). Overall, these results point to a multifaceted role of the Rnf complex in many cellular processes in *F. nucleatum*.

Genetic deletion of *rnfC* disrupts RadD-mediated coaggregation via blockage of lysine catabolism

A Tn5 insertion can potentially cause polar effects on transcription of downstream genes. Although this is unlikely the case here (Fig. S1A), we decided to generate non-polar, in-frame deletions of *rnf* genes utilizing our published protocols (24, 26, 37). Since all Tn5 mutants displayed similar phenotypes, we chose *rnfC* for further characterizations, as RnfC is predicted to be a peripheral membrane protein, enabling generation of polyclonal antibodies against a recombinant RnfC protein (Fig. S1B). To examine how the Rnf complex mediates polymicrobial interaction, this *rnfC* mutant (Δ*rnfC*) and other strains were subjected to the coaggregation assay, in which unwashed fusobacterial cells were mixed with *Streptococcus gordonii*, like the coaggregation assays done with *S. oralis* and *A. oris* as mentioned above (see Fig. 1C). As expected, deletion of *rnfC* abrogated fusobacterial coaggregation with *S. gordonii*, as compared to the parent strain (CW1), and this defect was rescued by ectopic expression of RnfC from a plasmid (Fig. 2A; the unwashed panel), supporting the polymicrobial nature of Rnf-associated coaggregation by *F. nucleatum* that is not limited to *S. oralis* and *A. oris*.

Because RadD is essential as the adhesin for fusobacterial coaggregation (23, 24), we examined if deletion of *rnfC* causes a defect in surface expression of RadD by immunofluorescence microscopy, wherein normalized fusobacterial cells of different strains were stained with antibodies against RadD (α-RadD), followed by counter-staining with Alexa 488-conjugated IgG. Microscopic examination presented in Fig. S2A revealed no significant defects of RadD-surface expression in the Δ*rnfC* mutant as compared to the parent strain. Consistent with this observation, western blotting of whole-cell lysates showed similar levels of RadD antigen production in all strains—parent, Δ*rnfC*, and its complement (Fig. S2B). Thus, the coaggregation defect of Δ*rnfC* is not due to reduced RadD expression.

Unexpectedly, when we utilized Δ*rnfC* cells free of the culture medium before mixing with *S. gordonii*, the mutant fusobacteria were able to adhere to oral streptococci at a level comparable to the parent strain (Fig. 2A; compare panels washed vs unwashed). This behavior of sensitivity to the culture medium mirrored that of a deletion mutant of *kamA*, which is defective in lysine catabolism and hence accumulates excess lysine in the culture medium (24). Given that lysine inhibits RadD-dependent coaggregation (23, 24), the results prompted us to examine the relative extracellular levels of lysine in these strains by using liquid chromatography-mass spectrometry as previously reported (24). Strikingly, compared to the parent strain, the extracellular level of lysine for the Δ*rnfC* mutant remained high and was quite comparable to that of the Δ*kamA* mutant (Fig. 2B). Thus, this accumulation of extracellular lysine is likely the inhibitor that blocks coaggregation by Δ*rnfC* mutant bacteria. To obtain support for this hypothesis, we re-performed

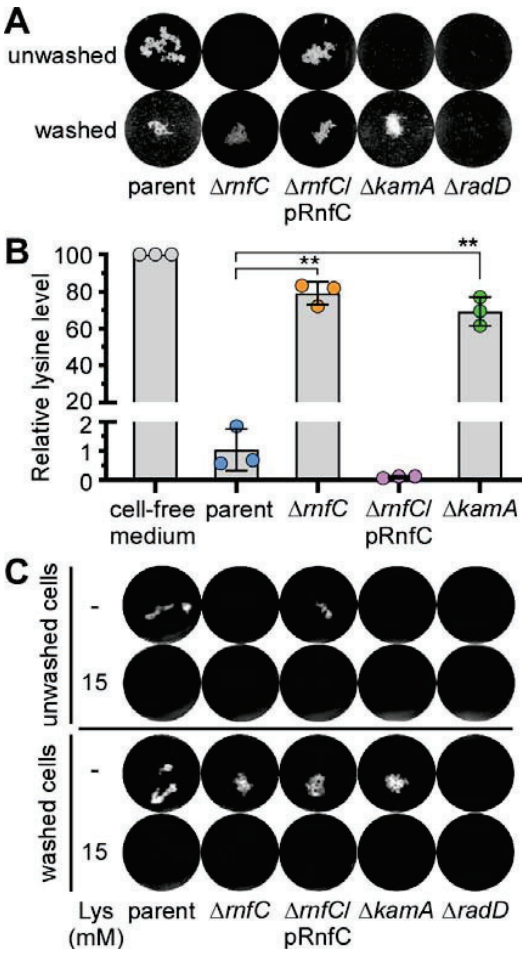

FIG 2 A non-polar, in-frame *rnfC* deletion mutant is defective in RadD-mediated coaggregation and lysine uptake. (A) The parent, *rnfC* deletion mutant, and *rnfC*-complemented strains were tested for their ability to co-aggregate with *S. gordonii*. Fusobacterial cells were washed or unwashed before being mixed in equal volumes with washed *S. gordonii* and imaged. Mutants devoid of *radD* or *kamA*, a lysine metabolic pathway gene (24), were used as references. (B) The relative level of lysine in the cell-free culture medium of indicated strains grown to stationary phase was determined by liquid chromatography-mass spectrometry, with the level of lysine in media without bacteria set to 100. (C) The same coaggregation experiment as (A) was performed with or without addition of 15 mM lysine. All results were obtained from three independent experiments performed in triplicate. Significance was calculated by a Student's *t*-test; $^{*}P < 0.05$; $^{**}P < 0.01$.

the coaggregation assay with the same set of strains in the absence or presence of 15 mM lysine added in the coaggregation mix. Regardless of whether fusobacterial cells were washed or not, the addition of lysine blocked fusobacterial coaggregation with *S. gordonii* as expected (Fig. 2C).

Since deletion of *kamA* leads to the accumulation of extracellular lysine (Fig. 2B) (24), we examined the transcript level of *kamA* in the Δ*rnfC* mutant by quantitative reverse transcription polymerase chain reaction (qRT-PCR). Remarkably, expression of *kamA* was significantly reduced in the absence of *rnfC*, as compared to the parent strain,

and this defect was rescued by ectopic expression of *rnfC* from a plasmid (Fig. S3). In addition, expression of *kamD*, another lysine metabolic gene in the *kamA* locus (24), mirrored that of *kamA* in these strains (Fig. S3). Altogether, the results indicate that the defect of RadD-mediated coaggregation by genetic disruption of *rnfC* is due to increased extracellular levels of lysine, likely due to the reduced expression of lysine metabolic genes by an as yet unexplored mechanism.

Genetic deletion of *rnf*C disrupts biofilm formation, growth, cell morphology, and hydrogen sulfide production

Next, to determine how biofilm formation is dependent on the Rnf complex, we first analyzed the non-polar, in-frame *rnfC* deletion mutant in the aforementioned biofilm assay using crystal violet staining (as described in Fig. 1B above). As expected, this mutant was also unable to form monospecies biofilms compared to the parent strain, and ectopic expression of RnfC on a plasmid was sufficient to restore biofilm formation (Fig. 3A). Since the Rnf complex plays a key role in energy conservation through several bacterial metabolic pathways (27, 38, 39), we reasoned that the defects in biofilm formation by *rnf* mutants could be due to alterations with respect to fusobacterial physiology. To investigate this further, we tested whether the Rnf complex is important in ATP biosynthesis by subjecting normalized fusobacterial cells to a microbial cell viability assay (BacTiter-Glo), which relies on the mono-oxygenation of luciferin catalyzed by luciferase in the presence of ATP. Indeed, compared to the parent strain, the Δ*rnfC* mutant drastically reduced ATP production, and complementation with an

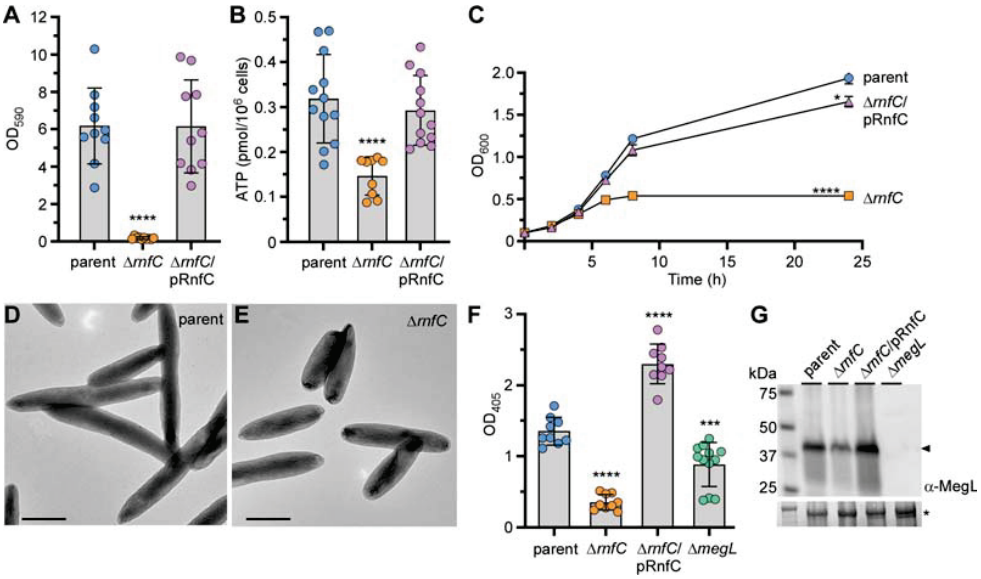

FIG 3 Deletion of *rnfC* causes pleiotropic defects. (A) 48-h grown biofilms of indicated strains were stained with 1% crystal violet and quantified by optical density measurement at 590 nm (OD_{590}). (B) ATP production of indicated strains was assessed by a luciferase assay using a BacTiter-Glo kit (Promega). Mid-log phase cells were mixed with equal volumes of the BacTiter-Glo reagent and incubated at room temperature for 2 min before measuring luminescence on a plate reader. Normalized cell suspensions were serially diluted and plated for bacterial enumeration and subsequent normalization of relative luminescent signal. (C) Bacterial growth of indicated strains was determined by optical density at 600 nm at timed intervals. (D–E) Mid-log phase cells of parent and Δ*rnfC* mutant strains were immobilized on carbon-coated nickel grids and stained with 1% uranyl acetate prior to imaging by electron microscopy; scale bars: 1 µm. (F) H_2S production of indicated strains was determined by the bismuth sulfide assay. (G) Protein samples obtained from the whole-cell lysates of normalized cultures of indicated strains were subjected to immunoblotting with antibodies against MegL (α-MegL). A Coomassie Blue stained band (*) was used as a loading control. All results were obtained from three independent experiments performed in triplicate. Significance was calculated by a Student's *t*-test; $^{*}P < 0.05$; $^{***}P < 0.001$; $^{****}P < 0.0001$.

RnfC-expressing plasmid rescued the defect (Fig. 3B). The Δ*rnfC* mutant was also severely defective in growth displaying premature growth cessation after the culture reached a suboptimal density (Fig. 3C). Intriguingly, the colony forming units (CFUs) of Δ*rnfC* cells grown to log phase and harvested for the ATP production assay or grown over the course of 24 h were comparable to that of the parent strain (Fig. S3). This similarity in the CFUs of both parent and Δ*rnfC* cells grown over time, although the latter shows reduced optical density, might be due to the morphological abnormality of the Δ*rnfC* mutant with short/stubby cells as examined by electron microscopy (Fig. 3D and E).

Potentially, the physiological deficits reported above might be due to reduced metabolism of amino acids, especially cysteine as it is one of eight important amino acids for fusobacteria (40). To test this hypothesis, we employed the aforementioned bismuth sulfide assay to measure hydrogen sulfide since it is a product of cysteine metabolism in *F. nucleatum* (25, 41–44). Consistent with the results of our Tn5 mutants, the Δ*rnfC* mutant showed a significant defect in H_2S production, and overexpression of RnfC from a plasmid substantially enhanced this process (Fig. 3F). Because the methionine γ-lyase MegL was previously shown to be responsible for the bulk of H_2S production from cysteine metabolism in *F. nucleatum* (25), we went on to determine the overall expression level of MegL in cells by immunoblotting of whole-cell lysates with antibodies against MegL (α-MegL). Remarkably, compared with the parent and rescued strains, the Δ*rnfC* mutant expressed a significantly reduced level of MegL (Fig. 3G). This reduction of MegL enzyme corresponded to a reduced level of *megL* mRNA as determined by qRT-PCR (Fig. S3). Notably, the expression of both *cysK1* and *cysK2*, which encode two additional H_2S-producing enzymes (24), was also reduced in the absence of *rnfC* (Fig. S4).

To ascertain that the physiological defects reported above are a reflection of the loss of Rnf function, we repeated these experiments with a non-polar, in-frame *rnfD* deletion mutant (Δ*rnfD*). Like the Δ*rnfC* mutant, the Δ*rnfD* mutant showed significant defects in coaggregation, biofilm formation, cell growth, and H_2S production, and these defects were rescued by ectopic expression of *rnfD* (Fig. S5). Altogether, these findings support our hypothesis that the biofilm formation defect caused by genetic disruption of the Rnf complex is not due to defects in cell viability or reduced cell numbers, but rather gross deficiencies in ATP biosynthesis and amino acid metabolism.

Loss of RnfC complex disrupt global *F. nucleatum* metabolism

To gain further insight into the function of the *F. nucleatum* Rnf complex in relation to the aforementioned phenotypes associated with genetic disruption of the Rnf complex, we performed metabolomic analysis of parent and Δ*rnfC* cells using ultra-performance liquid chromatography coupled to mass spectrometry. Among over 80 metabolites detected in these samples, 10 metabolites (Gln, Tyr, Ile, etc.) were elevated, whereas 7 metabolites, including purine ribonucleoside precursors, were significantly depleted in the Δ*rnfC* mutant, as compared to the parent strain (Fig. 4A).

To obtain a better view of the specific metabolic pathways altered upon loss of *rnfC*, we performed a quantitative pathway enrichment and pathway topology analysis of the parent and Δ*rnfC* cell using the free, web-based software, MetaboAnalyst 5.0. In keeping with our initial findings (Fig. 4A), several pathways involved in amino acid and purine metabolism were significantly enriched in the Δ*rnfC* mutant compared to the parent strain (Fig. 4B and C). Pathway analysis of the "Lys degradation," "His degradation," and "Ala/Asp/Gln metabolism" nodes in the topology analysis revealed that many amino acids are directly degraded into glutamate, which is subsequently fermented into the short-chain fatty acids, butyrate, and acetate (Fig. 4D). Significantly, the Δ*rnfC* mutant had elevated levels of urocanate, glutamine, N-acetyl-L-glutamate, lysine, and the lysine-degradation pathway intermediate, L-2-aminoadipate, relative to the parent strain (Fig. 4E through I), indicating possible disruptions in glutamate fermentation. Consistent with this result, we observed a reduced level of butyrate in this mutant as determined by high-performance liquid chromatography coupled to mass spectrometry (Fig. 4J). Additionally, as demonstrated by pathway analysis of the "Cys/Met metabolism"

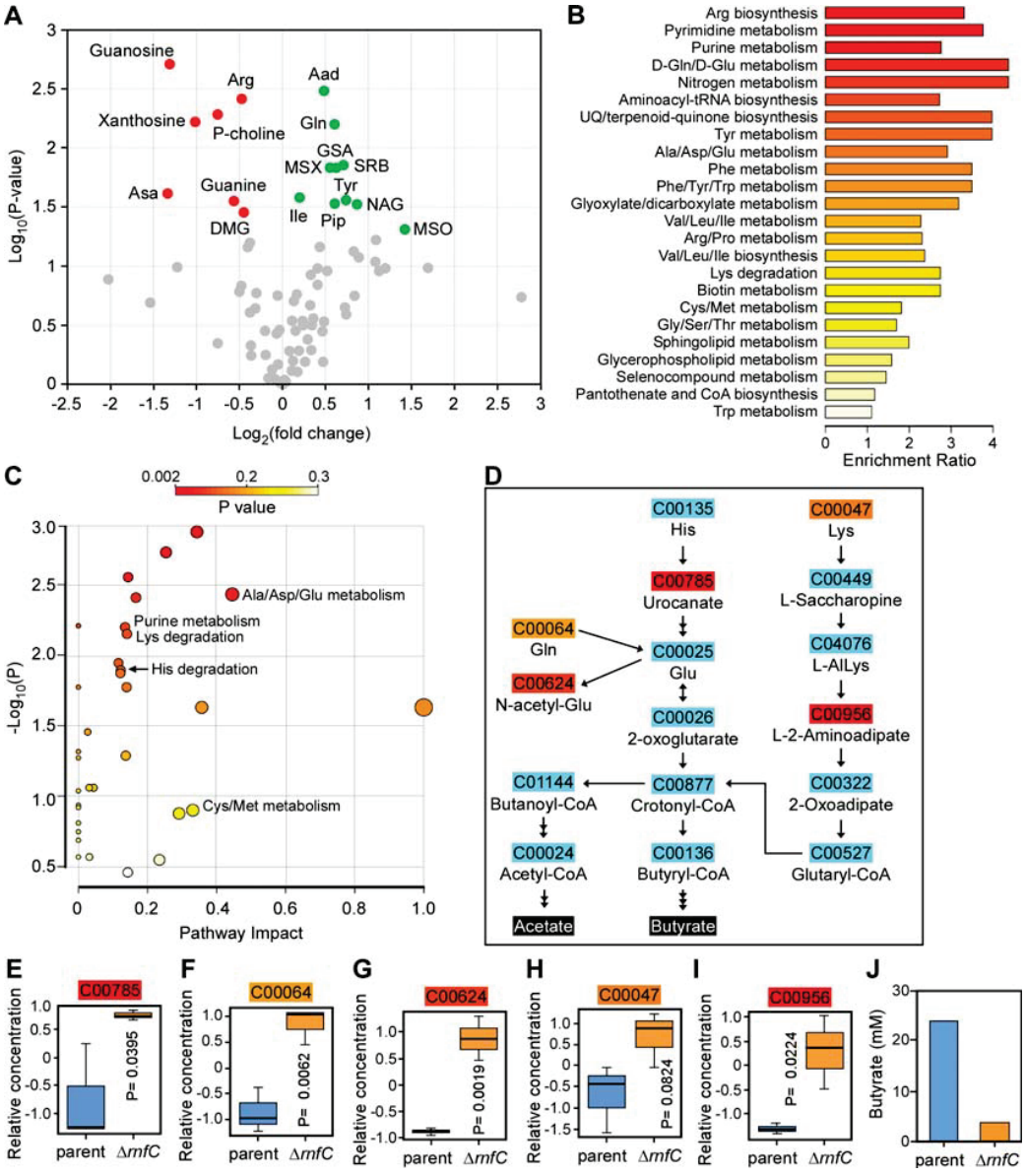

FIG 4 Deletion of *rnfC* disrupts amino acid metabolism. (A) The parent and Δ*rnfC* cells grown to mid-log phase were subjected to metabolomics analysis using liquid chromatography-mass spectrometry (LC-MS). Shown is a volcano plot of 81 differentially expressed metabolites (DEMs) between the parent and Δ*rnfC* mutant strains. Metabolites significantly depleted or enriched in the Δ*rnfC* strain, relative to the parent, are marked in red or green, respectively. (B) Shown is a graphical overview of quantitative enrichment analysis of DEMs between the parent and Δ*rnfC* strains generated using MetaboAnalyst 5.0. The top 24 pathway-associated metabolic sets in Δ*rnfC* compared to the parent strain were sorted based on their fold enrichment and *P*-values. (C) Pathway analysis was performed using MetaboAnalyst 5.0, which combines pathway enrichment and topology analysis. A range of *P*-values is shown from red to yellow. (D) Shown are amino acid metabolic nodes in *F. nucleatum*, based on the significance level in (C), generating acetate and butyrate. (E–I) The relative concentrations of DEMs in the amino acid nodes shown in (D) between the parent and Δ*rnfC* mutant strains are presented. *P*-values were calculated using the global test. (J) The relative level of butyrate (mM) in the overnight cultures of the parent and Δ*rnfC* strains was determined by LC-MS.

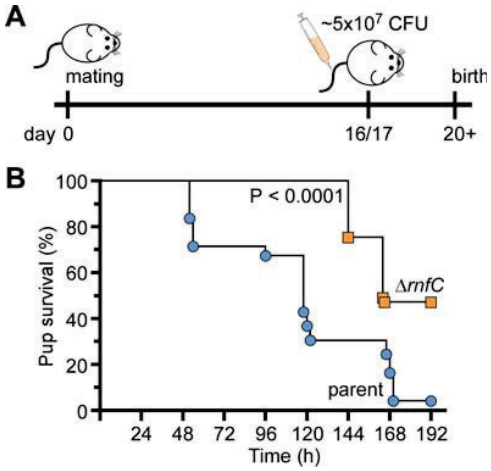

FIG 5 The *rnfC* mutant is attenuated in virulence. (A–B) Groups of pregnant CF-1 mice were infected with ~5.0 × 10^7 CFU/mL of the parent or Δ*rnfC* strain via tail vein injection at day 16 or 17 of gestation. Pup survival was recorded over time. Statistical analysis was determined by Mantel-Cox testing.

node from the topology analysis, hydrogen sulfide production is derived primarily from methionine degradation into L-homocysteine and subsequent L-cysteine degradation into pyruvate (Fig. S6A), both catalyzed by MegL (25). Correspondingly, elevated levels of methionine and slightly lower levels of the pathway intermediate, S-adenosyl-L-homocysteine, were observed in the Δ*rnfC* mutant, relative to the parent strain (Fig. S6B and C), suggesting the Rnf complex may also be important for methionine/cysteine metabolism. In sum, the results support a broad role of the Rnf complex in *F. nucleatum* metabolism.

The Rnf complex is required for *Fusobacterium nucleatum* virulence

Because genetic disruption of the Rnf complex causes significant defects in many virulence traits of *F. nucleatum* (Fig. 1 to 3), we sought to determine whether this complex contributes to *F. nucleatum* pathogenesis. Utilizing a mouse model of preterm birth as previously reported (24, 37), we infected via tail vein injection groups of five CF-1 pregnant mice at day 16/17 of gestation with roughly 5.0 × 10^7 CFU of either the parent or Δ*rnfC* strain, and pup delivery was monitored (Fig. 5A). Strikingly, the Δ*rnfC* mutant was severely attenuated in virulence, with nearly 50% of pups born alive by the end-point, while almost no pups survived infection by the parent strain within the same timeframe (Fig. 5B). Clearly, the Rnf complex plays a significant role in metabolism that is central to *F. nucleatum* pathogenesis.

DISCUSSION

The dual life of *F. nucleatum* as a commensal in the human oral cavity and an opportunistic pathogen in extra-oral sites raises an intriguing question as to how *F. nucleatum* is able to maintain its plasticity in metabolically changing environments. Here, we have demonstrated that the highly conserved multicomponent Rnf complex plays a central role in mediating metabolism of various amino acids in *F. nucleatum*, which impacts many physiological traits critical for fusobacterial virulence. Specifically, various *rnf* mutants emerged in unbiased forward genetic screens in which we sought to uncover genetic factors that govern two different aspects of *F. nucleatum* pathobiology—its ability to form biofilms and to co-aggregate with certain partner co-colonizers of the oral cavity. We then showed that that targeted disruption of the Rnf complex, via deletion

of *rnfC* or *rnfD*, not only causes severe defects in coaggregation and biofilm formation but also hydrogen sulfide production, cell morphology and growth, ATP production, and induction of preterm birth (Fig. 1 to 5; Fig. S4).

The ability of fusobacteria to co-aggregate with streptococci and other partners such as *A. oris* depends on a well-characterized adhesin RadD present on the fusobacterial cell surface. We have shown that the loss of Rnf complex function does not alter RadD expression or its display at the bacterial surface (Fig. S2). Rather, the defect in RadD-mediated interbacterial coaggregation appears to be a consequence of a defect in lysine metabolism mediated by the LMP, which in turn raises the level of extracellular lysine that can bind and inhibit RadD to block coaggregation with oral streptococci and *A. oris* (Fig. 2). Intriguingly, our results revealed that this reduced lysine metabolism parallels a decreased expression of the LMP genes, i.e., *kamA* and *kamD* (Fig. S3). As KamA is predicted to catalyze the conversion of incoming lysine to β-lysine, which is then converted to 3,5-diaminohyxanoate by KamD (24), the reduced level of *kamA* and *kamD* caused by *rnfC* deletion would certainly contribute to the accumulation of extracellular lysine that inhibits coaggregation by binding to and inactivating the adhesin RadD (24). Not only is the Δ*rnfC* mutant unable to aggregate with oral bacteria, but it is also defective in biofilm formation. Because the viability of Δ*rnfC* cells remains comparable to the parent strain throughout growth phases (Fig. S3), although the optical density of the former is less than the parent during stationary phase growth (Fig. 3C) likely due to the reduced cell size (Fig. 3D and E), we think that the defect in biofilm formation is a result of defects in metabolism leading to reduced ATP production. It is noteworthy that the growth rate of *rnf* mutants is similar to that of the parent and complement strains during the early exponential growth before plateauing at the midpoint for the remainder of the growth period (Fig. 3C). It is likely that these mutants are able to utilize available sugars until their exhaustion but unable to metabolize various amino acids.

Consistently, our metabolomic profiling further revealed that the defect in amino acid metabolism is not limited to lysine alone as aforementioned but, rather, the metabolism of many additional amino acids (viz. cysteine, histidine, and glutamate) is also affected (Fig. 4; Fig. S6). Our targeted metabolomic analysis also revealed defects in purine metabolism, which is supported by significant reduction in guanine, adenine, and their respective nucleoside precursors in the absence of *rnfC* (Fig. 4A through C). Given that *F. nucleatum* harbors several purine nucleotide biosynthetic pathways originating from many amino acids such as glutamine, glutamate, and/or aspartate, it is likely that the defects in purine metabolism in the Δ*rnfC* mutant also result from aberrant amino acid utilization. Critically, cysteine metabolism that generates hydrogen sulfide in *F. nucleatum* is mainly catalyzed by MegL, a conserved L-methionine γ-lyase (25). Logically, we expected that the defective cysteine metabolism in the Δ*rnfC* mutant would lead to reduced hydrogen sulfide production by the mutant. What we did not anticipate, however, is that the level of hydrogen sulfide production in the Δ*rnfC* mutant is significantly lower than that of the *megL* mutant (Fig. 3F), indicating the Rnf complex plays a broader role in amino acid metabolism.

Indeed, pathway and gene expression analyses demonstrated that multiple pathways leading to hydrogen sulfide production are significantly affected in the absence of *rnfC* (Fig. S6) and that expression of other cysteine metabolic genes, e.g., *cysK1* and *cysK2*, is markedly reduced (Fig. S4). Intriguingly, given CysK1 catalyzes the conversion of cysteine to hydrogen sulfide and L-lanthionine, an essential amino acid required for formation of fusobacterial peptidoglycan (45, 46), the reduced expression of *cysK1* by deletion of *rnfC* can be attributed to aberrant cell growth, short and stumpy cell size, coupled with reduced ATP production (Fig. 3). How the absence of *rnfC* reduces expression of LMP genes, *megL*, and *cysK1*/*cysK2* genes remains a significant puzzle. It is noteworthy that the expression of LMP genes and *megL* is controlled by the two-component transduction systems (TCSs), CarRS and ModRS, respectively (24, 25). One intriguing possibility, which remains to be tested in future studies, is that metabolic blockage by genetic disruption of the Rnf complex causes the accumulation of certain metabolites and intermediates that

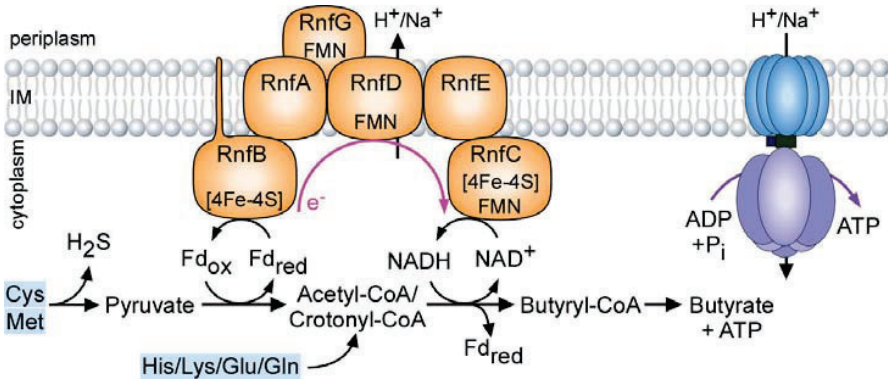

FIG 6 A working model of Rnf-mediated energy conservation through amino acid metabolism in *F. nucleatum*. See text for details.

may trigger gene expression responses from these TCSs and perhaps other transcriptional regulators.

How is the Rnf complex central to *F. nucleatum* metabolism and virulence? We propose that the *F. nucleatum* Rnf complex is a versatile metabolic exchange center that promotes metabolism of many amino acids, via the oxidation of reduced ferredoxin to the reduction of NAD^+ that generates an electrochemical ion gradient across the cytoplasmic membrane, leading to the formation of several key metabolites and ATP (Fig. 6). In particular, cysteine and methionine are metabolized into H_2S and pyruvate. The latter is oxidized to acetyl-CoA, leading to formation of butyryl-CoA and later butyrate, by reduction of ferredoxin (Fd_{ox}) and NAD. Electron shuffling from fd_{red} to NAD+ by the Rnf complex generates a sodium/proton gradient that powers the ATP synthase to generate ATP. In addition, the fermentative pathways of many amino acids (His/Lys/Glu/Gln) also lead to crotonyl-CoA that is coupled to reduction of ferrodoxin. As such, genetic disruption of the Rnf complex limits the amino acid fermentative capacity of *F. nucleatum* causing pleiotropic defects that hinder the virulence capabilities of this pathobiont as seen through defects in coaggregation, biofilm formation, cell morphology and growth, H_2S production, ATP biosynthesis, and induction of preterm birth. Given the wide conservation of the Rnf complex in many pathogens and its absence in eukaryotes, this multi-subunit respiratory enzyme may serve as an important target for broad anti-infective therapeutic strategies.

MATERIALS AND METHODS

Bacterial strains, plasmids, and media

The bacterial strains and plasmids used in this study are listed in Table S1. *F. nucleatum* cells were grown in tryptic soy broth supplemented with 1% Bacto peptone and 0.25% fresh cysteine (TSPC) or on TSPC agar plates in an anaerobic chamber (10% CO_2, 10% H_2, and 80% N_2). Heart infusion broth or heart infusion agar was used to culture *A. oris* and supplemented with 0.5% glucose to grow *S. oralis* and *S. gordonii*. *Escherichia coli* strains were grown in Luria broth. All bacterial strains, except *F. nucleatum*, were cultured in a 5% CO_2 incubator. When required, chloramphenicol or thiamphenicol were added into the medium at a concentration of 15 µg/mL and 5 µg/mL, respectively. All reagents were purchased from Sigma-Aldrich unless noted otherwise.

Plasmid construction

(i) To generate pRnfC, the primer set com-rnfC-F/R (Table S2) was used to amplify the *rnfC* coding sequence and its promoter region from chromosomal DNA of *F. nucleatum*

ATCC 23726, while appending the restriction sites KpnI/NdeI to the amplicon (35 cycles at annealing temperature of 55°C). The PCR product was digested with KpnI and NdeI restriction enzymes and cloned into pCWU6 (*SI* Table S2) precut with the same enzymes. (ii) To generate pRnfD, a segment encompassing the *rnfC* promoter region and the *rnfD* coding region was PCR-amplified from chromosomal DNA of *F. nucleatum* Δ*rnfC* (35 cycles at 56°C) using the primer set com-rnfD-F/R (Table S2), while appending NdeI and XhoI restriction sites to the amplicon. The PCR product was digested with NdeI and XhoI restriction enzymes and cloned into pCWU6 precut with the same enzymes. (iii) To generate pMCSG7-RnfC, the primer set, LIC-RnfC-F/R, was used to PCR-amplify the *rnfC* coding sequence from chromosomal DNA of *F. nucleatum* ATCC 23726, while appending adapter sequences for subsequent ligation-independent cloning into pMCSG7 as previously reported (47). All generated vectors were subjected to DNA sequence to confirm cloned sequences.

Gene deletion in *F. nucleatum*

Generation of non-polar, in-frame deletion mutants, Δ*rnfC* and Δ*rnfD*, was performed according to our published protocol (24, 26, 37), with primers for generation of deletion constructs listed in Table S2. All PCRs were performed with a 55°C annealing temperature for 35 cycles.

qRT-PCR

Overnight-grown (~17 h) fusobacterial cultures were normalized to optical density measurement at 600 nm (OD_{600}) of ~2.0, and cells were harvested by centrifugation for RNA extraction using RNeasy Mini Kits (Qiagen) according to the manufacturer's instructions, as described previously (25). Approximately 1 µg of purified RNA, free from DNA by treatment with DNase I (Qiagen), was used for cDNA synthesis using iScript RT supermix (Bio-Rad) based on the manufacturer protocol. Real-time PCR reactions were prepared using the SYBR Green PCR Master Mix with the appropriate primers (Table S2), and analysis was performed using the CFX96 Real-Time System (Bio-Rad). The $\Delta\Delta C_T$ method was used to calculate changes in gene expression between samples. Briefly, $\Delta\Delta C_T = \Delta C_{T1} - \Delta C_{T2}$, where $\Delta C_T = C_T$ (target) $- C_T$ (housekeeping gene). Fold changes were calculated as $\log_{10}(2^{\Delta\Delta Ct})$. The *16S* rRNA gene was used as reference. Reactions without reverse transcriptase were used as control to assess genomic DNA contamination.

Biofilm assay

Stationary-phase (~20 h) cells of fusobacterial strains normalized to an OD_{600} of ~0.6 in fresh TSPC were seeded into flat-bottom, multi-well plates (Greiner Bio-One) and grown anaerobically for 48 h at 37°C. Obtained biofilms were washed gently in phosphate-buffered saline (PBS) and dried before being stained with 0.2 mL of 1% crystal violet (wt/vol) solution for 10 min at room temperature with gentle shaking. Biofilms were gently washed with sterile water before being dried and imaged. For quantification, dried biofilms were de-stained with acetic acid (30% vol/vol) for 10 min at room temperature, followed by measurement at OD_{590}. Results were obtained from at least three independent experiments performed in triplicate. Statistical analysis was performed by GraphPad Prism 9.0.

Bacterial coaggregation assays

Fusobacterial interaction with bacterial partner strains was assessed using a previously published coaggregation assay (24), with some modifications. Briefly, overnight cultures (~20 h) of *F. nucleatum* and partner strains (*S. oralis*, *S. gordonii*, and *A. oris*) were harvested by centrifugation and washed twice in coaggregation buffer (0.02 M tris-buffered saline, 150 mM NaCl, 0.1 mM $CaCl_2$). Fusobacterial cells were normalized to an OD_{600} of ~0.4 in coaggregation buffer without or with 15 mM L-lysine, when indicated,

whereas partner strains were normalized to an OD_{600} of 2.0 in coaggregation buffer. Also, 0.25 mL aliquots of normalized fusobacterial and partner strains were mixed in multi-well plates (GenClone), and coaggregation was imaged. For the experiments using unwashed fusobacterial cells, a similar procedure was used, except that fusobacterial cultures were directly used without washing. All coaggregation assays were performed in an aerated condition. Results were obtained from at least three independent experiments performed in triplicate.

H_2S detection

Detection of H_2S was performed according to a published protocol with slight modification (25). Briefly, overnight cultures (~20 h) of fusobacterial cells were normalized to an OD_{600} of ~0.6 in TSPC, and 0.1 mL of normalized cell suspension was mixed with 0.1 mL of bismuth solution (0.4 M triethanolamine pH 8.0, 10 mM bismuth chloride, 20 mM pyridoxal 5-phosphate monohydride, 20 mM EDTA, 40 mM L-cysteine) and incubated at 37°C anaerobic for 1 h, at which point, images were taken and H_2S was quantified by OD_{405}. The results were presented as average of at least three independent experiments performed in triplicate.

Measurement of lysine levels by liquid chromatography-mass spectrometry

The relative lysine levels from the culture supernatant of various fusobacterial strains grown to a stationary phase (~20 h) were determined at the Metabolomics Core at Baylor College of Medicine, according to our previous publication (24). Significance analysis was performed by GraphPad Prism.

ATP quantification assay

Mid-log phase fusobacterial cells (OD_{600} of ~0.5) were harvested by centrifugation and combined in equal volumes (0.1 mL) with the BacTiter-Glo Reagent (Promega) in multi-well plates (Cellstar). The plates were incubated at room temperature in dark for ~2 min prior to measurement of relative luminescent unit using a plate reader (Tecan). ATP concentrations were determined from an ATP standard curve with ATP concentrations ranging from 1 nM to 1,000 nM. The results, presented as pmol/10^6 CFU, were obtained from at least three independent experiments performed in triplicate.

Quantification of CFU

For the ATP quantification assay, aliquots (0.1 mL) of fusobacterial cells harvested at mid-log phase and normalized to OD_{600} of 0.5 were serially diluted (10^0–10^{-7}) in a 96-well plate before spot plating 10 µL on TSPC agar plates supplemented with 5 µg/mL thiamphenicol when required. Plates were incubated in an anaerobic chamber at 37°C for 2 days before quantification. ATP levels of fusobacterial strains were normalized by their respective calculated CFU/mL. For CFU quantification over a 24-h growth period, stationary phase (~20 h) fusobacterial cultures were used to inoculate fresh cultures with starting OD_{600} of 0.1. Aliquots (0.1 mL) were taken at 8.5, 15, and 24 h of growth for spot plating and CFU/mL analysis. Results were obtained from three independent experiments performed in triplicate.

Western blotting

Expression of fusobacterial proteins was analyzed by immunoblotting with antibodies against RadD (α-RadD; 1:5,000), MegL (α-MegL; 1:5,000), FtsX (α-FtsX; 1:2,000), and RnfC (α-RnfC; 1:3,000). Generation of the first three antibodies was described elsewhere (24–26). For α-RnfC, the procedure was followed according to a previously published protocol (26). Briefly, *E. coli* BL21 (DE3) harboring pMCSG7-RnfC was used to purify recombinant protein RnfC by affinity chromatography. The purified protein was used for antibody production (Cocalico Biologicals, Inc.). For immunoblotting, overnight fusobacterial

cultures were normalized to an OD_{600} of 1.0, and 1 mL aliquots of bacterial cultures were taken for trichloroacetic acid precipitation and acetone wash, as previously reported (24). Protein samples obtained were suspended in SDS-containing sample buffer, separated by SDS-PAGE using 4%–15% Tris-Glycine gradient gels (RadD and MegL) or a 12% Tris-Glycine gel (RnfC), and immunoblotted by specific antibodies.

Electron microscopy

Electron microscopy was performed according to previously published protocols (24, 26). Briefly, overnight cultures of fusobacteria were harvested by centrifugation and re-suspended in PBS supplemented with 0.1 M NaCl. A drop of bacterial suspension was added to carbon-coated grids, stained with 1% uranyl acetate, and washed prior to imaging with an electron microscope (JEOL 1200).

Immunofluorescence microscopy

Overnight-grown (~20 h) fusobacterial cells were harvested by centrifugation and washed twice in PBS before normalizing to an OD_{600} of 0.5 in PBS. Also, 0.2 mL aliquots of cell suspension were used to coat circular glass coverslips placed in a 24-well plate for 20 min at room temperature. Cells were fixed with 2.5% formaldehyde (in PBS) for 20 min, washed with PBS, and blocked with 3% wt/vol bovine serum albumin for 1 h. Cells were incubated with α-RadD (1:200) for 1 h and then AlexaFluor 488 goat anti-rabbit IgG for another hour, followed by washing in PBS three times in the dark. Coverslips were mounted on glass slides with VECTASHIELD anti-fade mounting medium with DAPI (Vector Laboratories, Inc.). Cells were analyzed by a fluorescence microscope (Keyence BZ-X800).

Targeted metabolic analysis

Parent and Δ*rnfC* mutant cells were harvested by centrifugation from mid-log phase cultures in triplicate and normalized to an OD_{600} of 0.5 before drying in a speed vacuum concentrator (Thermo Scientific). Dried pellet samples were subjected to metabolomics analysis at the UC Riverside Metabolomics Core Facility as previously described with some modifications (48). In brief, 10 mg of dry pellet was extracted with 100 µL/mg of monophasic extraction solvent (30:30:20:20/acetonitrile, methanol, isopropanol, and water) by sonication on ice for 5 min, followed by 90-min vortexing at 4°C. Cell-free supernatants were collected by centrifugation (3,000 *g*) at 4°C for 30 min, and 1 mL aliquots were analyzed by a TQ-XS triple quadrupole mass spectrometer (Waters) coupled to an I-class UPLC system (Waters), with separations performed using a ZIC-pHILIC column (2.1 × 150 mm, 5 µM) (EMD Millipore). The mobile phases were (A) water supplemented with 15 mM ammonium bicarbonate titrated to a pH of 9.6 with ammonium hydroxide and (B) acetonitrile. The flow rate was 200 µL/min, and the columns were held at 50°C. The injection volume was 2 µL. The gradient was as follows: 0 min, 90% B; 1.5 min, 90% B; 16 min, 20% B; 18 min, 20% B; 20 min, 90% B; 28 min, 90% B. The MS was operated in multiple-reaction monitoring mode. Source and desolvation temperatures were 150°C and 600°C, respectively. Desolvation gas was set to 1,100 L/h and cone gas to 150 L/h. Collision gas was set to 0.15 mL/min. All gases were nitrogen except the collision gas of argon. Capillary voltage was 1 kV in positive ion mode and 2 kV in negative ion mode. Four quality control (QC) samples, generated by pooling equal aliquots of each sample, were analyzed periodically to monitor system stability and performance. Samples were analyzed in random order. Statistical analysis was performed relative to the parent strain and determined by a Student's *t*-test, using GraphPad Prism 9.0.

Raw mass spectral data for all 81 identified metabolites with corresponding Kyoto Encyclopedia of Genes and Genomes (KEGG) identifiers above for *F. nucleatum* ATCC 23726 were used to perform quantitative enrichment and pathway analysis using MetaboAnalyst 5.0 (49, 50). Statistical analysis was performed relative to the parent strain

and determined by the global test of MetaboAnalyst 5.0. The raw metabolomic data can be accessed from Github with the following link: https://github.com/Timbritton7/Raw-MetabolomicAnalysis_Britton.git.

Mouse model of preterm birth

The virulence potential of Δ*rnfC* was evaluated using a published mouse model of preterm birth (25, 37). Briefly, groups of five CF-1 (Charles River Laboratories) pregnant mice were infected with ~5 × 10^7 CFU of the parent or Δ*rnfC* strain at day 16 or 17 of gestation via tail vein injection. Pup survival was recorded for the next 7 days. Statistical analysis was determined via the Mantel-Cox text, using GraphPad Prism 9.0, and specified in corresponding figure legends.

ACKNOWLEDGMENTS

We thank Amancio De Souza (Metabolomics Core Facility, UCR) for technical assistance and our lab members for their discussion and critical review of the manuscript.

Research reported in this publication was supported by the National Institute of Dental & Craniofacial Research (NIDCR) of the National Institutes of Health under award numbers DE030895 (to C.W.) and DE026758 (to H.T.-T). T.A.B. was supported by the UCLA Dentist-Scientist and Oral Health-Researcher Training Program, NIDCR grant T90DE030860. D.F. was supported by the Ruth L. Kirschstein National Research Service Award (T32AI007323). The content is solely the responsibility of the authors and does not necessarily represent the official views of the National Institutes of Health.

T.A.B. and H.T.-T. designed research; T.A.B., C.W., Y.-W.C., D.F., Y.C., M.I.C., and T.T.L. performed research; T.A.B., C.W., Y.-W.C., and A.D. analyzed data; and T.A.B., A.D., and H.T.-T. wrote the paper.

AUTHOR AFFILIATIONS

[1]Molecular Biology Institute, University of California, Los Angeles, California, USA
[2]Department of Microbiology & Molecular Genetics, University of Texas McGovern Medical School, Houston, Texas, USA
[3]Division of Oral & Systemic Health Sciences, School of Dentistry, University of California, Los Angeles, California, USA
[4]Department of Medicine, Neag Comprehensive Cancer Center, University of Connecticut Health Center, Farmington, Connecticut, USA
[5]Department of Microbiology, Immunology & Molecular Genetics, University of California, Los Angeles, California, USA

AUTHOR ORCIDs

Timmie A. Britton http://orcid.org/0000-0002-1264-7878
Chenggang Wu http://orcid.org/0000-0002-5700-7188
Hung Ton-That http://orcid.org/0000-0003-1611-0469

FUNDING

Funder	Grant(s)	Author(s)
HHS | NIH | National Institute of Dental and Craniofacial Research (NIDCR)	DE026758	Hung Ton-That
HHS | NIH | National Institute of Dental and Craniofacial Research (NIDCR)	T90DE030860	Timmie A. Britton
HHS | NIH | National Institute of Dental and Craniofacial Research (NIDCR)	DE030895	Chenggang Wu

Funder	Grant(s)	Author(s)
HHS | NIH | NIAID | Division of Microbiology and Infectious Diseases, National Institute of Allergy and Infectious Diseases (DMID)	T32AI007323	Dana Franklin

AUTHOR CONTRIBUTIONS

Timmie A. Britton, Conceptualization, Formal analysis, Investigation, Writing – original draft | Chenggang Wu, Conceptualization, Formal analysis, Funding acquisition, Investigation | Yi-Wei Chen, Formal analysis, Investigation | Dana Franklin, Formal analysis, Investigation | Yimin Chen, Formal analysis, Investigation | Martha I. Camacho, Formal analysis, Investigation | Truc T. Luong, Formal analysis, Investigation | Asis Das, Formal analysis, Writing – review and editing | Hung Ton-That, Conceptualization, Formal analysis, Funding acquisition, Project administration, Supervision, Writing – original draft, Writing – review and editing

ETHICS APPROVAL

All animal procedures were approved by the UCLA Animal Research Committee (#ARC-2018–077).

ADDITIONAL FILES

The following material is available online.

Supplemental Material

Supplemental material (mBio01751-23-s0001.pdf). Supplemental figures and tables.

REFERENCES

1. Dewhirst FE, Chen T, Izard J, Paster BJ, Tanner ACR, Yu W-H, Lakshmanan A, Wade WG. 2010. The human oral microbiome. J Bacteriol 192:5002–5017. https://doi.org/10.1128/JB.00542-10
2. Caselli E, Fabbri C, D'Accolti M, Soffritti I, Bassi C, Mazzacane S, Franchi M. 2020. Defining the oral microbiome by whole-genome sequencing and resistome analysis: the complexity of the healthy picture. BMC Microbiol 20:120. https://doi.org/10.1186/s12866-020-01801-y
3. Kolenbrander PE, Andersen RN, Moore LV. 1989. Coaggregation of *Fusobacterium nucleatum*, *Selenomonas flueggei*, *Selenomonas infelix*, *Selenomonas noxia*, and *Selenomonas sputigena* with strains from 11 genera of oral bacteria. Infect Immun 57:3194–3203. https://doi.org/10.1128/iai.57.10.3194-3203.1989
4. Lancy P, Dirienzo JM, Appelbaum B, Rosan B, Holt SC. 1983. Corncob formation between *Fusobacterium nucleatum* and *Streptococcus sanguis*. Infect Immun 40:303–309. https://doi.org/10.1128/iai.40.1.303-309.1983
5. Coppenhagen-Glazer S, Sol A, Abed J, Naor R, Zhang X, Han YW, Bachrach G. 2015. Fap2 of *Fusobacterium nucleatum* is a galactose-inhibitable adhesin involved in coaggregation, cell adhesion, and preterm birth. Infect Immun 83:1104–1113. https://doi.org/10.1128/IAI.02838-14
6. Mutha NVR, Mohammed WK, Krasnogor N, Tan GYA, Choo SW, Jakubovics NS. 2018. Transcriptional responses of *Streptococcus gordonii* and *Fusobacterium nucleatum* to coaggregation. Mol Oral Microbiol 33:450–464. https://doi.org/10.1111/omi.12248
7. Wu T, Cen L, Kaplan C, Zhou X, Lux R, Shi W, He X. 2015. Cellular components mediating coadherence of *Candida albicans* and *Fusobacterium nucleatum*. J Dent Res 94:1432–1438. https://doi.org/10.1177/0022034515593706
8. Rickard AH, Gilbert P, High NJ, Kolenbrander PE, Handley PS. 2003. Bacterial coaggregation: an integral process in the development of multi-species biofilms. Trends Microbiol 11:94–100. https://doi.org/10.1016/s0966-842x(02)00034-3
9. Kolenbrander PE, Andersen RN. 1989. Inhibition of coaggregation between *Fusobacterium nucleatum* and *Porphyromonas* (Bacteroides) *gingivalis* by lactose and related sugars. Infect Immun 57:3204–3209. https://doi.org/10.1128/iai.57.10.3204-3209.1989
10. Karched M, Bhardwaj RG, Asikainen SE. 2015. Coaggregation and biofilm growth of granulicatella spp. with *Fusobacterium nucleatum* and *Aggregatibacter actinomycetemcomitans*. BMC Microbiol 15:114. https://doi.org/10.1186/s12866-015-0439-z
11. Polak D, Shapira L, Weiss EI, Houri-Haddad Y. 2012. The role of coaggregation between *Porphyromonas gingivalis* and *Fusobacterium nucleatum* on the host response to mixed infection. J Clin Periodontol 39:617–625. https://doi.org/10.1111/j.1600-051X.2012.01889.x
12. Yamaguchi-Kuroda Y, Kikuchi Y, Kokubu E, Ishihara K. 2023. Porphyromonas gingivalis diffusible signaling molecules enhance *Fusobacterium nucleatum* biofilm formation via gene expression modulation. J Oral Microbiol 15:2165001.
13. Han YW, Shen T, Chung P, Buhimschi IA, Buhimschi CS. 2009. Uncultivated bacteria as etiologic agents of intra-amniotic inflammation leading to preterm birth. J Clin Microbiol 47:38–47. https://doi.org/10.1128/JCM.01206-08
14. Payne MS, Bayatibojakhi S. 2014. Exploring preterm birth as a polymicrobial disease: an overview of the uterine microbiome. Front Immunol 5:595. https://doi.org/10.3389/fimmu.2014.00595
15. Parhi L, Alon-Maimon T, Sol A, Nejman D, Shhadeh A, Fainsod-Levi T, Yajuk O, Isaacson B, Abed J, Maalouf N, Nissan A, Sandbank J, Yehuda-Shnaidman E, Ponath F, Vogel J, Mandelboim O, Granot Z, Straussman R, Bachrach G. 2020. Breast cancer colonization by *Fusobacterium nucleatum* accelerates tumor growth and metastatic progression. Nat Commun 11:3259. https://doi.org/10.1038/s41467-020-16967-2
16. Udayasuryan B, Ahmad RN, Nguyen TTD, Umaña A, Monét Roberts L, Sobol P, Jones SD, Munson JM, Slade DJ, Verbridge SS. 2022. *Fusobacterium nucleatum* induces proliferation and migration in pancreatic cancer cells through host autocrine and paracrine signaling. Sci Signal 15:eabn4948. https://doi.org/10.1126/scisignal.abn4948

17. Rubinstein MR, Wang X, Liu W, Hao Y, Cai G, Han YW. 2013. *Fusobacterium nucleatum* promotes colorectal carcinogenesis by modulating E-cadherin/beta-catenin signaling via its FadA adhesin. Cell Host Microbe 14:195–206. https://doi.org/10.1016/j.chom.2013.07.012
18. Abed J, Emgård JEM, Zamir G, Faroja M, Almogy G, Grenov A, Sol A, Naor R, Pikarsky E, Atlan KA, Mellul A, Chaushu S, Manson AL, Earl AM, Ou N, Brennan CA, Garrett WS, Bachrach G. 2016. Fap2 mediates *Fusobacterium nucleatum* colorectal adenocarcinoma enrichment by binding to tumor-expressed gal-GaLNAc. Cell Host Microbe 20:215–225. https://doi.org/10.1016/j.chom.2016.07.006
19. Parhi L, Abed J, Shhadeh A, Alon-Maimon T, Udi S, Ben-Arye SL, Tam J, Parnas O, Padler-Karavani V, Goldman-Wohl D, Yagel S, Mandelboim O, Bachrach G. 2022. Placental colonization by *Fusobacterium nucleatum* is mediated by binding of the Fap2 lectin to placentally displayed Gal-GaLNAc. Cell Rep 38:110537. https://doi.org/10.1016/j.celrep.2022.110537
20. Rubinstein MR, Baik JE, Lagana SM, Han RP, Raab WJ, Sahoo D, Dalerba P, Wang TC, Han YW. 2019. Fusobacterium nucleatum promotes colorectal cancer by inducing Wnt/beta-catenin modulator annexin A1. EMBO Rep 20:e47638. https://doi.org/10.15252/embr.201847638
21. Xu M, Yamada M, Li M, Liu H, Chen SG, Han YW. 2007. FadA from *Fusobacterium nucleatum* utilizes both secreted and nonsecreted forms for functional oligomerization for attachment and invasion of host cells. J Biol Chem 282:25000–25009. https://doi.org/10.1074/jbc.M611567200
22. Ikegami A, Chung P, Han YW. 2009. Complementation of the *fadA* mutation in *Fusobacterium nucleatum* demonstrates that the surface-exposed Adhesin promotes cellular invasion and placental colonization. Infect Immun 77:3075–3079. https://doi.org/10.1128/IAI.00209-09
23. Kaplan CW, Lux R, Haake SK, Shi W. 2009. The *Fusobacterium nucleatum* outer membrane protein RadD is an arginine-inhibitable adhesin required for inter-species adherence and the structured architecture of multispecies biofilm. Mol Microbiol 71:35–47. https://doi.org/10.1111/j.1365-2958.2008.06503.x
24. Wu C, Chen Y-W, Scheible M, Chang C, Wittchen M, Lee JH, Luong TT, Tiner BL, Tauch A, Das A, Ton-That H. 2021. Genetic and molecular determinants of polymicrobial interactions in *Fusobacterium nucleatum*. Proc Natl Acad Sci U S A 118:e2006482118. https://doi.org/10.1073/pnas.2006482118
25. Chen Y-W, Camacho MI, Chen Y, Bhat AH, Chang C, Peluso EA, Wu C, Das A, Ton-That H. 2022. Genetic determinants of hydrogen sulfide biosynthesis in Fusobacterium Nucleatum are required for bacterial fitness, antibiotic sensitivity, and virulence. mBio 13:e0193622. https://doi.org/10.1128/mbio.01936-22
26. Wu C, Al Mamun AAM, Luong TT, Hu B, Gu J, Lee JH, D'Amore M, Das A, Ton-That H. 2018. Forward genetic dissection of biofilm development by *Fusobacterium nucleatum*: novel functions of cell division proteins FtsX and EnvC. mBio 9:e00360-18. https://doi.org/10.1128/mBio.00360-18
27. Schmehl M, Jahn A, Meyer zu Vilsendorf A, Hennecke S, Masepohl B, Schuppler M, Marxer M, Oelze J, Klipp W. 1993. Identification of a new class of nitrogen fixation genes in *Rhodobacter capsulatus*: a putative membrane complex involved in electron transport to nitrogenase. Mol Gen Genet 241:602–615. https://doi.org/10.1007/BF00279903
28. Reyes-Prieto A, Barquera B, Juárez O. 2014. Origin and evolution of the sodium -pumping NADH: ubiquinone oxidoreductase. PLoS One 9:e96696. https://doi.org/10.1371/journal.pone.0096696
29. Biegel E, Müller V. 2010. Bacterial Na+-translocating ferredoxin:NAD+ oxidoreductase. Proc Natl Acad Sci U S A 107:18138–18142. https://doi.org/10.1073/pnas.1010318107
30. Biegel E, Schmidt S, Müller V. 2009. Genetic, immunological and biochemical evidence for a Rnf complex in the acetogen *Acetobacterium woodii*. Environ Microbiol 11:1438–1443. https://doi.org/10.1111/j.1462-2920.2009.01871.x
31. Neumann-Schaal M, Jahn D, Schmidt-Hohagen K. 2019. Metabolism the difficile way: the key to the success of the pathogen *Clostridioides difficile*. Front Microbiol 10:219. https://doi.org/10.3389/fmicb.2019.00219
32. Weghoff MC, Bertsch J, Müller V. 2015. A novel mode of lactate metabolism in strictly anaerobic bacteria. Environ Microbiol 17:670–677. https://doi.org/10.1111/1462-2920.12493
33. Seedorf H, Fricke WF, Veith B, Brüggemann H, Liesegang H, Strittmatter A, Miethke M, Buckel W, Hinderberger J, Li F, Hagemeier C, Thauer RK, Gottschalk G. 2008. The genome of *Clostridium kluyveri*, a strict anaerobe with unique metabolic features. Proc Natl Acad Sci U S A 105:2128–2133. https://doi.org/10.1073/pnas.0711093105
34. Hreha TN, Mezic KG, Herce HD, Duffy EB, Bourges A, Pryshchep S, Juarez O, Barquera B. 2015. Complete topology of the RNF complex from *Vibrio cholerae*. Biochemistry 54:2443–2455. https://doi.org/10.1021/acs.biochem.5b00020
35. Koo MS, Lee JH, Rah SY, Yeo WS, Lee JW, Lee KL, Koh YS, Kang SO, Roe JH. 2003. A reducing system of the superoxide sensor SoxR in *Escherichia coli*. EMBO J 22:2614–2622. https://doi.org/10.1093/emboj/cdg252
36. Liu Y, Chen H, Van Treuren W, Hou B-H, Higginbottom SK, Dodd D. 2022. *Clostridium sporogenes* uses reductive stickland metabolism in the gut to generate ATP and produce circulating metabolites. Nat Microbiol 7:695–706. https://doi.org/10.1038/s41564-022-01109-9
37. Peluso EA, Scheible M, Ton-That H, Wu C. 2020. Genetic manipulation and virulence assessment of *Fusobacterium nucleatum*. Curr Protoc Microbiol 57:e104. https://doi.org/10.1002/cpmc.104
38. Biegel E, Schmidt S, González JM, Müller V. 2011. Biochemistry, evolution and physiological function of the Rnf complex, a novel ion-motive electron transport complex in prokaryotes. Cell Mol Life Sci 68:613–634. https://doi.org/10.1007/s00018-010-0555-8
39. Tremblay P-L, Zhang T, Dar SA, Leang C, Lovley DR, Newman DK. 2013. The Rnf complex of *Clostridium ljungdahlii* is a proton-translocating ferredoxin:NAD+ oxidoreductase essential for autotrophic growth. mBio 4:e00406-12. https://doi.org/10.1128/mBio.00406-12
40. Dzink JL, Socransky SS. 1990. Amino acid utilization by *Fusobacterium nucleatum* grown in a chemically defined medium. Oral Microbiol Immunol 5:172–174. https://doi.org/10.1111/j.1399-302x.1990.tb00418.x
41. Fukamachi H, Nakano Y, Yoshimura M, Koga T. 2002. Cloning and characterization of the L-cysteine desulfhydrase gene of *Fusobacterium nucleatum*. FEMS Microbiol Lett 215:75–80. https://doi.org/10.1111/j.1574-6968.2002.tb11373.x
42. Yoshida Y, Suwabe K, Nagano K, Kezuka Y, Kato H, Yoshimura F. 2011. Identification and enzymic analysis of a novel protein associated with production of hydrogen sulfide and L-serine from L-cysteine in *Fusobacterium nucleatum* subsp. *nucleatum* ATCC 25586. Microbiology (Reading) 157:2164–2171. https://doi.org/10.1099/mic.0.048934-0
43. Yoshida Y, Ito S, Kamo M, Kezuka Y, Tamura H, Kunimatsu K, Kato H. 2010. Production of hydrogen sulfide by two enzymes associated with biosynthesis of homocysteine and lanthionine in *Fusobacterium nucleatum* subsp. Microbiology (Reading) 156:2260–2269. https://doi.org/10.1099/mic.0.039180-0
44. Suwabe K, Yoshida Y, Nagano K, Yoshimura F. 2011. Identification of an L-methionine gamma-lyase involved in the production of hydrogen sulfide from L-cysteine in *Fusobacterium nucleatum* subsp. *nucleatum* ATCC 25586. Microbiology (Reading) 157:2992–3000. https://doi.org/10.1099/mic.0.051813-0
45. Vasstrand EN, Hofstad T, Endresen C, Jensen HB. 1979. Demonstration of lanthionine as a natural constituent of the peptidoglycan of *Fusobacterium nucleatum*. Infect Immun 25:775–780. https://doi.org/10.1128/iai.25.3.775-780.1979
46. Fredriksen A, Vasstrand EN, Jensen HB. 1991. Peptidoglycan precursor from *Fusobacterium nucleatum* contains lanthionine. J Bacteriol 173:900–902. https://doi.org/10.1128/jb.173.2.900-902.1991
47. Siegel SD, Amer BR, Wu C, Sawaya MR, Gosschalk JE, Clubb RT, Ton-That H. 2019. Structure and mechanism of LcpA, a phosphotransferase that mediates glycosylation of a gram-positive bacterial cell wall-anchored protein. mBio 10:e01580-18. https://doi.org/10.1128/mBio.01580-18
48. Vliet SMF, Dasgupta S, Sparks NRL, Kirkwood JS, Vollaro A, Hur M, Zur Nieden NI, Volz DC. 2019. Maternal-to-zygotic transition as a potential target for niclosamide during early embryogenesis. Toxicol Appl Pharmacol 380:114699. https://doi.org/10.1016/j.taap.2019.114699
49. Xia J, Psychogios N, Young N, Wishart DS. 2009. Metaboanalyst: a web server for metabolomic data analysis and interpretation. Nucleic Acids Res 37:W652–60. https://doi.org/10.1093/nar/gkp356
50. Pang Z, Zhou G, Ewald J, Chang L, Hacariz O, Basu N, Xia J. 2022. Using MetaboAnalyst 5.0 for LC-HRMS spectra processing, multi-omics integration and covariate adjustment of global metabolomics data. Nat Protoc 17:1735–1761. https://doi.org/10.1038/s41596-022-00710-w

Appendix A: Supporting Information for The respiratory enzyme complex Rnf is vital for metabolic adaptation and virulence in *Fusobacterium nucleatum*

A-1: Tables and Figures

Appendix Table A-1: Bacterial strains and plasmids used in this study

Strains & Plasmids	Description	Reference
Strain		
F. nucleatum ATCC 23726	Type strain	(1)
F. nucleatum CW1	Derivative of 23726; lacking *galK* (Δ*galK*)	(1)
F. nucleatum radD::Tn5	Derivative of ATCC 23726 with Tn5 insertion into *radD* at position 5615 (10386)	(2)
F. nucleatum rnfA::Tn5	Derivative of ATCC 23726 with Tn5 insertion into *rnfA* at position 511 (585)	(1)
F. nucleatum rnfB::Tn5	Derivative of ATCC 23726 with Tn5 insertion into *rnfB* at position 222 (1158)	(2)
F. nucleatum rnfC::Tn5	Derivative of ATCC 23726 with Tn5 insertion into *rnfC* at position 222 (1326)	(2)
F. nucleatum Δ*rnfC*	Isogenic derivative of CW1 lacking *rnfC*	This study
F. nucleatum Δ*rnfD*	Isogenic derivative of CW1 lacking *rnfD*	This study
F. nucleatum Δ*megL*	Isogenic derivative of CW1 lacking *megL*	This study
F. nucleatum Δ*radD*	isogenic derivative of CW1 lacking *radD*)	(1)
F. nucleatum Δ*kamA*	Isogenic derivative of CW1 lacking *kamA*	(2)
A. oris MG1	Type strain	(3)
S. oralis 34	RPS positive	(4)
S. gordonii DL1	Type strain	(5)
Plasmid		
pCWU6	Derivative of pHS30	(1)
pCM-GalK	*C. perfringens* vector expressing *galK*	(1)
pMCSG7-RnfC	Recombinant vector expressing His-tagged RnfC	This study
pRnfC	Derivative of pCWU6 expressing *rnfC* under the control of a *rpsJ* promoter	This study
pRnfD	Derivative of on pCWU6 expressing *rnfD* under the control of a *rpsJ* promoter	This study
pGalK--Δ*rnfC*	pCM-galK derivative; *rnfC* deletion vector	This study
pGalK--Δ*rnfD*	pCM-galK derivative; *rnfD* deletion vector	This study
pGalK--Δ*radD*	pCM-galK derivative; *radD* deletion vector	(2)
pGalK--Δ*megL*	pCM-galK derivative; *megL* deletion vector	(6)
pGalK--Δ*kamA*	pCM-galK derivative; *kamA* deletion vector	(2)

Appendix Table A-2: Primers used in this study

Primer	Sequence[a]	Used for
rnfC-up-F	GGCGGGATCCATGAACTTTGAAGAAATAGATTTTTATATT	pGalK-Δ*rnfC*
rnfC-up-R	GGCGGGATCCTTAAAGGAGCTCCTATATGTTGTAAAAG	pGalK-Δ*rnfC*
rnfC-dn-F	GGCGGGTACCGTCCTATGGGGCTTGCACCACTTATG	pGalK-Δ*rnfC*
rnfC-dn-R	GGCGAAGCTTGCTAGTTGCTTCTGGTAAAACTTCTTTT	pGalK-Δ*rnfC*
com-rnfC-F	GGCGGGTACCGGATAGTAGAAGTGCATTTAAAGATT	pRnfC
com-rnfC-R	GGCGGGATCCCTACTTTTTCTTAGCTCTTAATTTAG	pRnfC
LIC-RnfC-F	TACTTCCAATCCAATGCAATGAAAGGAGTGTTT	pMCSG7-RnfC
LIC-RnfC-R	TTATCCACTTCCAATGTTACTACTTTTTCTTAGCTC	pMCSG7-RnfC
rnfD-up-F	CGCGGATCCAAAGGTATTGTTGGTATAGGAG	pGalK-Δ*rnfD*
rnfD-up-R	CCCATCCACTAAACTTAAACAATATGAGGAGCTGGTCCTGT	pGalK-Δ*rnfD*
rnfD-dn-F	TGTTTAAGTTTAGTGGATGGGTTTGCATTGGGATTAGGAGTTT	pGalK-Δ*rnfD*
rnfD-dn-R	CGCGTCGACAAATAATCCTAATACCTTATATAAG	pGalK-Δ*rnfD*
com-rnfD-F	GGGAATTCCATATGGTTTAGGAAATCCGGGCAAA	pRnfD
com-rnfD-R	CCGCTCGAGAGCTGCTATTAGACCAAGGA	pRnfD
radD-up-F	AAAGTCGACATGGTTTAGTGAAAGATTATTCAAAAT	pGalK-Δ*radD*
radD-up-R	AAAGGTACCATTTGCTCCA AAATCTATTT TATCA	pGalK-Δ*radD*
radD-dn-F	AAAGGTACCTCATCATCACCAATATTTAAGTCATTAG	pGalK-Δ*radD*
radD-dn-R	AAAGAGCTCCATAAATATCCTCAAAATATGAGTG	pGalK-Δ*radD*
kamA-up-F	GGCGTGAGCTCCAGAGATAGAAGTTTTTGATAAGGGTA	pGalK-Δ*kamA*
kamA-up-R	GGCGAGGTACCGTTTACCTTTCTACTACCATACCATAAT	pGalK-Δ*kamA*
kamA-dn-F	GGCGAGGTACCGGTACCAAAATAAAAAATGTTAGATAC	pGalK-Δ*kamA*
kamA-dn-R	GGCGAGTCGACAAGTAGCAATTTTTTCATTATTAGGAT	pGalK-Δ*kamA*
megL-up-F	CGCGGATCCGACATTCTCTTGAATTATAAAAAAAATCTG	pGalK-Δ*megL*
megL-up-R	AAAACTGCAGCCATTATAGATTTCTTTCCCATAACC	pGalK-Δ*megL*
megL-dn-F	TAACTTTACTCATTTGTCTTAATTCCTTAC	pGalK-Δ*megL*
RT-megL-F	CACAAGACTAGGCAATCCTACA	RT-PCR *megL*
RT-megL-R	GCTCCCATACCAGATGACATAG	RT-PCR *megL*
RT-cysK1-F	AACAGGGACAGGAGGTAGTT	RT-PCR *cysK1*
RT-cysK1-R	AGATGAAGCAGGCTCAACAG	RT-PCR *cysK1*
RT-cysK2-F	GCTACAAGTGGAAACACAGGA	RT-PCR *cysK2*
RT-cysK2-R	TCACTCATCCAATCTGGCATATAA	RT-PCR *cysK2*
RT-kamA-F	TCTCAATGGCAACTGGATTCTC	RT-PCR *kamA*
RT-kamA-R	TGCAGCATGGTCAACTGTATAA	RT-PCR *kamA*
RT-kamD-F	GTGCTGATGTTGTTGCAGTTAT	RT-PCR *kamD*
RT-kamD-R	TTCTTGTGTTGCCATTGTTCC	RT-PCR *kamD*
RT-radD-F	GCAGCAGCACCAACAATAAAT	RT-PCR *radD*
RT-radD-R	GGTGCTTCAGGAGGTGTTATC	RT-PCR *radD*
RT-16s-F	GGTTAAGTCCCGCAACGA	RT-PCR *16s*
RT-16s-R	CATCCCCACCTTCCTCCTAC	RT-PCR *16s*

[a] Underlined are restriction site sequences.

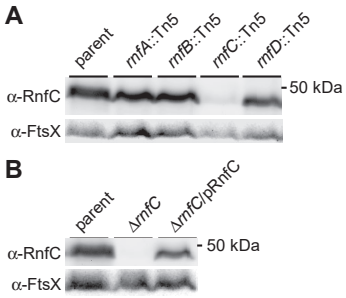

Appendix Figure A-1: Expression analysis of RnfC by western blotting. (A) Protein samples in the whole-cell lysates prepared from the parent and Tn5 mutant strains were subjected to SDS-PAGE and immunoblotted with antibodies against RnfC (α-RnfC). (B) Immunoblotting of whole-cell lysates of the parent, its isogenic rnfC deletion mutant ΔrnfC, and rnfC-complemented ΔrnfC/pRnfC strains was performed with α-RnfC. Blotting with antibody against FtsX (the membrane-bound cell-division protein) was used as the loading control. Results represent three independent experiments performed in triplicate.

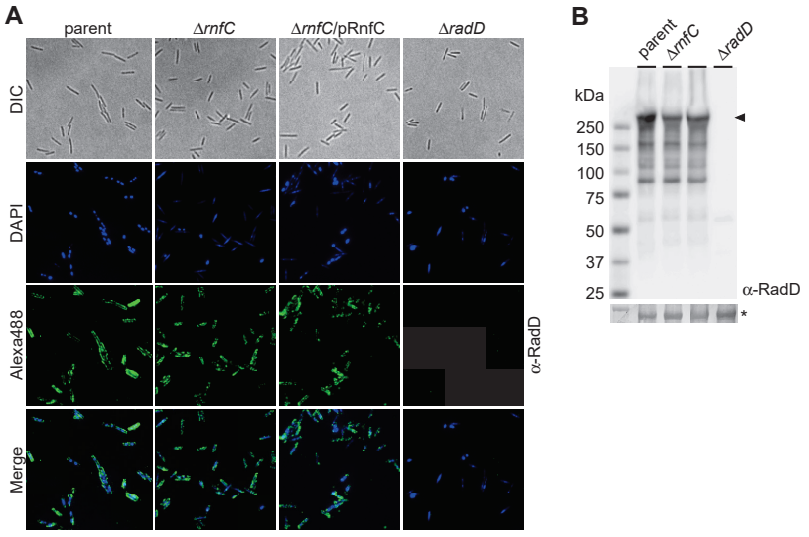

Appendix Figure A-2: RnfC is dispensable for surface display of RadD. (A) Overnight-grown cells of indicated fusobacterial strains were first stained with an antibody against RadD (α-RadD) and then Alexa Fluor 488-conjugated secondary antibody (green), as well as DAPI (blue). Surface display of RadD was analyzed by fluorescence microscopy. (B) Expression of RadD was analyzed by immunoblotting of protein samples in the whole-cell lysates obtained from the indicated strains. A Coomassie-stained band (*) was used as loading control. The results presented are representative of three independent experiments performed in triplicate.

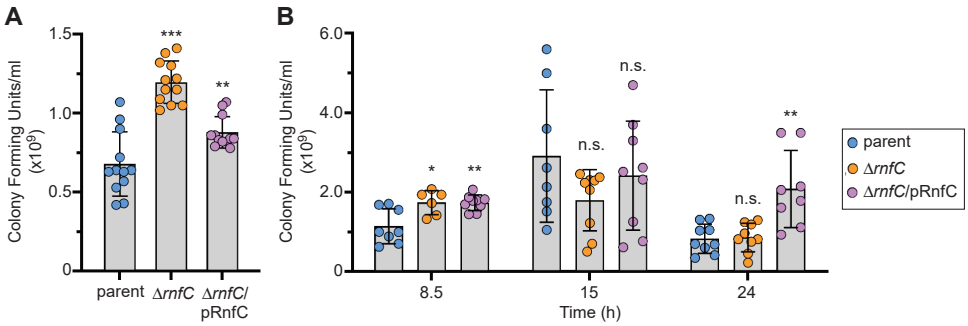

Appendix Figure A-3: Colony forming units of the Δ*rnfC* mutant are comparable to the parent strain. (A) Normalized overnight cultures of the parent, Δ*rnfC*, complementing strains were used to inoculate fresh cultures grown to mid-log phase (OD600 of 0.5). Aliquots were taken for ATP quantification (see Fig. 3B) and bacterial numeration expressed as colony forming unit per ml (CFU/ml). (B) Normalized overnight cultures of indicated strains were used to inoculate fresh cultures that were grown for 24. Aliquots were taken at indicated times for bacterial numeration (CFU/ml). Results represent three independent experiments performed in triplicate. Significance was calculated by a student's t-test; *P < 0.05; **P < 0.01; ***P < 0.001.

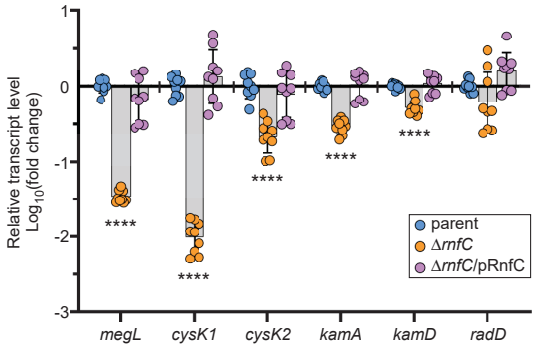

Appendix Figure A-4: Deletion of rnfC significantly reduces expression of genes coding for enzymes involved in H2S production and lysine catabolism. Normalized overnight cultures of the parent, in ΔrnfC, and ΔrnfC/pRnfC strains were used to isolate total RNA. The expression levels of megL, cysK1, cysK2, kamA, kamD, and radD in these strains were determined by qRT-PCR. Results were obtained from three independent experiments performed in triplicate. All qRT-PCR data were normalized to the transcript abundance of 16s rRNA for each sample. Significance was calculated by a student's t-test; ****, P < 0.0001.

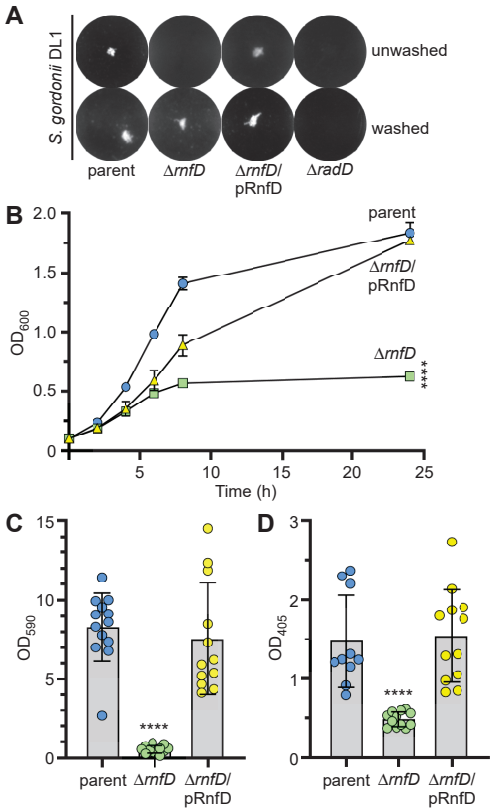

Appendix Figure A-5: Deletion of rnfD causes pleiotropic defects. (A) Interaction between S. gordonii DL1 and indicated fusobacterial strains was determined by a coaggregation assay, with fusobacterial cells washed or unwashed prior to mixing with gordonii. A radD mutant was used as a negative control. (B) Bacterial growth of indicated strains was monitored by optical density at 600 nm over 24 h. (C) Biofilms of indicated strains were cultivated for 48 h under anaerobic conditions. Quantification of biofilm production was determined by 1% crystal violet staining. (D) Normalized overnight cultures of indicated fusobacterial strains were used to determine hydrogen sulfide production by a bismuth assay. Results represent three independent experiments performed in triplicate, and significance calculated by a student's t-test; ****, P< 0.0001.

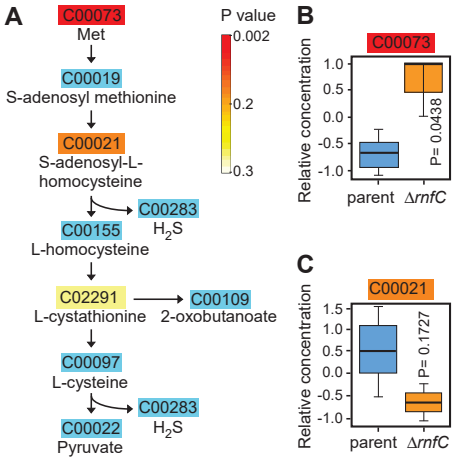

Appendix Figure A-6: Deletion of rnfC alters methionine and cysteine metabolism. (A) Using the MetaboAnalyst 5.0 web-based software, pathway analysis was performed on differentially expressed metabolites between the parent and ΔrnfC strain (see Fig. 4C). Shown is the generated pathway from the "Cys/Met metabolism" node. The level of significance for a metabolite abundantly detected in these two strains is indicated by yellow to red (P value ranging from 0.3 to 0.002). KEGG identification numbers of metabolites are highlighted in light blue. (B-C) Shown are relative concentrations of methionine (B) and S-adenosyl-L-homocysteine (C); statistical significance was calculated using the Global test.

Appendix A-2: References

1. Wu C, Al Mamun AAM, Luong TT, Hu B, Gu J, Lee JH, D'Amore M, Das A, Ton-That H. 2018. Forward Genetic Dissection of Biofilm Development by *Fusobacterium nucleatum*: Novel Functions of Cell Division Proteins FtsX and EnvC. mBio 9.

2. Wu C, Chen YW, Scheible M, Chang C, Wittchen M, Lee JH, Luong TT, Tiner BL, Tauch A, Das A, Ton-That H. 2021. Genetic and molecular determinants of polymicrobial interactions in *Fusobacterium nucleatum*. Proc Natl Acad Sci U S A 118.

3. Wu C, Mishra A, Yang J, Cisar JO, Das A, Ton-That H. 2011. Dual function of a tip fimbrillin of *Actinomyces* in fimbrial assembly and receptor binding. J Bacteriol 193:3197-206.

4. Wu C, Huang IH, Chang C, Reardon-Robinson ME, Das A, Ton-That H. 2014. Lethality of sortase depletion in *Actinomyces oris* caused by excessive membrane accumulation of a surface glycoprotein. Mol Microbiol 94:1227-41.

5. Hsu SD, Cisar JO, Sandberg AL, Kilian M. 1994. Adhesive properties of viridans streptococcal species. Microb Ecol Health Dis 7:125-37.

6. Chen YW, Camacho MI, Chen Y, Bhat AH, Chang C, Peluso EA, Wu C, Das A, Ton-That H. 2022. Genetic Determinants of Hydrogen Sulfide Biosynthesis in *Fusobacterium nucleatum* Are Required for Bacterial Fitness, Antibiotic Sensitivity, and Virulence. mBio 13:e0193622.

Chapter 3 Inactivation of the *Fusobacterium nucleatum* Rnf complex reduces FadA-mediated amyloid formation and tumor development

Timmie A. Britton[1], Ju Huck Lee[2,3], Chungyu Chang[4], Aadil H. Bhat[4], Yi-Wei Chen[4], Rusul Mohammed Ali[5], Chenggang Wu[6], Asis Das[7], and Hung Ton-That[1,4,5]

[1]*Molecular Biology Institute, University of California, Los Angeles, California, USA;* [2]*Department of Microbiology & Molecular Genetics, University of Texas McGovern Medical School, Houston, Texas, USA;* [3]*Korean Collection for Type Cultures, Korea Research Institute of Bioscience and Biotechnology, Daejeon, Republic of Korea*; [4]*Division of Oral & Systemic Health Sciences, School of Dentistry, University of California, Los Angeles, California, USA;* [5]*Department of Microbiology, Immunology & Molecular Genetics, University of California, Los Angeles, Los Angeles, CA, USA;* [6]*Department of Microbiology & Molecular Genetics, University of Texas McGovern Medical School, Houston, Texas, USA;* [7]*Department of Medicine, Neag Comprehensive Cancer Center, University of Connecticut Health Center, Farmington, CT, USA*

[1]To whom correspondence may be addressed; email htonthat@dentistry.ucla.edu

Running Title: Rnf-associated amyloid and tumor formation

Keywords: Rnf complex, metabolism, two-component system, amyloid, tumor, colorectal cancer

3.1 Abstract. The Gram-negative oral anaerobe *Fusobacterium nucleatum* is an oncobacterium that promotes carcinogenesis of colorectal cancer, and the amyloid-forming adhesin FadA is integral to this process. Previous studies suggest that the highly conserved *Rhodobacter* nitrogen-fixation (Rnf) complex modulates the virulence potential of this pathobiont via metabolic signaling; however, a mechanism for this modulation remains unknown. Here, we show that genetic disruption of the Rnf complex, via *rnfC* deletion, significantly reduced the transcript level of *fadA*, relative to the wildtype. This was accompanied with near complete abolition of the precursor form of FadA (pFadA) and reduced surface assembly of FadA at the mature cell pole. Noticeably, *rnfC* deletion caused a severe defect in osmotic stress-induced amyloid formation that was rescued by ectopic expression of *rnfC*. Gene deletion analysis identified three response regulators – CarR, ArlR, and S1 – that modulate expression of pFadA, without affecting its transcript level, suggesting that these response regulators control expression of factors that process FadA. Consistently, deletion of *rnfC*, *arlR*, and *s1* significantly reduced expression of the signal peptidase-encoding gene *lepB*, and CRISPR-induced depletion of *lepB* nearly abolished FadA expression. Importantly, while *rnfC* deletion did not affect the ability of mutant cells to adhere to cancer cells HCT116, *rnfC* deficiency significantly diminished fusobacterial invasion of HCT116. In line with the role of FadA in tumor formation, the *rnfC* mutant was markedly defective in promotion of spheroid tumors. Evidently, the Rnf complex modulates expression of FadA and formation of FadA-associated amyloids and tumors via regulation of LepB by multiple response regulators.

3.2 Importance. In the opportunistic pathogen *Fusobacterium nucleatum*, the *Rhodobacter* nitrogen-fixation (Rnf) complex plays an important role in the pathophysiology of this oral pathobiont, since genetic disruption of this conserved respiratory enzyme negatively impacts a wide range of metabolic pathways, as well as bacterial virulence in mice. Nonetheless, how Rnf deficiency weakens the virulence potential of *F. nucleatum* is not well understood. Here, we demonstrate that genetic disruption of the Rnf complex reduces surface assembly of adhesin

FadA and FadA-mediated amyloid formation, via regulation of signal peptidase LepB by multiple response regulators. As FadA is critical in the carcinogenesis of colorectal cancer (CRC), the Rnf-deficient mutant reduces its ability to invade CRC cells and promote spheroid tumor growth. Thus, this work uncovers a molecular linkage between the Rnf complex and gene regulation, likely via metabolic signaling, that maintains the virulence potential of this oncobacterium in various cellular niches.

3.3 Introduction. Originally discovered in the phototrophic bacterium *Rhodobacter capsulatus* and shown to fix nitrogen, hence named as Rnf for *Rhodobacter* nitrogen fixation (1), the Rnf complex is known to catalyze the oxidation of reduced ferredoxin and the reduction of NAD+, establishing an ion-motive force and permitting substrate import and ATP biosynthesis (1-4). This respiratory enzyme, comprised of 6 to 7 subunits, is highly conserved in Gram-positive and Gram-negative bacteria (4), with genes coding for the Rnf subunits clustered into an operon; for example, the *rnfABCDGEH* cluster of *R. capsulatus* (5), the *rnfABCDGE* of *Escherichia coli* (6), and the *rnfCDGEAB* cluster of *Clostridium tetani* and *Fusobacterium nucleatum* (7, 8). Although the role of the Rnf complex in energy conservation has been well documented (4, 9-11), its role in bacterial pathogenesis has begun to emerge. In the Gram-positive gut bacterium *Clostridium sporogenes*, a *rnfB* mutant is attenuated for growth in the mouse gut (12), and in the Gram-negative oral anaerobe *F. nucleatum*, a mutant devoid of *rnfC* reduces its virulence in a mouse model of preterm birth (8). It is noteworthy that although the fusobacterial *rnfC* mutant exhibits slow growth and cell morphological defects, its colony forming units (CFUs) are as similar as the parent strain (8), suggesting that the virulence attenuation of this mutant may not be due to reduced bacterial burden. While the role of the *C. sporogenes* Rnf complex in metabolism has been implicated in gut colonization (12), how genetic disruption of the Rnf complex affects *F. nucleatum* virulence remains unknown.

Considered as an opportunistic pathogen associated with adverse pregnancy outcomes (13, 14), *F. nucleatum* is an oncobacterium that has been linked to the promotion of colorectal cancer (CRC) (15-18). Among a few known adhesins, FadA plays a crucial role in fusobacterial pathogenesis. A mutant lacking *fadA* is defective in placental colonization and stimulation of CRC cell growth (18, 19). Through FadA and E-cadherin, *F. nucleatum* induces expression of Annexin A1 in cancerous cells, with Annexin A1 acting as a modulator of Wnt/ β-catenin signaling (20). FadA exists in two forms – the precursor full-length form (pFadA) of 129 residues and the secreted mature FadA (mFadA) missing its signal peptide (21). An active FadA complex (FadAc), comprised of mFadA and pFadA, is sufficient to promote CRC cell growth via FadA binding to E-cadherin on CRC cells (18). Under stress and disease conditions, FadA also forms surface amyloid-like structures – involving pFadA-assisted crosslinking of FadA filaments – that are critical for CRC progression in mice (22). Noticeably, secretion of FadA requires a Fap2-like autotransporter (22), with Fap2 previously shown to mediate fusobacterial binding to Gal-GalNAc, a biomarker that is abundantly expressed by adenocarcinomas (23).

RadD is another adhesin that has recently been shown to promote fusobacterial binding to CRC cells (24). Originally identified as the major coaggregation factor that mediates fusobacterial adherence to many oral bacteria (25, 26), RadD directly binds to CD147, a glycoprotein that is highly expressed on the surface of tumor cells, triggering a PI3K-AKT-NF-κB-MMP9 cascade to enhance tumorigenesis (24). This suggests that *F. nucleatum* may utilize multiple pathways to promote tumorigenesis and CRC progression. It is noteworthy that genetic disruption of the *F. nucleatum* Rnf complex, via *rnfC* deletion, abrogates fusobacterial binding to oral bacteria without interfering with surface expression of RadD (26). This proved to be due to global metabolic defects leading to accumulation of environmental lysine, which binds to RadD and inhibits RadD-mediated bacterial binding to oral bacteria (26). Intriguingly, *rnfC* deletion reduces expression of *megL*, coding for the L-methionine γ-lyase MegL that mediates

methionine/cysteine metabolism (27). Nonetheless, how genetic disruption of the Rnf complex affects gene expression in *F. nucleatum* remains to be investigated.

Here, we show that genetic disruption of the Rnf complex, via *rnfC* deletion, decreases surface expression of FadA and FadA-mediated amyloid formation under osmotic stress, via an indirect regulation by several response regulators. In fact, these regulators control the expression of the signal peptidase LepB that processes the precursor form of FadA. As FadA plays an important role of the carcinogenesis of CRC, inactivation of Rnf reduces fusobacterial ability to invade CRC cells and promote tumor growth. Our study presented here reveals a molecular linkage between the Rnf complex and gene regulation, likely via metabolic signaling, the modulates *F. nucleatum* virulence.

3.4 Results

3.4.1 Genetic disruption of the Rnf complex reduces surface expression of FadA and FadA-mediated amyloid formation. To further characterize the impact of Rnf-mediated metabolism on fusobacterial virulence, we examined the expression of FadA and Fap2, previously identified adhesins that play an important role in bacterial colonization and CRC promotion (14, 20, 23), since genetic disruption of the Rnf complex reduces expression of MegL (8). Protein samples from the equivalent whole-cell lysates of *F. nucleatum* strains were analyzed by western blotting with a polyclonal antibody against FadA (α-FadA) that detects both precursor (pFadA) and mature (mFadA) forms (28). Remarkably, deletion of *rnfC* (Δ*rnfC*) drastically reduced expression of pFadA, coupled with increased expression of mFadA as compared to the parent and complement strains (Fig. 1A). To examine whether the reduced expression of pFadA is due to the reduced expression of *fadA* transcripts, we obtained equivalent mRNA samples for quantitative reverse transcription polymerase chain reaction (qRT-PCR) analysis. Consistently, we found a 10-fold reduction of *fadA* expression in the Δ*rnfC* mutant, relative to the parent strain (Fig. 1B). Since

FadA is displayed on the bacterial cell surface (22), we probed for surface FadA by immunofluorescence microscopy (IFM), whereby normalized fusobacterial cells were first stained with α-FadA and then Alexa488-conjugated IgG, with DAPI staining the nucleus. Compared to the FadA signal of the parent strain, the FadA signal of Δ*rnfC* was significantly reduced, and this defect was rescued by ectopic expression of FadA (Fig. 1C & 1D). Furthermore, we observed distinct localization of surface FadA at the cell pole (Fig. 1C).

To uncover the spatiotemporal dynamics of FadA deposition on the fusobacterial cell surface, we employed fluorescently-tagged D-amino acids (FDAAs), which are covalently incorporated into the bacterial cell wall by endogenous transpeptidases without disrupting bacterial metabolism or cell growth; as such, these compounds are used to probe peptidoglycan biosynthesis (29, 30). Subsequently, fusobacterial cells were grown in the presence of HCC-amino-D-alanine (HADA) for 14 h prior to being treated with Rf470DL for 3 h. Fusobacteria were then fixed for staining with α-FadA and Alexa488-conjugated IgG (Fig. 1E). As shown in Fig. 1E, HADA labeled oldest peptidoglycan at the cell poles of two dividing cells, while Rf470DL marked newly synthesized peptidoglycan. Noticeably, the FadA signal was mainly observed at the old cell pole, although the signal was also observed along the cell envelope, albeit with much lower intensity (Fig. 1E).

Next, using the same set of samples above, we analyzed surface expression of the outer membrane protein Fap2 by immunoblotting with antibodies against Fap2 (α-Fap2), surprisingly revealing that expression of Fap2 significantly increased in the Δ*rnfC* mutant, relative to the parent and complement strains (Fig. 2A & 2B). Consistent with the western blot analysis, deletion of *rnfC* resulted in increased surface signal of Fap2 that appeared to be punctate (Fig. 2C & 2D).

Given that under stress conditions FadA forms amyloids on the cell surface that can be visualized by IFM using antibodies raised against human amyloid beta 42 (α-Aβ42) (22), we

performed a similar experiment and found that *F. nucleatum* grown in high salt concentrations (100 mM NaCl) produced markedly more FadA amyloids than cells grown without NaCl (Fig. 2A). Consistent with the above results (Fig. 1), formation of FadA amyloids was significantly reduced in the Δ*rnfC* mutant, as compared to the parent and complement strains (Fig. 3B & 3C). Together, the results indicate that genetic disruption of the RnfC complex, via *rnfC* deletion, causes reduction in the expression of *fadA* and FadA, which in turn reduces formation of surface FadA amyloids, while increasing expression of the outer membrane adhesin Fap2.

3.4.2 Expression of FadA is modulated by several response regulators of two-component systems.

We next investigated how genetic disruption of the Rnf complex affects *fadA*. Given that the response regulator CarR of the two-component system (TCS) CarRS regulates *megL* expression (26), we determined whether *fadA* is also transcriptionally regulated. By bioinformatics analysis, we identified 7 TCS's in *F. nucleatum* including ModRS, CarRS, and ArlRS (Table S1) (26, 31, 32). The response regulator CarR modulates a large regulon including *megL*, *radD*, and many lysine metabolic genes (26), whereas ModR regulates genes coding for factors involved in oxidative stress, metabolism, and many other processes (31). It is unclear about the regulon of ArlR, although its homolog in *Staphylococcus aureus* control expression of genes involved in adhesion, autolysis, and proteolysis (33). Others response regulators of *F. nucleatum* are predicted to be homologous to CheY, EutV, S1, and YdbB (Table S1). To examine whether these response regulators control expression of FadA, we generated corresponding non-polar, in-frame deletion mutants and analyzed protein and gene expression in these strains by western blotting and qRT-PCR, respectively. Among these response regulator mutants, the *carR* (Δ*carR*), *arlR* (Δ*arlR*), and *s1* (Δ*s1*) mutants displayed significant reduction of FadA expression (Fig. 4A & 4B). Intriguingly, these deletion mutants had no effect on the expression level of *fadA* transcripts (Fig. 4C), suggesting the response regulators CarR, ArlR, and S1 may play a role in post-translational modification of FadA via unknown factors.

3.4.3 Genetic disruption of the Rnf complex reduces expression of response regulator-encoding genes and signal peptidase *lepB*. We previously postulated that metabolic blockage by genetic disruption of the Rnf complex may trigger gene expression responses from the TCSs of *F. nucleatum* (8). To examine this possibility, we measured the transcript levels of these response regulators in the presence or absence of *rnfC* using qRT-PCR. Remarkably, mRNA expression of all seven response regulators was strongly reduced in the *rnfC* mutant as compared to the parent strain, and this reduction of gene expression was restored to the wild-type level by complementation of *rnfC* (Fig. 5A). Since FadA contains a signal peptide sequence (28), which may be cleaved by the signal peptidase LepB, we determined whether *rnf* deletion also affects *lepB* expression. Indeed, compared to the parent and rescued strains, the *rnfC* mutant expressed a reduced level of *lepB* (Fig. 5B). Because the response regulators CarR, ArlR, and S1 might modulate the expression of FadA without affecting its transcript level (Fig. 4), we examined by qRT-PCR whether these regulators control expression of *lepB*. As shown in Fig. 5C, although deletion of *carR* did not significantly reduce the *lepB* transcript level, deletion of *arlR* or *s1* decreased expression of *lepB*.

The results above suggest that LepB is the major signal peptidase that processes FadA. To examine if this is the case, we employed a recently developed gene-editing method for *F. nucleatum*, based on CRISPR (34), to conditionally inactivate *lepB* as *lepB* is essential in *F. nucleatum* (35). Remarkably, when the CRISPR system was induced, we observed multifold reduction of *lepB* (Fig. 5D), concomitant of near complete abolishment of FadA (Fig. 5E). Together, the results establish the molecular linkage between the Rnf complex and gene regulation that controls expression of the signal peptidase LepB, which in turn processes FadA post-translationally.

3.4.4 Genetic disruption of the Rnf complex reduces bacterial invasion of cancer cells and

tumor formation. As the FadA adhesin is critical for fusobacterial binding, invasion, and proliferation of CRC cells (18, 20), we reasoned that FadA reduced expression in the *rnfC* mutant might account for the reduced ability of this mutant to adhere, invade, and/or induce CRC tumor formation. To test this, we subjected *F. nucleatum* strains to adherence/invasion and spheroid formation assays as previously reported (31, 36). For adherence, CRC HCT116 cells were infected with fusobacteria at a multiplicity of infection (MOI) of 50 for 4 h and washed prior to cell lysis for enumeration of fusobacterial colony forming units (CFUs), whereas for invasion infected HCT116 cells were treated with gentamicin prior to washing and lysing for bacterial enumeration. Unexpectedly, deletion of *rnfC* did not affect fusobacterial adherence to CRC cells (Fig. 6A). In contrast, deletion of *rnfC* significantly reduced fusobacterial invasion of CRC cells, and the defect was rescued by ectopic expression of *rnfC* (Fig. 6B).

To determine if *rnfC* deletion affects CRC tumor development, we treated HCT116 cells with various fusobacterial strains at the MOI of 50 for 72 h before imaging and quantification of spheroids. Remarkably, HCT116 cells treated with the parent strain formed larger spheroids than HCT116 cells treated with the *rnfC* mutant, relative to the untreated samples (PBS) (Fig. 6C & 6D). Consistent with the role of FadA in tumor development, deletion of *fadA* reduced the ability of fusobacteria to form spheroids (Fig. 6C & 6D; Δ*fadA*). To examine the effect of Rnf on stimulating tumor growth, pre-grown HCT116 spheroids were infected with fusobacteria 48 h before imaging and quantification. Consistent with the above results, the Δ*rnfC* and Δ*fadA* mutants were defective in inducing spheroid formation (Fig. 6E & 6F). Together, the results demonstrate that the Rnf complex metabolically modulates expression of FadA and FadA-associated amyloid formation via two-component transduction systems.

3.5 Discussion. The human oral cavity is home to a rich diversity of microorganisms that encounter consistent changes in nutrient and redox availability depending on factors such as age, diet, health, and microbial composition. As such, metabolic flexibility is key to microbial fitness in

these environments (37). Once regarded as a harmless oral commensal, *F. nucleatum* is well-known for its ability to disseminate outside the oral cavity, via hematogenous or digestive routes, and colonize a wide variety of host tissues, potentiating several diseases, the most studied of which include preterm birth (14, 19, 38, 39) and colorectal cancer (17, 18, 22, 40). How *F. nucleatum* maintains metabolic plasticity to enhance its virulence capabilities despite encountering various metabolic landscapes is of current interest. We recently show *F. nucleatum* encodes a functional ferredoxin:NAD^+ oxidoreductase termed the Rhodobacter nitrogen-fixation (Rnf) complex, which acts as a versatile metabolic exchange center to conserve energy via the production of a ion-motive force (IMF) from the oxidation of multiple amino acids (Lys, His, Glu, Gln, Met, Cys). As a result, the Rnf complex expands the redox range of this anaerobic, pluritropic pathogen, metabolically stimulating a multitude of pathophysiological traits outside the oral cavity to promote preterm birth in a mouse model of infection (8).

To decipher a mechanism for how defects in Rnf-mediated metabolism negatively impact fusobacterial virulence, we sought to examine the expression of multiple outer membrane adhesins associated with fusobacterial placental colonization and colorectal carcinogenesis. The highly virulent fusobacterial adhesin A (FadA) mediates *F. nucleatum* colonic colonization and drives tumorigenesis via formation of a trimeric complex with E-cadherin and Annexin A1, the latter of which was recently discovered to modulate Wnt/β-catenin signaling in colorectal cancer cells (20). At the same time, FadA-mediated *F. nucleatum* internalization promotes inflammation through NF-κβ signaling (18), contributing to ulcerative colitis (41, 42) and autoimmune disorders (43). Here, we have discovered that loss of Rnf via deletion of *rnfC* abolishes expression of FadA and FadA-associated amyloid accompanied by global reductions in the expression of several two-component system (TCS) response regulators responsible for expression of the LepB signal peptidase required for FadA post-translational processing. Consequently, *rnfC* mutants are drastically inept at invading colorectal cancer cells and inducing tumor formation (Fig. 1 – Fig. 6).

FadA exists in two forms, a full-length, signal peptide-containing pre-FadA (pFadA) form consisting of 129 amino acids that anchors secreted mature FadA (mFadA) monomers, which do not contain the 18-amino acid signal peptide, to the inner membrane (28). Together, pFadA and mFadA form a functional complex, FadAc, that exists as membrane-bound extracellular α-helical filaments, comprised of repeating mFadA monomers linked in a head-to-tail manner via a novel structural motif, the leucine chain (44). Shockingly, deletion of *rnfC* abrogates pFadA production (Fig. 1A), as well as *fadA* mRNA transcript expression (Fig. 1B). As pFadA regulates filament length and width and is required for the formation of a functional complex (28, 45), we assessed the expression of FadA on the fusobacterial outer membrane using immunofluorescence microscopy (IFM), which confirmed deletion of *rnfC* significantly hinders expression of FadA on the fusobacterial cell surface (Fig. 1C & 1D). Interestingly, FadA seemed to localize primarily to the fusobacterial cell tip, a phenotype not observed in other studies (19), and sequential labeling using fluorescently-tagged D-amino acids revealed FadA is increasingly deposited at the mature cell pole (Fig. 1E). These data align with previous reports that FadA expression increases in stationary-phase cells as they encounter nutrient-limiting conditions (22), and may explain why FadA is largely absent from newly-formed cell envelopes. Monopolar localization of FadA could also aid in host cell invasion, which was previously shown to require pFadA (28). Intriguingly, previous studies have noted the galactose-inhibitable adhesin, Fap2, may be necessary for FadA secretion (22). However, counter to our expectations, Fap2 expression was significantly increased in Δ*rnfC* mutants (Fig. 2), suggesting defects in *fadA* expression among *rnfC* mutants may instead be due to aberrant post-translational processing of FadA.

In both nutrient-limiting and disease conditions, *F.* nucleatum secretes ‘amyloid-like’ FadA which serves as a scaffold for biofilm formation, host cell binding, and promotes acid tolerance (22). Implicated in several human cognitive disorders, including dementia and Alzheimer’s, amyloid are aggregates of proteins with a fibrillar morphology and cross-β-sheet secondary

structure (46). The term, ‘amyloid-like’, is reserved for a subset of structures lacking cross-β-sheets, yet harbor similar biochemical properties of amyloid, including fiber formation, the ability to resist ionic detergents, and be stained with dyes such as thioflavin T or antibodies against human amyloid beta 42 (α-Aβ42) (22). Taking the latter approach, we confirmed the formation of fusobacterial FadA-associated amyloid-like protein aggregates under high salt conditions (Fig. 2A), mimicking osmotic stress found in the human bloodstream and proximal colon, where a bulk of electrolytes are absorbed (47, 48). Furthermore, deletion of *rnfC* abrogated FadA-mediated amyloid formation (Fig. 2B-2C), confirming the Rnf complex metabolically drives FadA-amyloid production, likely useful for host cell binding and promoting tolerance to bile acids found abundantly in the human digestive tract (49, 50).

Bioinformatic analysis revealed *F. nucleatum* ATCC 23726 encodes seven TCSs (Table S1), some of which regulate the expression of notable adhesins such as RadD and Fap2, as well as many metabolic enzymes (MegL, KamA), and have been shown to promote extra-oral disease in mouse models of infection (26, 31). To decipher the mechanism by which *rnfC* genetic disruption negatively impacts FadA production, we generated in-frame genetic deletion mutants of all seven response regulators and probed for FadA expression by western blot. Amazingly, multiple response regulator mutants, including Δ*carR*, Δ*arlR*, Δ*s1*, had significantly less pFadA (Fig. 4A & 3B), as observed with Δ*rnfC* cells (Fig. 1A). However, these response regulators had little-to-no effect on *fadA* transcript abundance (Fig. 3C), suggesting FadA post-translational processing is regulated synergistically via several fusobacterial two component regulatory systems.

In line with these findings, *rnfC*-deletion strongly reduced transcript expression of all seven response regulators (Fig. 5A), highlighting the importance of fusobacterial amino acid fermentation for the activation of two-component system signaling. As FadA contains a signal peptide and is thus cleaved by a signal peptidase, we probed for the transcript expression of the

major fusobacterial signal peptidase, *lepB*, in Δ*rnfC* cells (Fig. 5B). Compared to the parent or the RnfC complement, these mutants (Δ*rnfC*) had nearly 10-fold less *lepB* transcript, and examination of *lepB* expression in Δ*carR*, Δ*arlR*, and Δ*s1* mutants revealed multiple fusobacterial TCSs regulate this major signal peptidase (Fig. 5C). As previous efforts to delete *lepB* failed, indicating its essentiality to fusobacterial survival, we employed a conditional CRISPR interference system to deplete *lepB* (Fig. 5D) and measured the expression of FadA by western blot (Fig. 5E). While uninduced cultures had had less FadA, which may be due to leaky promoter activity, depletion of *lepB* with theophylline caused a near-complete abolishment of FadA, indicating LepB is required for processing FadA, defects in which may lead to FadA protein degradation due to an inability to transport pFadA across the fusobacterial inner membrane. Together, these data suggest fusobacterial amino acid catabolism is required for the production of an as of yet unidentified signal necessary for TCS activation and synergistic regulation of LepB-mediated FadA processing. It is worth noting no genes encoding quorum-sensing proteins, such as LuxI or LuxS, exist in *F. nucleatum* (51), despite characterization of autoinducer-2 (AI-2) production and its role in *Fn* biofilm formation (52, 53) and colorectal cancer (54). AI-2 is produced from methionine degradation into S-adenosyl-L-homocysteine (SAH), which is further detoxified into adenine and the substrate for LuxS-catalyzed AI-2 biosynthesis, S-ribosyl-L-homocysteine (SRH) (55). Interestingly, previous metabolic screening of Δ*rnfC* mutant cells revealed significantly less methionine, adenine, and SAH intermediates compared to the parent strain (8). It is therefore tempting to speculate *rnfC*-deletion reduces production of autoinducer-2, which in turn may account for global TCS inactivation. Additional characterization of AI-1 and AI-2 synthases in *F. nucleatum*, as well as the potential role for autoinducers to activate fusobacterial two-component system signaling is warranted.

As FadA is a prominent adhesin required for fusobacterial colorectal colonization, invasion, and enhancement of CRC (14, 18, 19, 28, 56), we examined the ability for mutant fusobacteria deficient in Rnf-metabolism via deletion of *rnfC* to invade and stimulate tumor

formation of human colorectal cancer cells, HCT116, in vitro. Unexpectedly, *rnfC*-deletion had no noticeable impact on colorectal cancer cell adhesion (Fig. 6A), suggesting Fap2- and RadD-binding to Gal-GalNAc- and CD147-expressing CRC cells, respectively, is sufficient for fusobacterial colonization (24, 56). Nevertheless, this mutant (Δ*rnfC*) was severely attenuated in CRC cell invasion (Fig. 6B). As the signal peptide-containing pFadA form is required for fusobacterial stimulation of CRC cell growth (18), we developed a procedure to monitor HCT116 spheroid formation in vitro as a model for colorectal tumor formation. Spheroids are spontaneous 3D aggregates of proliferating, necrotic, and quiescent cells first introduced in the 1970's (57). Since then, spheroids have been used to model and study a number of pathologies (58-60), including the role of E-cadherin in cancer progression (61). Astonishingly, Δ*rnfC* mutant cells were largely unable to induce formation of HCT116 spheroids in vitro (Fig. 6C – Fig. 6D), nor could these mutants promote growth of pre-formed spheroids (Fig. 6E – Fig. 6F). In conclusion, the Rnf complex expands the metabolic versatility of *F. nucleatum* through its role in amino acid metabolism, driving two-component system signaling required for LepB-mediated FadA expression. As such, deletion of *rnfC* greatly hinders fusobacterial colorectal cancer cell invasion and tumor formation, as shown in our working model (Fig. 7). Given the high conservation of Rnf in many anaerobic bacterial pathogens, and its absence from eukaryotes, this ancient respiratory enzyme serves as an attractive drug target to treat *Fn*-related malignancies.

3.6 Materials and methods

3.6.1 Bacterial strains, plasmids, and media. All bacterial strains and plasmids used in this study are listed in *Supplemental Material (SM)* Table S2. *F. nucleatum* strains were grown in tryptic soy broth supplemented with 1% Bacto Peptone and 0.25% fresh L-cysteine (TSPC) or on TSPC agar plates at 37°C in an anaerobic chamber as previous described (8). *Escherichia coli* strains were grown in Luria Broth (LB) at 37°C. When required, chloramphenicol, thiamphenicol, or

penicillin G were added to the medium at a concentration of 15 μg/mL, 5 μg/mL, or 10 μg/mL, respectively. All reagents were purchased from Sigma-Aldrich unless noted otherwise.

3.6.2 Plasmid construction. (i) pMCSG7-based plasmids: pMCSG7 was used to clone vectors expressing recombinant proteins FadA, CarR, and Fap2 for antibody production, and vectors pMCSG7-FadA, pMCSG7-CarR, and pMCSG7-Fap2 were created with the primer sets using ligation-independent cloning (LIC) as previously reported (62). Briefly, a pair of primers (LIC-FadA-F/R, LIC-CarR-F/R, or LIC-Fap2-F/R listed in *SM* Table S3) was used to amplify part of coding sequences of *fadA* (corresponding residues 48-129), *carR* (residues 2-224), and *fap2* (residues 3401-3786) from the chromosomal DNA of *F. nucleatum* ATCC 23726. Generated amplicons were inserted into pMCSG7, and the resulting plasmids were introduced into *E. coli* DH5α for propagation and verification by DNA-sequencing. Verified clones were then introduced into *E. coli* BL21 (DE3) for protein expression.

(ii) pRnfC: The primer pair com-rnfC-F/R (Table S3) was used to amplify the *rnfC* coding region and its promoter from *F. nucleatum* ATCC 23726 chromosomal DNA. KpnI and NdeI restriction sites were appended to the amplicon, and the PCR product was digested and cloned into pCWU6 as previously described (63). The generated vector was subjected to DNA sequencing for confirmation.

(iii) Gene deletion plasmids: pCM-GalK (Table S2) was used to generate vectors for deletion of *fadA*, *arlR*, *cheY*, *eutV*, *s1*, and *ypdB* according to a published protocol (27). Briefly, 1-kb flanking regions upstream and downstream of individual genes of interest were PCR amplified using a specific set of primers (Table S3), and the PCR products were cloned into pCM-GalK. The generated vectors were subjected to DNA sequencing for confirmation.

3.6.3 Gene deletion in *F. nucleatum*. Using the generated gene deletion plasmids mentioned above (see Table S2), non-polar, in-frame deletion mutants, Δ*fadA*, Δ*arlR*, Δ*cheY*, Δ*ypdB,* Δ*eutV,* and Δs1, were generated as previously described (8, 26, 63).

3.6.4 Depletion of *F. nucleatum lepB* by CRISPRi. The CRISPRi-based plasmid pZP4C (34) was used to generate pZP4C-lepB (Table S2). For PCR amplification of a single guide RNA (sgRNA) that targets *lepB* (RS05265), primers, Sg-lepB_F and Sg-RNA-R (Table S3), were used with *F. nucleatum* ATCC 23726 chromosomal DNA as template. The generated sgRNA cassette was cloned into pZP4C between MscI and NotI restriction sites. The generated vector was transformed into *E. coli* DH5α for DNA amplification and verification prior to being introduced into ATCC 23726 by electroporation. Transformants were selected on TSPC agar plates containing thiamphenicol (5 μg/ml). Overnight cultures of obtained colonies anaerobically grown in TSPC broth supplemented with thiamphenicol at 37^{o}C were used to inoculate fresh cultures with a starting optical density at 600 nm (OD_{600}) of 0.1 in the presence or absence of 2mM theophylline. The resulting cultures were grown in an anaerobic chamber for 18 h prior to being normalized to an OD_{600} of 1.0 for western blotting analysis.

3.6.5 Western blotting. Expression of fusobacterial proteins were analyzed by immunoblotting with antibodies against FadA (α-FadA; 1:8000), CarR (α-CarR; 1:5000), and Fap2 (α-Fap2; 1:4000). The antibodies were generated using *E. coli* BL21 (DE3) strains harboring pMCSG7-FadA, pMCSG7-CarR, or pMCSG7-Fap2 (mentioned above) as previously described (27, 64). Briefly, cell-free lysates obtained from *E. coli* cell cultures were subjected to protein purification by affinity chromatography. The purified proteins were used for antibody production (Cocalico Biologicals, Inc.). To perform immunoblots, overnight (~17 h) fusobacterial cultures were harvested and normalized by OD_{600}. 1 ml-aliquots of normalized cultures were subjected to protein precipitation by trichloroacetic acid (TCA), followed by acetone wash as previously described (63). Protein samples were suspended SDS-containing sample buffer with 6M urea, separated by SDS-

PAGE using a 4-15% Tris-Glycine gradient gel (Nacalai USA, Inc.), and immunoblotted with specific antibodies. When indicated, band intensity was calculated using ImageJ.

3.6.6 qRT-PCR. Fusobacterial strains were cultured overnight (~17 h) and normalized to OD_{600} of ~2.0. Normalized cells harvested by centrifugation were used to extract total RNA using the RNeasy Mini Kit (Qiagen) according to manufacturer's instructions and as previously described (8, 27). Approximately 1 µg of purified RNA, free from DNA by treatment with DNase I (Qiagen), was reverse transcribed into cDNA using iScript RT supermix (Bio-Rad) according to the manufacturer's protocol. Obtained cDNA was used for qRT-PCR with appropriate primers (Table S3) and SYBR Green PCR Master Mix (Bio-Rad). The $\Delta\Delta C_T$ method was used to calculate fold changes in gene expression between samples. Briefly, $\Delta\Delta C_T = \Delta C_{T1} - \Delta C_{T2,}$ where $\Delta C_T = C_T$(target) - C_T(housekeeping gene). The *16S* rRNA gene was used as a reference and reactions without reverse transcriptase used as a control to assess genomic DNA contamination.

3.6.7 Immunofluorescence microcopy. Immunofluorescence microscopy was performed as previously described (8). Circular glass coverslips were placed in a 24-well plate and 0.2 mL aliquots of poly-L-lysine were used to coat the surface for 15 min before washing with sterile water and air-drying for 2 h. Fusobacterial cells grown overnight (~17 h) with or without 100 mM sodium chloride (NaCl) were harvested by centrifugation and washed twice before being normalized to OD_{600} of ~ 0.3. Aliquots (~0.2 mL) of resulting cell suspensions were used to coat the surface of poly-L-lysine-treated glass coverslips and incubated at room temperature for 20 min. Cells were fixed using 2.5% formaldehyde (in PBS) for 20 min, washed with PBS, and blocked for 1 h with 3% wt/vol bovine serum albumin (FadA, Fap2) or 5% skim milk (amyloid), both diluted in PBS supplemented with tween-20 (PBST). Cells were incubated with α-FadA (1:300), α-Fap2 (1:200), or α-Aβ42 (1:500) for 1 h and then AlexaFluor488- (FadA, Fap2) or AlexaFluor594-conjugated (amyloid) goat anti-rabbit IgG (1:200) for another hour in the dark, followed by washing in PBS three times. Coverslips were mounted on glass slides with VECTASHIELD anti-fade mounting

medium containing DAPI (Vector Laboratories, Inc.). Images were taken using a fluorescence microscope (Keyence BZ-X800) and fluorescent units normalized and quantified using ImageJ.

For cell labeling with fluorescently-tagged D-amino acids (FDAAs), the experiment was performed as previously described (29, 65), with some modification. Briefly, overnight cultures of fusobacterial strains were used to inoculate fresh cultures normalized to OD_{600} of 0.05 in TSPC containing 0.5 mM HADA (Bio-Techne). Cells were grown for 14 h, harvested by centrifugation, washed in PBS, and inoculated in fresh cultures normalized to OD_{600} of 0.3 in TSPC containing 0.5 mM Rf470DL (Bio-Techne). Cells were grown for 3 h before being washed twice in PBS. The resulting cell suspensions were used for labeling with α-FadA and AlexaFluor488 as described above.

3.6.8 Adherence and invasion of colorectal cancer cells. Adherence and invasion assays were performed as previously described (31), with minor modifications. Human colorectal cancer cells, HCT116 (American Type Culture Collection), were grown in Dulbecco's modification of Eagle's medium (DMEM) supplemented with 10% FBS and 1% penicillin G in 24-well tissue culture-treated plates. HCT116 cells cultured to 80% confluency were washed with DMEM supplemented with 10% FBS to remove penicillin G and infected at an MOI (multiplicity of infection) of 50 with indicated fusobacterial strains grown to mid-exponential phase in TSPC. For adherence, fusobacteria were allowed to adhere HCT116 colorectal cancer cells for 4 h before gently washing twice with PBS to remove unattached fusobacterial cells. For invasion, a similar procedure was employed, except that after 3 h of infection, HCT116 colorectal cancer cells were treated with PBS supplemented with gentamicin (200 μg/mL) for 1 h to kill all extracellular fusobacteria, followed by washing twice in PBS. To enumerate fusobacterial cells, HCT116 cells were lysed in distilled water for 10 min, followed by serial dilution on TSPC plates for CFU counts.

3.6.9 Formation and growth of CRC spheroid tumors. HCT116 cells were grown in DMEM supplemented with 10% FBS and 1% penicillin G to 80% confluency and seeded into 24-well ultra-low attachment plates. For spheroid formation, HCT116 cells were immediately infected with fusobacterial strains grown to mid-exponential phase at an MOI of 50 for 72 h. For measurement of spheroid growth, mammalian cells were allowed to grow for 24 h before challenging with fusobacterial strains grown to mid-exponential phase at an MOI of 50 for 48 h. Resulting spheroids were imaged using phase-contrast microscopy and their surface area quantified using ImageJ.

Acknowledgements

We thank our lab members for their discussion and critical review of the manuscript. Research reported in this publication was supported by the National Institute of Dental & Craniofacial Research (NIDCR) of the National Institutes of Health (NIH) under Award Number DE026758 (to H.T.-T). T.A.B. was supported by the UCLA Dentist-Scientist and Oral Health-Researcher Training Program, NIDCR Grant T90DE030860, and the UCLA Eugene V. Cota Robles fellowship. The content is solely the responsibility of the authors and does not necessarily represent the official views of the NIH.

Author contributions

T.A.B. and H.T.-T. designed research; T.A.B., J.H.L., C.C., Wu C, B.A.H., and R.M.A., performed research; T.A.B. H.T.-T. analyzed data; and T.A.B. and H.T.-T. wrote the paper.

Declaration of interests

The authors declare no competing interests.

3.7 Figures

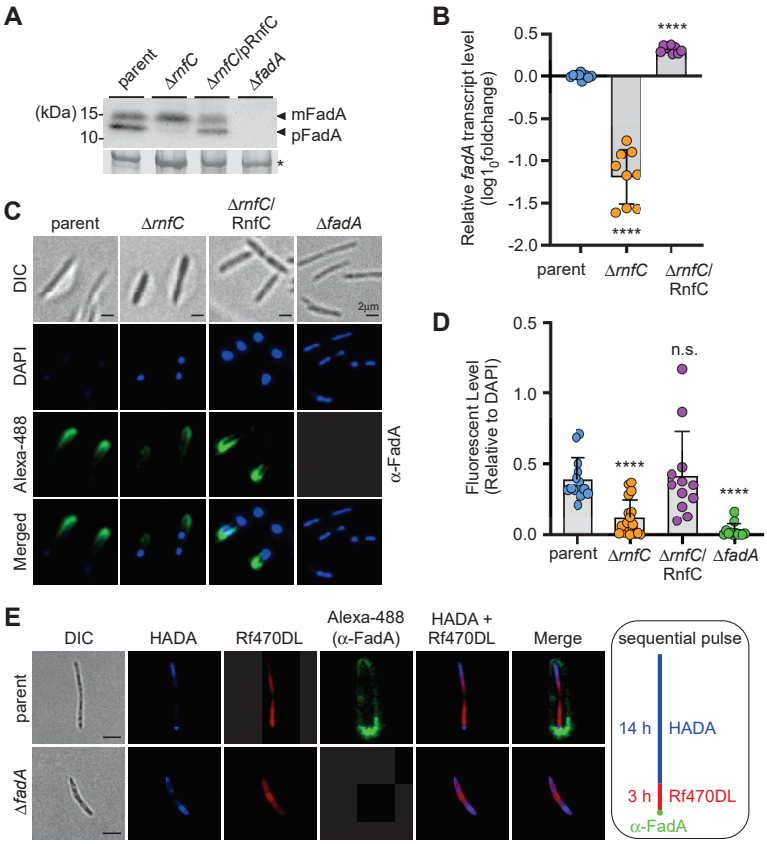

Figure 1: Genetic disruption of the Rnf complex, via *rnfC* deletion, reduces expression of FadA. (A) Protein samples obtained from whole-cell lysates of normalized cultures from indicated fusobacterial strains were subjected to immunoblotting with antibodies against FadA (α-FadA). Black arrows mark the precursor form of FadA (pFadA) and mature FadA (mFadA), with a Coomassie Blue stained band (*) used as a loading control. (B) Normalized overnight cultures of indicated strains were used to isolate total RNA for qRT-PCR to determine the transcript levels of fadA. All qRT-PCR data was normalized by *16s* rRNA transcript abundance for each sample. (C) Overnight cultures of indicated strains were first stained with α-FadA, followed by Alexa488-conjugated secondary antibodies (green), as well as DAPI (blue). Surface localization of FadA was visualized by a fluorescence microscope, and representative images are shown. (D) FadA signal relative to DAPI signal from indicated strains shown in panel C was quantified and presented. (E) Cells of parent and Δ*fadA* mutant strains grown to log-phase were harvested and sequentially labeled with fluorescent dyes HADA and Rf470DL for 14 h and 3 h, respectively, followed by labeling with α-FadA and Alexa488 as described in panel C. Samples were analyzed by fluorescence microscopy. All results were obtained from three independent experiments performed in triplicate. Significance was calculated by a Student's t-test; **** $P < 0.0001$.

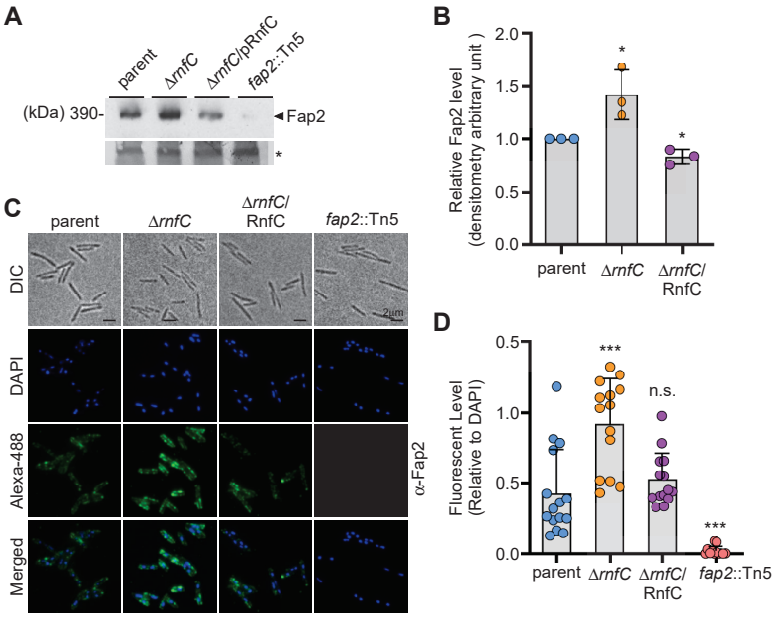

Figure 2: Deletion of *rnfC* increases expression of Fap2. (A) Protein samples obtained from whole-cell lysates of normalized cultures from indicated strains grown overnight were subjected to immunoblotting with antibodies against Fap2 (α-Fap2), with a Coomassie Blue stained band (*) used as a loading control. (B) Fap2 signal of indicated strains from three independent experiments in panel A was quantified by densitometry. (C) Overnight cultures of indicated strains were stained with α-Fap2, followed by Alexa488-conjugated secondary antibodies (green), as well as DAPI (blue). Surface localization of Fap2 was visualized by a fluorescence microscope. (D) Fap2 signal, relative to DAPI signal from indicated strains in panel C, was quantified by ImageJ. All results were obtained from three independent experiments performed in triplicate. Significance was calculated by a Student's t-test; * $P \leq 0.05$; ** $P < 0.01$.

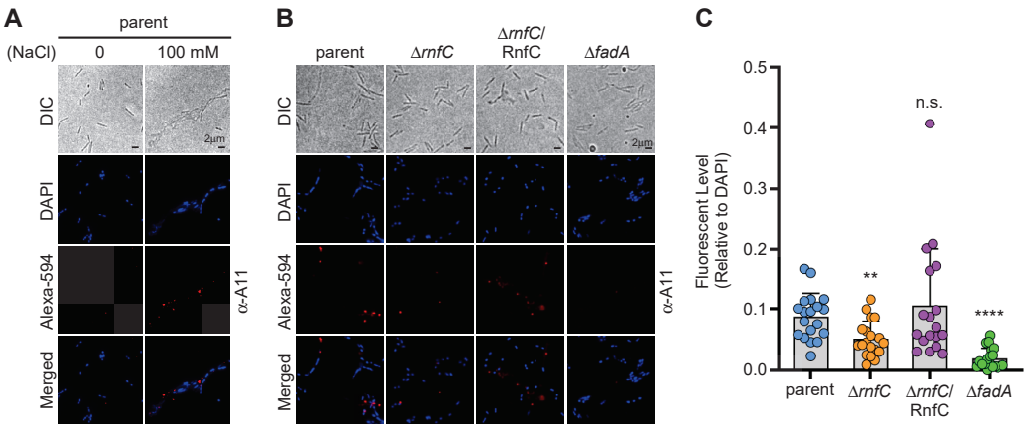

Figure 3: Genetic disruption of the Rnf complex reduces formation of FadA-mediated amyloids. (A) Parental cells grown overnight in the presence or absence of 100 mM NaCl were harvested for immunofluorescence microscopy. Cells were first stained with antibodies against human amyloid beta 42 (α-A11), followed by staining with Alexa594-conjugated secondary antibodies (red), as well as DAPI (blue), prior to microscopic analysis. (B-C) A similar experimental procedure was performed with the indicated strains. Quantification of amyloid signal, via Alexa594, relative to DAPI signal in these strains is shown in panel C. All results were obtained from three independent experiments performed in triplicate. Significance was calculated by a Student's t-test; **, $P < 0.01$ and ****, $P < 0.0001$.

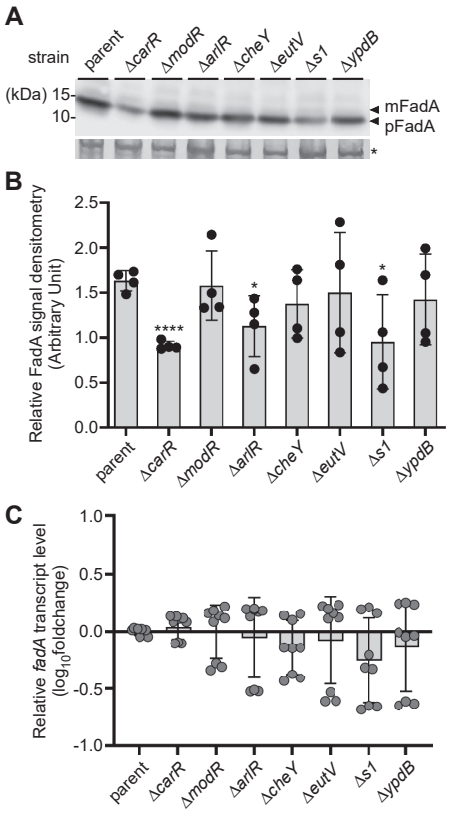

Figure 4: Expression of FadA is modulated by several response regulators of fusobacterial two-component systems. (A) Protein samples obtained from whole-cell lysates of normalized overnight cultures of indicated strains were subjected to immunoblotting with antibodies against α-FadA. Arrows mark pFadA and mFadA, with a Coomassie Blue stained band (*) used as a loading control. (B) FadA signal of strains in panel A was quantified from three independent experiments by densitometry. (C) Normalized overnight cultures of indicated strains were used to isolate total RNA for qRT-PCR to determine the expression level of *fadA*, with *16s* rRNA transcript abundance used as control. All data was obtained from three independent experiments performed in triplicate. Significance was calculated by a Student's t-test; *, $P \leq 0.05$ and ****, $P < 0.0001$.

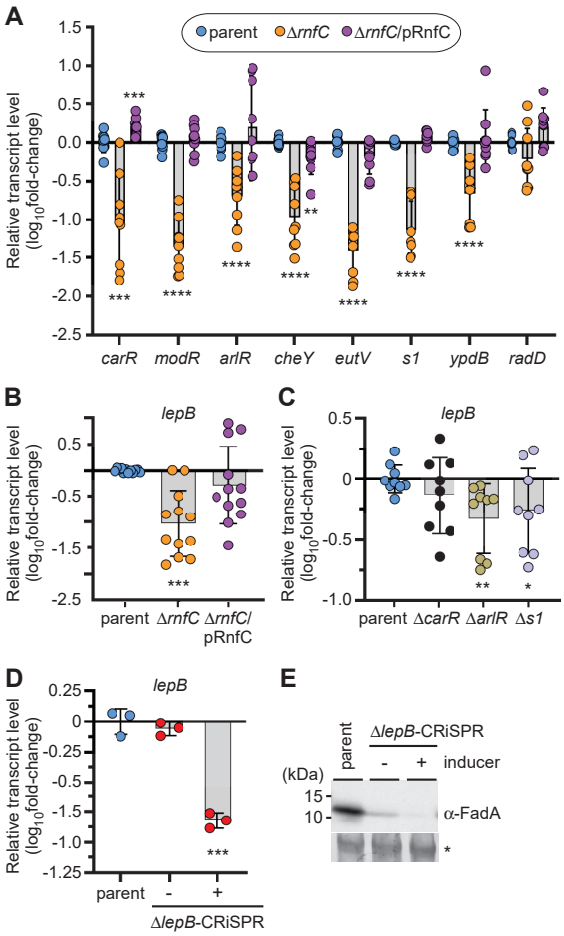

Figure 5: The Rnf complex modulates LepB-regulated cleavage of FadA. (A-C) Equivalent overnight cultures of indicated strains were used to isolate total RNA for qRT-PCR to determine the expression levels of *carR*, *modR*, *arlR*, *cheY*, *eutV*, *s1*, *ypdB*, and *radD* (panel A), as well as *lepB* (panels B-C), with *16s* rRNA used as control. (D-E) The parent and CRISPRi strains were grown overnight in the presence (+) or absence (-) of 2 mM theophylline (inducer). Normalized cells were harvested for RNA extraction and qRT-PCR, with 16s rRNA used as control (panel E). In a parallel experiment, normalized cells were used for preparation of whole-cell lysates for immunoblotting with α-FadA. A Coomassie Blue stained band (*) was used as a loading control (panel E). All data was obtained from three independent experiments performed in triplicate. Significance was calculated by a Student's t-test; * P < 0.05; ** P < 0.01; *** P < 0.001; **** P < 0.0001.

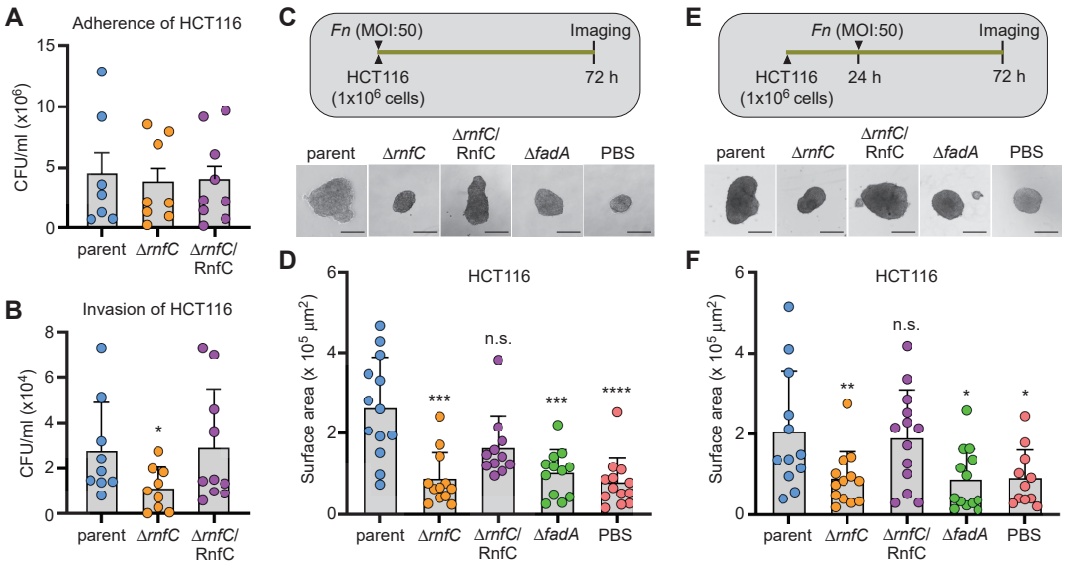

Figure 6: Genetic disruption of the Rnf complex reduces bacterial invasion of cancer cells and tumor formation. (A) HCT116 cells were infected with indicated fusobacterial strains at an MOI of 50 for 4 h before being washed off unadhered bacteria and lysed for bacterial enumeration as colony forming units per mL (CFU/mL). (B) A similar procedure as A was performed, except that HCT16 cells were treated with 200 μg/mL gentamycin before lysis for bacterial enumeration. (C-D) HCT116 cells were infected with indicated strains at an MOI of 50 for 72 h, with PBS used as control, and the resulting spheroids were microscopically analyzed (panel C) and quantified (panel D). (E-F) HCT116 cells were allowed to form spheroids for 24 h and treated with indicated strains at an MOI of 50. The resulting spheroids were microscopically analyzed (panel E) and quantified (panel F). All results were obtained from three independent experiments performed in triplicate. Significance was calculated by a Student's t-test; * $P \leq 0.05$; ** $P < 0.01$; *** $P < 0.001$; **** $P < 0.0001$.

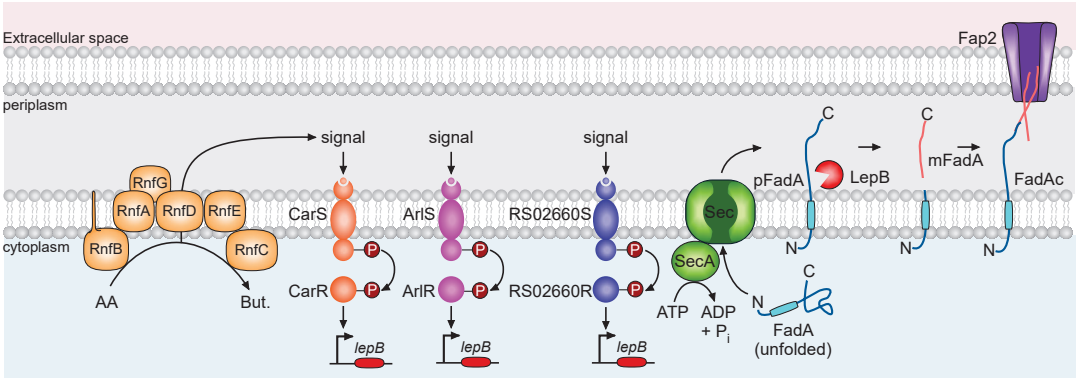

Figure 7: A working model of Rnf-mediated virulence through the FadA adhesin in *F. nucleatum.* See text for details.

3.8 References

1. **Schmehl M, et al.** 1993. Identification of a new class of nitrogen fixation genes in Rhodobacter capsulatus: a putative membrane complex involved in electron transport to nitrogenase. Mol Gen Genet 241:602-15.
2. **Reyes-Prieto A, et al.** 2014. Origin and evolution of the sodium -pumping NADH: ubiquinone oxidoreductase. PLoS One 9:e96696.
3. **Biegel E, Muller V.** 2010. Bacterial Na+-translocating ferredoxin:NAD+ oxidoreductase. Proc Natl Acad Sci U S A 107:18138-42.
4. **Biegel E, et al.** 2011. Biochemistry, evolution and physiological function of the Rnf complex, a novel ion-motive electron transport complex in prokaryotes. Cell Mol Life Sci 68:613-34.
5. **Jouanneau Y, et al.** 1998. Overexpression in Escherichia coli of the rnf genes from Rhodobacter capsulatus--characterization of two membrane-bound iron-sulfur proteins. Eur J Biochem 251:54-64.
6. **Koo MS, et al.** 2003. A reducing system of the superoxide sensor SoxR in Escherichia coli. EMBO J 22:2614-22.
7. **Bruggemann H, et al.** 2003. The genome sequence of Clostridium tetani, the causative agent of tetanus disease. Proc Natl Acad Sci U S A 100:1316-21.
8. **Britton TA, et al.** 2024. The respiratory enzyme complex Rnf is vital for metabolic adaptation and virulence in Fusobacterium nucleatum. mBio 15:e0175123.
9. **Schmidt S, et al.** 2009. The ins and outs of Na(+) bioenergetics in Acetobacterium woodii. Biochim Biophys Acta 1787:691-6.
10. **Buckel W, Thauer RK.** 2013. Energy conservation via electron bifurcating ferredoxin reduction and proton/Na(+) translocating ferredoxin oxidation. Biochim Biophys Acta 1827:94-113.

11. **Rosenbaum FP, Muller V.** 2021. Energy conservation under extreme energy limitation: the role of cytochromes and quinones in acetogenic bacteria. Extremophiles 25:413-424.

12. **Liu Y, et al.** 2022. Clostridium sporogenes uses reductive Stickland metabolism in the gut to generate ATP and produce circulating metabolites. Nat Microbiol 7:695-706.

13. **Han YW.** 2015. Fusobacterium nucleatum: a commensal-turned pathogen. Curr Opin Microbiol 23:141-7.

14. **Han YW, et al.** 2004. Fusobacterium nucleatum induces premature and term stillbirths in pregnant mice: implication of oral bacteria in preterm birth. Infect Immun 72:2272-9.

15. **Brennan CA, Garrett WS.** 2019. Fusobacterium nucleatum - symbiont, opportunist and oncobacterium. Nat Rev Microbiol 17:156-166.

16. **Kostic AD, et al.** 2012. Genomic analysis identifies association of Fusobacterium with colorectal carcinoma. Genome Res 22:292-8.

17. **Kostic AD, et al.** 2013. Fusobacterium nucleatum potentiates intestinal tumorigenesis and modulates the tumor-immune microenvironment. Cell Host Microbe 14:207-15.

18. **Rubinstein MR, et al.** 2013. Fusobacterium nucleatum promotes colorectal carcinogenesis by modulating E-cadherin/beta-catenin signaling via its FadA adhesin. Cell Host Microbe 14:195-206.

19. **Ikegami A, et al.** 2009. Complementation of the fadA mutation in Fusobacterium nucleatum demonstrates that the surface-exposed adhesin promotes cellular invasion and placental colonization. Infect Immun 77:3075-9.

20. **Rubinstein MR, et al.** 2019. Fusobacterium nucleatum promotes colorectal cancer by inducing Wnt/beta-catenin modulator Annexin A1. EMBO Rep doi:10.15252/embr.201847638.

21. **Han YW, et al.** 2005. Identification and characterization of a novel adhesin unique to oral fusobacteria. J Bacteriol 187:5330-40.

22. **Meng Q, et al.** 2021. Fusobacterium nucleatum secretes amyloid-like FadA to enhance pathogenicity. EMBO Rep 22:e52891.

23. **Abed J, et al.** 2016. Fap2 Mediates Fusobacterium nucleatum Colorectal Adenocarcinoma Enrichment by Binding to Tumor-Expressed Gal-GalNAc. Cell Host Microbe 20:215-25.

24. **Zhang L, et al.** 2024. The adhesin RadD enhances Fusobacterium nucleatum tumour colonization and colorectal carcinogenesis. Nat Microbiol 9:2292-2307.

25. **Kaplan CW, et al.** 2009. The Fusobacterium nucleatum outer membrane protein RadD is an arginine-inhibitable adhesin required for inter-species adherence and the structured architecture of multispecies biofilm. Mol Microbiol 71:35-47.

26. **Wu C, et al.** 2021. Genetic and molecular determinants of polymicrobial interactions in Fusobacterium nucleatum. Proc Natl Acad Sci U S A 118.

27. **Chen YW, et al.** 2022. Genetic Determinants of Hydrogen Sulfide Biosynthesis in Fusobacterium nucleatum Are Required for Bacterial Fitness, Antibiotic Sensitivity, and Virulence. mBio 13:e0193622.

28. **Xu M, et al.** 2007. FadA from Fusobacterium nucleatum utilizes both secreted and nonsecreted forms for functional oligomerization for attachment and invasion of host cells. J Biol Chem 282:25000-9.

29. **Kuru E, et al.** 2012. In Situ probing of newly synthesized peptidoglycan in live bacteria with fluorescent D-amino acids. Angew Chem Int Ed Engl 51:12519-23.

30. **Kuru E, et al.** 2019. Mechanisms of Incorporation for D-Amino Acid Probes That Target Peptidoglycan Biosynthesis. ACS Chem Biol 14:2745-2756.

31. **Scheible M, et al.** 2022. The Fused Methionine Sulfoxide Reductase MsrAB Promotes Oxidative Stress Defense and Bacterial Virulence in Fusobacterium nucleatum. mBio 13:e0302221.

32. **Fan R, et al.** 2022. Expression, Purification, and Characterization of the Recombinant, Two-Component, Response Regulator ArlR from Fusobacterium nucleatum. Appl Biochem Biotechnol 194:2093-2107.

33. **Fournier B, Hooper DC.** 2000. A new two-component regulatory system involved in adhesion, autolysis, and extracellular proteolytic activity of Staphylococcus aureus. J Bacteriol 182:3955-64.

34. **Zhou P, et al.** 2024. Use of CRISPR interference for efficient and rapid gene inactivation in Fusobacterium nucleatum. Appl Environ Microbiol 90:e0166523.

35. **Bibek GC, et al.** 2023. Development of a Xylose-Inducible Promoter and Riboswitch Combination System for Manipulating Gene Expression in Fusobacterium nucleatum. bioRxiv doi:10.1101/2023.04.24.538132.

36. **Galeano Nino JL, et al.** 2022. Effect of the intratumoral microbiota on spatial and cellular heterogeneity in cancer. Nature 611:810-817.

37. **Baker JL, et al.** 2024. The oral microbiome: diversity, biogeography and human health. Nat Rev Microbiol 22:89-104.

38. **Han YW, et al.** 2009. Uncultivated bacteria as etiologic agents of intra-amniotic inflammation leading to preterm birth. J Clin Microbiol 47:38-47.

39. **Parhi L, et al.** 2022. Placental colonization by Fusobacterium nucleatum is mediated by binding of the Fap2 lectin to placentally displayed Gal-GalNAc. Cell Rep 38:110537.

40. **Gur C, et al.** 2015. Binding of the Fap2 protein of Fusobacterium nucleatum to human inhibitory receptor TIGIT protects tumors from immune cell attack. Immunity 42:344-355.

41. **Li DH, et al.** 2021. Fecal Fusobacterium nucleatum harbored virulence gene fadA are associated with ulcerative colitis and clinical outcomes. Microb Pathog 157:104964.

42. **Li D, et al.** 2024. Oral inoculation of Fusobacterium nucleatum exacerbates ulcerative colitis via the secretion of virulence adhesin FadA. Virulence 15:2399217.

43. **Hong M, et al.** 2023. Fusobacterium nucleatum aggravates rheumatoid arthritis through FadA-containing outer membrane vesicles. Cell Host Microbe 31:798-810 e7.

44. **Nithianantham S, et al.** 2009. Crystal structure of FadA adhesin from Fusobacterium nucleatum reveals a novel oligomerization motif, the leucine chain. J Biol Chem 284:3865-72.

45. **Temoin S, et al.** 2012. Signal peptide of FadA adhesin from Fusobacterium nucleatum plays a novel structural role by modulating the filament's length and width. FEBS Lett 586:1-6.

46. **Sunde M, et al.** 1997. Common core structure of amyloid fibrils by synchrotron X-ray diffraction. J Mol Biol 273:729-39.

47. **Kiela PR, Ghishan FK.** 2016. Physiology of Intestinal Absorption and Secretion. Best Pract Res Clin Gastroenterol 30:145-59.

48. **Cummings JH.** 1975. Absorption and secretion by the colon. Gut 16:323-9.

49. **Zeng H, et al.** 2019. Secondary Bile Acids and Short Chain Fatty Acids in the Colon: A Focus on Colonic Microbiome, Cell Proliferation, Inflammation, and Cancer. Int J Mol Sci 20.

50. **Degirolamo C, et al.** 2011. Bile acids and colon cancer: Solving the puzzle with nuclear receptors. Trends Mol Med 17:564-72.

51. **Kapatral V, et al.** 2002. Genome sequence and analysis of the oral bacterium Fusobacterium nucleatum strain ATCC 25586. J Bacteriol 184:2005-18.

52. **Jang YJ, et al.** 2013. Autoinducer 2 of Fusobacterium nucleatum as a target molecule to inhibit biofilm formation of periodontopathogens. Arch Oral Biol 58:17-27.

53. **Ryu EJ, et al.** 2016. D-Galactose as an autoinducer 2 inhibitor to control the biofilm formation of periodontopathogens. J Microbiol 54:632-637.

54. **Wu J, et al.** 2019. Autoinducer-2 of Fusobacterium nucleatum promotes macrophage M1 polarization via TNFSF9/IL-1beta signaling. Int Immunopharmacol 74:105724.

55. **Vendeville A, et al.** 2005. Making 'sense' of metabolism: autoinducer-2, LuxS and pathogenic bacteria. Nat Rev Microbiol 3:383-96.

56. **Fardini Y, et al.** 2011. Fusobacterium nucleatum adhesin FadA binds vascular endothelial cadherin and alters endothelial integrity. Mol Microbiol 82:1468-80.

57. **Sutherland RM, et al.** 1971. Growth of Multicell Spheroids in Tissue Culture as a Model of Nodular Carcinomas. Jnci-Journal of the National Cancer Institute 46:113-+.

58. **Gunti S, et al.** 2021. Organoid and Spheroid Tumor Models: Techniques and Applications. Cancers (Basel) 13.

59. **Luo L, et al.** 2022. Application Progress of Organoids in Colorectal Cancer. Front Cell Dev Biol 10:815067.

60. **Yau JNN, Adriani G.** 2023. Three-dimensional heterotypic colorectal cancer spheroid models for evaluation of drug response. Front Oncol 13:1148930.

61. **Lin RZ, et al.** 2006. Dynamic analysis of hepatoma spheroid formation: roles of E-cadherin and beta1-integrin. Cell Tissue Res 324:411-22.

62. **Luong TT, et al.** 2021. Ribonuclease J-Mediated mRNA Turnover Modulates Cell Shape, Metabolism and Virulence in Corynebacterium diphtheriae. Microorganisms 9.

63. **Wu C, et al.** 2018. Forward Genetic Dissection of Biofilm Development by Fusobacterium nucleatum: Novel Functions of Cell Division Proteins FtsX and EnvC. mBio 9.

64. **Siegel SD, et al.** 2019. Structure and Mechanism of LcpA, a Phosphotransferase That Mediates Glycosylation of a Gram-Positive Bacterial Cell Wall-Anchored Protein. mBio 10.

65. **Chimileski S, et al.** 2024. Tip extension and simultaneous multiple fission in a filamentous bacterium. Proc Natl Acad Sci U S A 121:e2408654121.

Appendix B: Supporting Information for Inactivation of the *Fusobacterium nucleatum* Rnf complex reduces FadA-mediated amyloid formation and tumor development

B-1: Tables

Appendix Table B-1: Response Regulators in *F. nucleatum* ATCC 23726

Gene ID	Homolog Type	Associated Process[a]	Reference
C4N14_RS05840	ArlR	Adhesion, autolysis, proteolysis	(1, 2)
C4N14_RS09320	CarR	Lysine metabolism, coaggregation	(3)
C4N14_RS07475	CheY	Chemotaxis	(4)
C4N14_RS02760	EutV	Ethanolamine utilization	(5)
C4N14_RS04330	ModR	Oxidative stress response	(6)
C4N14_RS02660	S1 RNA binding	Transcription	This study
C4N14_RS04495	YpdB	Autolysis	(7)

[a]Based on the available information of homologous response regulators.

Appendix Table B-2: Bacterial strains and plasmids used in this study

Strains & Plasmids	Description	Reference
Strain		
F. nucleatum ATCC 23726	Wild-type (WT) strain	(8)
F. nucleatum CW1	Δ*galK*; an isogenic derivative of 23726	(8)
F. nucleatum fap2::Tn5	Derivative of 23726 with Tn5 insertion mapped to *fap2* at position 2054 (11361)	(3)
F. nucleatum Δ*rnfC*	Isogenic derivative of CW1 lacking *rnfC*	(9)
F. nucleatum Δ*fadA*	Isogenic derivative of CW1 lacking *fadA*	This study
F. nucleatum Δ*carR*	Isogenic derivative of CW1 lacking *carR*	(3)
F. nucleatum Δ*modR*	Isogenic derivative of CW1 lacking *modR*	(6)
F. nucleatum Δ*arlR*	Isogenic derivative of CW1 lacking *arlR*	This study
F. nucleatum Δ*cheY*	Isogenic derivative of CW1 lacking *cheY*	This study
F. nucleatum Δ*eutV*	Isogenic derivative of CW1 lacking *eutV*	This study
F. nucleatum Δ*s1*	Isogenic derivative of CW1 lacking *s1*	This study
F. nucleatum Δ*ypdB*	Isogenic derivative of CW1 lacking *ypdB*	This study
Plasmid		
pCWU6	Derivative of pHS30	(8)
pMCSG7	ligation-independent cloning vector	(10)
pZP4C	CRISPR-based vector	(11)
pCM-GalK	*C. perfringens* vector expressing *galK*	(8)
pMCSG7-FadA	pMCSG7 expressing FadA	This study
pMCSG7-CarR	pMCSG7 expressing CarR	This study
pMCSG7-Fap2	pMCSG7 expressing Fap2	This study
pRnfC	pCWU6 expressing RnfC under the control of the *rpsJ* promoter	(9)
pZP4C-lepB	Derivative of pZP4C for *lepB* depletion	This study
pGalK-Δ*fadA*	pCM-galK derivative; *rnfC* deletion vector	This study
pGalK-Δ*arlR*	pCM-galK derivative; *arlR* deletion vector	This study
pGalK-Δ*cheY*	pCM-galK derivative; *cheY* deletion vector	This study
pGalK-Δ*eutV*	pCM-galK derivative; *eutV* deletion vector	This study
pGalK-Δs*1*	pCM-galK derivative; *s1* deletion vector	This study
pGalK-Δ*ypdB*	pCM-galK derivative; *ypdB* deletion vector	This study

Appendix Table B-3: Primers used in this study

Primer	Sequence	Used for
rnfC-up-F	GGCGGGATCCATGAACTTTGAAGAAATAGATTTTTATATT	pGalK-Δ*rnfC*
rnfC-up-R	GGCGGGATCCTTAAAGGAGCTCCTATATGTTGTAAAAG	pGalK-Δ*rnfC*
rnfC-dn-F	GGCGGGTACCGTCCTATGGGGCTTGCACCACTTATG	pGalK-Δ*rnfC*
rnfC-dn-R	GGCGAAGCTTGCTAGTTGCTTCTGGTAAAACTTCTTTT	pGalK-Δ*rnfC*
Com-rnfC-F	GGCGGGTACCGGATAGTAGAAGTGCATTTAAAGATT	pRnfC
Com-rnfC-R	GGCGGGATCCCTACTTTTTCTTAGCTCTTAATTTAG	pRnfC
fadA-up-F	GGCGGGTACCCTTAACATAAGTTTACTATGATTT	pGalK-Δ*fadA*
fadA-up-R	TAATAGCTTTTTGTTGTTCCGAAGCAGAAACAGCTAATACTGC	pGalK-Δ*fadA*
fadA-dn-F	GGAACAACAAAAAGCTATTATTTC	pGalK-Δ*fadA*
fadA-dn-R	CGCGGATCCCTTCTTCTTCAGCATATTCAATTC	pGalK-Δ*fadA*
LIC-FadA-F	TACTTCCAATCCAATGCAATGCAAAAGGAAAAAGAACTTTC	pMCSG7-FadA
LIC-FadA-R	TTATCCACTTCCAATGTTACTATCTTATTTTTTGAATTTTTTC	pMCSG7-FadA
LIC-Fap2-F	TACTTCCAATCCAATGCAGATAATTATGGACAAATAACAGGTGTTGCAATG	pMCSG7-FadA
LIC-Fap2-R	TTATCCACTTCCAATGTTATTAGAATATAACTCTTAGTCCTACTCCACCTC	pMCSG7-FadA
LIC-CarR-F	TACTTCCAATCCAATGCA AAAATTTTAGTAGTTGAAGATG	pMCSG7-CarR
LIC-CarR-R	TTATCCACTTCCAATGTTATTCATCTTCTTTAAGAACATAGCC	pMCSG7-CarR
arlR-up-F	GGCGGGTACCCTGTATAGAATATAAAGCTATGGA	pGalK-Δ*arlR*
arlR-up-R	CTCTTGAACAAGACAACCCCAAATTTTATTCATCTTCCTCACCC	pGalK-Δ*arlR*
arlR-dn-F	GGGGTTGTCTTGTTCAAGAGA	pGalK-Δ*arlR*
arlR-dn-R	CGCGGATCCCAAAACTTAAATTATCTATAACTTC	pGalK-Δ*arlR*
cheY-up-F	CGCGGATCCCAAAACTTAAATTATCTATAACTTC	pGalK-Δ*cheY*
cheY-up-R	CATAAATACTCATTTCTGGGTCTACCTTCCTCCATTGAAAGGGC	pGalK-Δ*cheY*
cheY-dn-F	GTAGACCCAGAAATGAGTATTTATG	pGalK-Δ*cheY*
cheY-dn-R	AGAGTCGTCGACCAATGATTGCAATAGTTACAGGTG	pGalK-Δ*cheY*
eutV-up-F	AGAGGAGCTCGATTTACCTTTTGATGAAAGAG	pGalK-Δ*eutV*
eutV-up-R	AGAGGGTACCCTTGTAAGTGTTTCATCTTCCAC	pGalK-Δ*eutV*
eutV-dn-F	AGAGGGTACCGAAAGAGCCAAAGGAATAGTTATG	pGalK-Δ*eutV*
eutV-dn-R	AGAGGTCGACCTAAGTAAACTTGCCACTGTCTG	pGalK-Δ*eutV*
s1-up-F	AGAGGAGCTCCAGAAGATGCTACAACTGATG	pGalK-Δ*s1*
s1-up-R	AGAGGGTACCCTGTACTTCATCTAAATTTCCTG	pGalK-Δ*s1*
s1-dn-F	AGAGGGTACCGGAAGTAGGAATGGAACTTG	pGalK-Δ*s1*
s1-dn-R	AGAGGTCGACCTAGGTAATAGTAATCATCACC	pGalK-Δ*s1*
ypdB-up-F	GGCGGAGCTCGTGAAATTGTAGCAGGAAACCAAG	pGalK-Δ*ypdB*
ypdB-up-R	GGCGGGTACCCTCTTGCAGGCAATTCATCTTC	pGalK-Δ*ypdB*
ypdB-dn-F	GGCGGGTACCCTATGCAACAGCTATACCTGTAAG	pGalK-Δ*ypdB*
ypdB-dn-R	GGCGGTCGACCTTAGGCAGTTCAAGAGAGG	pGalK-Δ*ypdB*
RT-fadA-F	CAAGCTGACGCTGCTAGA	RT-PCR *fadA*

RT-fadA-R	GCTTGAAGTCTTTGAGCTCTTT	RT-PCR *fadA*
RT-carR-F	TTGACAGCAAGAGATGGAATAG	RT-PCR *carR*
RT-carR-R	CTTCTCACAAGAGCTCTAATTCT	RT-PCR *carR*
RT-modR-F	CTTCAACGGGAGAAGAGGCA	RT-PCR *modR*
RT-modR-R	AGCCGTTTGTGCATAATCAAAAT	RT-PCR *modR*
RT-arlR-F	CTTGGGTGAGGAAGATGAATAA	RT-PCR *arlR*
RT-arlR-R	CATAAGCAGAGTCAACAGAGTAG	RT-PCR *arlR*
RT-cheY-F	ATGGTGTGTTGGGAGTAAAG	RT-PCR *cheY*
RT-cheY-R	TGCTCCTGCTTCAAAGAAA	RT-PCR *cheY*
RT-eutV-F	GGCTATGATGTTGTAGGAGAAG	RT-PCR *eutV*
RT-eutV-R	TTAGCAACCTTTAGTCCAGAAA	RT-PCR *eutV*
RT-s1-F	GGAACGGCTTCAAGAGAAA	RT-PCR *s1*
RT-s1-R	AGCTCCTGCTTCATTAACTATC	RT-PCR *s1*
RT-ypdB-F	GCCTGATATGAATGGAATTAGTC	RT-PCR *ypdB*
RT-ypdB-R	TTTATCTCAAAGGCATCAACAG	RT-PCR *ypdB*
RT-radD-F	GCAGCAGCACCAACAATAAAT	RT-PCR *radD*
RT-radD-R	GGTGCTTCAGGAGGTGTTATC	RT-PCR *radD*
RT-16s-F	GGTTAAGTCCCGCAACGA	RT-PCR *16s*
RT-16s-R	CATCCCCACCTTCCTCCTAC	RT-PCR *16s*
Sg-lepB_F	CCAAATTTCCTATATAAAATCTTGTTTTAGAGCTAGAAATAGCAAGTT	CRISPRi-lepB
Sg-RNA-R	GATCCGCGGCCGCTAGTCAG	CRISPRi-lepB

[a] Underlined are restriction site sequences.

B-2: References

1. Fournier B, Hooper DC. 2000. A new two-component regulatory system involved in adhesion, autolysis, and extracellular proteolytic activity of Staphylococcus aureus. J Bacteriol 182:3955-64. https://doi.org/10.1128/JB.182.14.3955-3964.2000.
2. Fan R, Li Z, Shi X, Wang L, Zhang X, Dong Y, Quan C. 2022. Expression, Purification, and Characterization of the Recombinant, Two-Component, Response Regulator ArlR from Fusobacterium nucleatum. Appl Biochem Biotechnol 194:2093-2107. https://doi.org/10.1007/s12010-021-03785-5.
3. Wu C, Chen YW, Scheible M, Chang C, Wittchen M, Lee JH, Luong TT, Tiner BL, Tauch A, Das A, Ton-That H. 2021. Genetic and molecular determinants of polymicrobial interactions in Fusobacterium nucleatum. Proc Natl Acad Sci U S A 118. https://doi.org/10.1073/pnas.2006482118.
4. Stock A, Koshland DE, Jr., Stock J. 1985. Homologies between the Salmonella typhimurium CheY protein and proteins involved in the regulation of chemotaxis, membrane protein synthesis, and sporulation. Proc Natl Acad Sci U S A 82:7989-93. https://doi.org/10.1073/pnas.82.23.7989.
5. Fox KA, Ramesh A, Stearns JE, Bourgogne A, Reyes-Jara A, Winkler WC, Garsin DA. 2009. Multiple posttranscriptional regulatory mechanisms partner to control ethanolamine utilization in Enterococcus faecalis. Proc Natl Acad Sci U S A 106:4435-40. https://doi.org/10.1073/pnas.0812194106.
6. Scheible M, Nguyen CT, Luong TT, Lee JH, Chen YW, Chang C, Wittchen M, Camacho MI, Tiner BL, Wu C, Tauch A, Das A, Ton-That H. 2022. The Fused Methionine Sulfoxide Reductase MsrAB Promotes Oxidative Stress Defense and Bacterial Virulence in Fusobacterium nucleatum. mBio 13:e0302221. https://doi.org/10.1128/mbio.03022-21.

7. Nikolskaya AN, Galperin MY. 2002. A novel type of conserved DNA-binding domain in the transcriptional regulators of the AlgR/AgrA/LytR family. Nucleic Acids Res 30:2453-9. https://doi.org/10.1093/nar/30.11.2453.

8. Wu C, Al Mamun AAM, Luong TT, Hu B, Gu J, Lee JH, D'Amore M, Das A, Ton-That H. 2018. Forward Genetic Dissection of Biofilm Development by Fusobacterium nucleatum: Novel Functions of Cell Division Proteins FtsX and EnvC. mBio 9. https://doi.org/10.1128/mBio.00360-18.

9. Britton TA, Wu C, Chen YW, Franklin D, Chen Y, Camacho MI, Luong TT, Das A, Ton-That H. 2024. The respiratory enzyme complex Rnf is vital for metabolic adaptation and virulence in Fusobacterium nucleatum. mBio 15:e0175123. https://doi.org/10.1128/mbio.01751-23.

10. Siegel SD, Amer BR, Wu C, Sawaya MR, Gosschalk JE, Clubb RT, Ton-That H. 2019. Structure and Mechanism of LcpA, a Phosphotransferase That Mediates Glycosylation of a Gram-Positive Bacterial Cell Wall-Anchored Protein. mBio 10. https://doi.org/10.1128/mBio.01580-18.

11. Zhou P, G CB, Stolte F, Wu C. 2024. Use of CRISPR interference for efficient and rapid gene inactivation in Fusobacterium nucleatum. Appl Environ Microbiol 90:e0166523. https://doi.org/10.1128/aem.01665-23.

Chapter 4

Visualization of a cell wall hydrolase inhibitor in *Fusobacterium nucleatum* by immunofluorescence microscopy

Published in *Methods in Molecular Biology*

Visualization of a Cell Wall Hydrolase Inhibitor in *Fusobacterium nucleatum* by Immunofluorescence Microscopy

Kevin To, Timmie Britton, and Hung Ton-That

Abstract

Innately present in tears, saliva and mucosal secretions, lysozyme provides a critical defensive strategy to the host by cleaving the β-1,4-glycosidic bonds between *N*-acetylmuramic acid and *N*-acetyl-D-glucosamine residues of peptidoglycan of invading bacteria, leading to bacterial lysis. To counter this class of cell wall hydrolase enzymes, bacteria produce several lysozyme inhibitors, a representative of which, MliC, was identified in *Escherichia coli*, *Pseudomonas aeruginosa*, and various bacterial species. The Gram-negative oral anaerobe *Fusobacterium nucleatum* encodes an uncharacterized lipoprotein homologous to MliC, whose localization is unknown. Here, we provide an experimental procedure to localize this MliC-like lipoprotein by employing immunofluorescence microscopy. In principle, this protocol can be used for any bacterial system to monitor protein localization.

Key words Immunofluorescence, Cell wall hydrolase, Membrane permeabilization, *Fusobacterium nucleatum*, Gram-negative bacteria, Lysozyme inhibitor

1 Introduction

Immunofluorescence microscopy (IFM) is a standard technique widely used to detect the presence, abundance, localization, and organization of biomolecules with high specificity in microbiological samples. For example, IFM was used to localize members of the RNA degradation & processing complex to a specialized cytoplasmic compartment [1] and cell division proteins FtsZ, FtsA, and ZipA to a cytoplasmic cell division ring in *Escherichia coli* [2]. This technique relies on the specificity between fluorescently conjugated antibodies and their cognate antigen. Briefly, bacterial cells are immobilized on a microscope slide and can be permeabilized to facilitate antibody access across the cell envelope. Indirect

Kevin To and Timmie Britton contributed equally with all other contributors.

Hung Ton-That (ed.), *The Bacterial Cell Wall: Methods and Protocols*, Methods in Molecular Biology, vol. 2727,
https://doi.org/10.1007/978-1-0716-3491-2_3,

immuno-labeling requires the addition of a secondary antibody, conjugated to a fluorophore, while direct immuno-labeling omits the secondary antibody and conjugates the fluorophore to the primary antibody. Indirect IFM achieves a much higher fluorescent readout due to amplification of the signal with multiple fluorescently conjugated secondary antibodies.

Using IFM, we present here a protocol to localize a lipoprotein that contains a membrane-bound lysozyme inhibitor of c-type lysozyme (MliC) domain in *Fusobacterium nucleatum* – a Gram-negative oral anaerobe that is associated with oral disease, preterm birth, and colorectal cancer [3]. A highly conserved and ancient constituent of the innate immune system of mammals, lysozyme protects hosts from pathogenic bacteria by hydrolyzing peptidoglycan. Unfortunately, bacteria have evolved to counter the activity of cell wall hydrolase enzymes via the production of lysozyme inhibitors. First identified as Ivy (Inhibitor of vertebrate lysozyme) in *E. coli* [4] and later renamed as MliC [5], MliC proteins have been identified in many other bacteria, including *Pseudomonas aeruginosa* and *Salmonella* Typhi [5]. MliC proteins are predicted to anchor to the periplasmic side of the outer membrane [6, 7]. In *F. nucleatum*, MliC is a lipoprotein that harbors a lipobox [8], presumably promoting the membrane localization of this protein. Using *F. nucleatum* MliC as an experimental model, we provide a detailed procedure to visualize protein dynamics within the bacterial cell envelope. This procedure can be used for protein visualization in other Gram-negative bacteria.

2 Materials

All solutions should be prepared with sterile molecular grade water.

2.1 Coverslip Preparation

1. No. 1 coverslip (12 mm diameter).
2. 0.01% poly-L-lysine solution: prepare this solution from lyophilized poly-L-lysine hydrobromide in water.

2.2 Preparation of F. nucleatum Cells for Fixation

1. *Fusobacterium nucleatum* strains: Δ*mliC*, Δ*mliC*/pMliC, and CW1 (parent) [9].
2. TSPC: Tryptic Soy Broth (TSB) supplemented with 1% Bacto peptone and 0.25% freshly made L-cysteine.
3. 1.5 mL Eppendorf tubes.
4. Phosphate buffered saline (PBS), pH 7.4.
5. 4% formaldehyde in PBS.

2.3 Permeabilization of Bacterial Cells

1. 70% ethanol.
2. TEG Buffer: 25 mM Tris-HCl, pH 8.0, 10 mM EDTA, 50 mM glucose.
3. 50 μg/mL lysozyme solution in TEG buffer.
4. End-to-end rotator.

2.4 Immunolabelling of Cells

1. 3% bovine serum albumin (BSA) solution.
2. Primary antibodies: rabbit anti-MliC (α-MliC).
3. Secondary antibodies: goat anti-rabbit IgG AlexaFluor 488 conjugate.

2.5 Mounting and Fluorescence Microscopy

1. Microscope slides (25 mm × 75 mm × 1 mm).
2. Anti-fade Mounting Medium with DAPI.
3. Hanks' Balanced Salt Solution (HBSS): 1.67 mM $CaCl_2.2H_2O$, 0.81 mM $MgSO_4$, 5.37 mM KCl, 0.44 mM KH_2PO_4, 4.17 mM $NaHCO_3$, 0.27 M NaCl, 0.34 mM Na_2HPO_4, 5.55 mM D-glucose, pH 7.4.
4. FM™ 4–64 Dye: 500 μg/mL in HBSS.
5. Nail polish.
6. Dumont angled tweezers.
7. Fluorescence microscope with appropriate fluorescence filters.

3 Methods

3.1 Coverslip Preparation

1. Coat one side of coverslips with 150 μL of poly-L-lysine solution and let settle for at least 5 min (*see* **Note 1**).
2. Aspirate poly-L-lysine solution off coverslips and thoroughly rinse the coated surface with sterile molecular grade water.
3. Allow to air-dry for at least 2 h.

3.2 Preparation of F. nucleatum Cells for Fixation

1. Aseptically transfer a single colony of individual *F. nucleatum* strains to 5 mL of TSPC and grow the cultures at 37 °C in an anaerobic chamber.
2. Adjust the cell cultures to OD_{600} of 1.0 in 1.5 mL Eppendorf tubes and pellet the cells by centrifugation in a microfuge at 6000 × *g* for 2 min.
3. Wash the cell pellets twice in PBS and discard the supernatants.
4. For detection of non-surface proteins, proceed to Subheading 3.3.
5. For detection of outer membrane surface proteins, resuspend the cell pellets in 1 mL of PBS, transfer 150 μL of cell suspension to individual coated coverslips (*see* Subheading 3.1),

incubate at room temperature for 20 min, and aspirate the cell suspension.

6. To fix cells, apply 150 µL of 4% formaldehyde solution (*see* **Note 2**) onto coverslips and incubate at room temperature for 20 min.
7. Wash coverslips once with 150 µL of PBS (*see* **Note 3**) and aspirate PBS.
8. Proceed to Subheading 3.4.

3.3 Permeabilization of Bacterial Cells

1. Resuspend the pellets prepared from **step 3** of Subheading 3.2 in 1 mL of 4% formaldehyde and incubate at room temperature for 30 min.
2. Pellet cells by centrifugation at 6000 × *g* for 2 min and wash cell pellets twice in 1 mL of PBS.
3. Discard the supernatants, resuspend the cell pellets in 1 mL of 70% ethanol, and incubate at room temperature for 1 h on an end-to-end rotator.
4. Harvest the cells by centrifugation at 6000 × *g* for 2 min and discard the supernatants.
5. Resuspend the pellets in 0.5 mL of TEG Buffer, add 0.5 mL of 50 µg/mL lysozyme solution in TEG, and incubate at room temperature for 30 min.
6. Transfer 150 µL of the cell suspension above to the coated coverslips (Subheading 3.1) and incubate at room temperature for 5 min.
7. Carefully aspirate the remaining solution from the coverslips and wash cells bound to the coverslips with 150 µL of PBS.
8. Proceed to Subheading 3.4.

3.4 Immunolabeling of Cells

1. Block cells on the coverslips with 150 µL of 3% BSA solution at room temperature for at least 1 h and aspirate the solution.
2. Dilute the primary antibody in 3% BSA (1:200 dilution) and add 150 µL of the primary antibody solution onto coverslips and incubate at room temperature for 1 h.
3. Wash coverslips three times with PBS (*see* **Note 3**).
4. Dilute the secondary antibody in 3% BSA and add 150 µL of the secondary antibody solution onto coverslip and incubate at room temperature for 1 h *in the dark* for remaining steps to prevent photobleaching (*see* **Note 4**).
5. Wash coverslips three times with 150 µL of PBS.

3.5 Mounting and Fluorescence Microscopy

1. Add one drop of Anti-fade Mounting Medium with DAPI onto a microscope slide.
2. To visualize bacterial membranes, add 1–2 μL of FM 4-64 dye (500 μg/mL) onto the microscope slide and mix with DAPI above.
3. Using Dumont angled tweezers, invert coverslip and mount face down onto the microscope slide, allowing to sit for 1 min in the dark.
4. Carefully apply nail polish along the perimeter of the coverslips to seal and dry for 5 min (*see* **Note 5**).
5. Image via a fluorescence microscope, using the appropriate channel for the indicated excitation and emission spectra (*see* **Note 6**).

4 Notes

1. May incubate coverslips with poly-L-lysine solution overnight.
2. Store 4% formaldehyde solution at 4 °C.
3. For each wash, gently pipette PBS up and down near the edge of coverslips and leave PBS on coverslips for at least 5 min prior to aspiration.
4. Use a small box to cover coverslips as to keep them in dark. Avoid exposing coverslips containing fluorescently labeled secondary antibodies to light.
5. Prepared glass slides can be stored at −20 °C for future imaging; however, moisture at −20 °C may lessen the integrity of the seal. If reimaging, one may need to apply nail polish to reseal.
6. For AlexaFluor 488, use the green fluorescence channel (max excitation and emission at 490 nm and 525 nm, respectively). For DAPI, use the blue fluorescence channel (max excitation and emission at 350 nm and 470 nm, respectively). For the FM 4-64 dye, use the red fluorescence channel (max excitation and emission at 515 nm and 640 nm, respectively) (Fig. 1).

Acknowledgments

We thank Dr. Chungyu Chang and our laboratory members for the critical review of this manuscript. Work reported in this publication was supported by the National Institute of Dental and Craniofacial Research (NIDCR) of the National Institutes of Health (NIH) under the award number DE026758 (to H.T.-T.). The content presented in this publication is solely the responsibility of the authors and does not necessarily reflect the viewpoints of the National Institutes of Health.

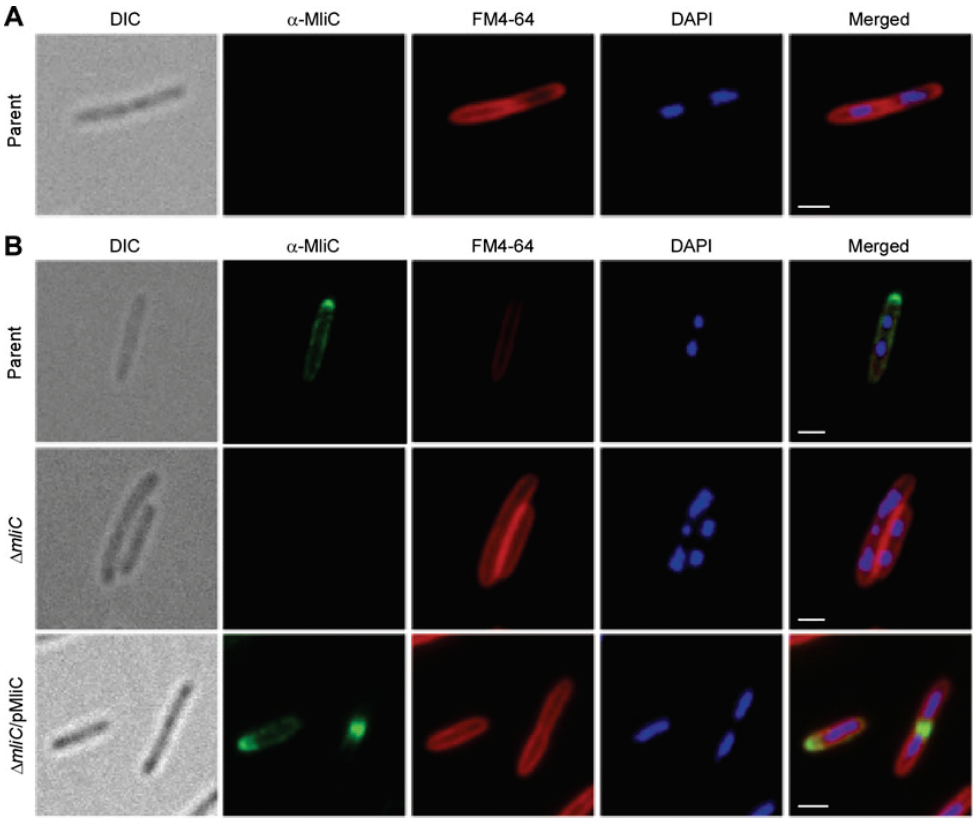

Fig. 1 Immunofluorescent microscopy of MliC. (**a**) Non-permeabilized cells of the parent strain and (**b**) permeabilized cells of the parent, Δ*mliC*, and Δ*mliC*/pMliC strains were stained with α-MliC (green), FM 4-64 (red), and DAPI (blue). Fluorescence signal was analyzed by a fluorescence microscope equipped with appropriate filters. Overlay of fluorescent images is shown (merged), with scale bars of 1 μm. Note, no MliC signal was detected in non-permeabilized cells, indicating MliC is not displayed on the extracellular side of the outer membrane

References

1. Taghbalout A, Yang Q, Arluison V (2014) The *Escherichia coli* RNA processing and degradation machinery is compartmentalized within an organized cellular network. Biochem J 458(1): 11–22. https://doi.org/10.1042/BJ20131287
2. Rueda S, Vicente M, Mingorance J (2003) Concentration and assembly of the division ring proteins FtsZ, FtsA, and ZipA during the *Escherichia coli* cell cycle. J Bacteriol 185(11): 3344–3351. https://doi.org/10.1128/JB.185.11.3344-3351.2003
3. Han YW (2015) *Fusobacterium nucleatum*: a commensal-turned pathogen. Curr Opin Microbiol 23:141–147. https://doi.org/10.1016/j.mib.2014.11.013
4. Monchois V, Abergel C, Sturgis J, Jeudy S, Claverie JM (2001) *Escherichia coli ykfE* ORFan gene encodes a potent inhibitor of C-type lysozyme. J Biol Chem 276(21):18437–18441. https://doi.org/10.1074/jbc.M010297200
5. Callewaert L, Aertsen A, Deckers D, Vanoirbeek KG, Vanderkelen L, Van Herreweghe JM,

Masschalck B, Nakimbugwe D, Robben J, Michiels CW (2008) A new family of lysozyme inhibitors contributing to lysozyme tolerance in gram-negative bacteria. PLoS Pathog 4(3): e1000019. https://doi.org/10.1371/journal.ppat.1000019

6. Tokuda H, Matsuyama S (2004) Sorting of lipoproteins to the outer membrane in *E. coli*. Biochim Biophys Acta 1693(1):5–13. https://doi.org/10.1016/j.bbamcr.2004.02.005
7. Narita S, Tokuda H (2007) Amino acids at positions 3 and 4 determine the membrane specificity of Pseudomonas aeruginosa lipoproteins. J Biol Chem 282(18):13372–13378. https://doi.org/10.1074/jbc.M611839200
8. Hayashi S, Wu HC (1990) Lipoproteins in bacteria. J Bioenerg Biomembr 22(3):451–471. https://doi.org/10.1007/BF00763177
9. Wu C, Al Mamun AAM, Luong TT, Hu B, Gu J, Lee JH, D'Amore M, Das A, Ton-That H (2018) Forward genetic dissection of biofilm development by *Fusobacterium nucleatum*: novel functions of cell division proteins FtsX and EnvC. mBio 9(2). https://doi.org/10.1128/mBio.00360-18

Chapter 5 Conclusions and Impact

5.1 Summary of Research Findings

The human oral cavity is home to over 700 microbial species and constitutes the second largest consortia of microorganisms in the human body (1, 2). Here, bacteria, fungi, protozoa, and viruses compete for a broad range of metabolites in various oral niches, spawning a complex habitat that directly influences health and disease (3). Understanding the impact specific microbial members have on oral health is therefore of great interest. In the subgingival pocket, below the gumline, resides a thinly rod-shaped anaerobic bacterium named *Fusobacterium nucleatum*, originally thought to be a commensal due to its interaction with harmless oral colonizers, however is now known to drive periodontitis. This is in large part due to the expression of many outer membrane proteins (RadD, Fap2, FomA, FadA) that serve as molecular adhesins, while also contributing to halitosis via the production of toxic and foul-smelling hydrogen sulfide (H_2S) gas (4-14). Worst of all, this periodontal pathogen can spread and colonize many extra-oral sites, where it promotes several malignancies (15-17), gastrointestinal (GI) disorders (18-20), and adverse pregnancy outcomes (APOs) (21, 22). Thanks to advances in genetic tools, researchers have identified a number of fusobacterial factors required for the virulence of this oral pathobiont outside the oral cavity, most of which being outer membrane adhesins due to the lack of any major secretion systems (23). Nonetheless, what remains to be studied is how *F. nucleatum* metabolically adapts to highly dynamic extra-oral environments to sustain its virulence potential and colonize a plethora of host tissues.

Informed by our genome-wide transposon mutagenesis screens for biofilm- and coaggregation-defective factors (24, 25), we report that the highly conserved prokaryotic *Rhodobacter* nitrogen-fixation (Rnf) complex, encoded in a six-gene operon (*rnfCDGEAB)*, is central to fusobacterial metabolic adaptation and virulence by conserving energy via an ion-motive force (IMF) and ATP biosynthesis from amino acid metabolism (26). Rnf is a ferredoxin-NAD^+ oxidoreductase discovered in the nitrogen-fixating bacterium, *Rhodobacter capsulatus*, in

1993 (27). Since then, researchers have divulged that Rnf expands the metabolic versatility of several prokaryotes in low-energy environments, conserving energy from nitrogen-fixation (28-30), carbon-dioxide fixation (31-33), amino acid metabolism (34-37), metabolic resource sharing (38, 39), and methanogenesis (40, 41). However, its impact on bacterial virulence has yet to be investigated.

Here, we find that genetic disruption of the NADH-binding *rnfC* (Δ*rnfC*) subunit abrogates fusobacterial biofilm formation and polymicrobial interaction (or coaggregation) associated with the RadD adhesin. The defect in coaggregation is not due to a loss of RadD but an inability by these mutants to metabolize extracellular lysine, resulting in an accumulation of this amino acid in the culture media, subsequently binding and blocking RadD-mediated interaction with nearby oral colonizers, in our case *Streptococcus gordonii*. Indeed, removal of extracellular lysine via washing Δ*rnfC* cells restores coaggregation, while the addition of lysine inhibits this process. These phenotypes mirror that of a mutant (Δ*kamA*) unable to metabolize extracellular lysine. Shockingly, deletion of *rnfC* causes pleotropic defects in *F. nucleatum* physiology as well, as these mutants are defective in bacterial cell growth, have altered cell morphology, and reduced expression of toxic H_2S gas as well as the enzymes (MegL, CysK1, CysK2) responsible for H_2S production from methionine and cysteine metabolism. Targeted metabolic profiling further demonstrated that the degradation of several amino acids, including histidine, lysine, glutamine, glutamate, methionine, and cysteine, were altered in Δ*rnfC* cells, thereby reducing ATP biosynthesis and several central carbon metabolites, such as butyrate. As a result, these mutants are severely attenuated in an *in vivo* mouse model of preterm birth (26).

We conclude that the indispensable role of the Rnf complex in amino acid fermentation is central to *F. nucleatum* pathophysiology. Nevertheless, outside of its effect on RadD-mediated polymicrobial interaction via its role in lysine metabolism, a mechanism for how this respiratory enzyme modulates the virulence potential of this pathobiont via metabolic signaling is still unclear. As mentioned, the Gram-negative oral anaerobe, *F. nucleatum*, promotes carcinogenesis in

several extra-oral sites, most notably the colon. The amyloid-forming adhesin, FadA, is vital to this process by binding and disrupting colorectal tight junction integrity while simultaneously activating expression of oncogenes via the Wnt/β-catenin signaling pathway (17, 42). Furthermore, FadA binding to the epithelial tight junction protein, E-cadherin, upregulates expression of annexin A1 (ANXA1), a modulator of Wnt/β-catenin signaling highly expressed on proliferating colorectal cancer (CRC) cells (43). Combined with the amyloid-like properties of FadA, this adhesin allows *F. nucleatum* to intimately associate with the colorectal crypt, driving carcinogenesis through an annexin A1-mediated positive feedback loop.

Amazingly, we find that genetic disruption of the Rnf complex, via *rnfC*-deletion, significantly reduces the transcript level of *fadA* relative to wildtype fusobacteria, which was accompanied with near complete abolition of the precursor form of FadA (pFadA) and reduced surface assembly of FadA at the mature cell pole. Importantly, deletion of *rnfC* led to a significant reduction of osmotic stress-induced amyloid formation, mediated by FadA, which could be rescued by ectopic expression of RnfC on a plasmid. Among the seven response regulators predictably identified in *F. nucleatum*, deletion of three (*carR*, *alrR*, and *s1*) significantly reduced pFadA expression at the protein level, while the transcript level of *fadA* remained unaltered. These data suggest a synergistic regulatory model of FadA post-translational processing. Intriguingly, deletion of *rnfC* reduced transcript expression of genes encoding all seven response regulators, including those affecting pFadA production, *carR*, *arlR*, and *s1*. We also observed a significant transcript loss of the major fusobacterial signal peptidase, *lepB*, in Δ*rnfC* mutant cells. Furthermore, deletion of *carR*, *alrR*, or *s1* also negatively impacts *lepB* transcript abundance. As *lepB* is an essential gene in *F. nucleatum*, we disrupted its expression by CRISPR interference (CRISPRi) which shockingly resulted in a near complete abrogation of FadA protein production. Taken together, we hypothesize that global metabolic defects in ∆*rnfC* cells negatively impacts the expression of an unidentified signal required for fusobacterial two-component system activation, which in turn reduces expression of the LepB signal peptidase required for pFadA

processing into its mature form (mFadA). As a result, most of the pFadA is unable to be processed in the fusobacterial inner membrane, and thus subsequently degraded to prevent cellular toxicity. As LepB production is not completely abolished, the minimal processing that does occur results in an accumulation of mFadA in Δ*rnfC* mutants, allowing for a reduced number of functional FadA adhesin (FadAc) to be formed at the mature *F. nucleatum* cell pole as visualized by immunofluorescence microscopy. Importantly, while *rnfC*-deletion did not affect the ability of mutant cells to adhere to cancer cells (HCT116), possibly due to the unaltered expression of RadD and Fap2 in these mutants, RnfC deficiency significantly diminished fusobacterial invasion of HCT116 cells. Consistent with the role of FadA in tumor formation, the *rnfC* mutant was markedly defective in promotion of spheroid tumors. Given the indispensable role of the Rnf complex to fusobacterial metabolic adaptation and virulence, coupled with its absence from eukaryotes, it may serve as an attractive target for therapeutic intervention.

Given a key virulence trait of *F. nucleatum* is the expression of outer membrane adhesins, our lab has developed a novel immunofluorescence microscopy technique to visualize proteins within and outside of the bacterial cell wall (44). As evident in our earlier studies described in chapters 2 and 3, we have used this tool to localize fusobacterial adhesins on the extracellular-side of the outer membrane, however visualization of proteins within the cell wall is more challenging given the difficulty of mediating antibody access across the outer membrane and/or peptidoglycan layer. *F. nucleatum* encodes an uncharacterized lipoprotein homologous to MliC, a lysozyme inhibitor whose specific location is unknown (45). Lysozyme is present in saliva, tears, and mucosal secretions and serves as an important attribute to mammalian innate immunity against bacterial pathogens by targeting β-1,4-glycosidic bonds between repeating N-acetylmuramic acid and N-acetyl-D-glucosamine sugars of the peptidoglycan backbone. The lysozyme inhibitor, MliC, contains a lipobox and is thus predicted to localize to the membrane (46-48). Using this cutting-edge technique, we demonstrate that the *F. nucleatum* MliC homolog is not

detected in non-permeabilized cells, but co-localizes with a membrane-specific dye, suggesting its localization to the periplasmic-facing side of the outer membrane, as predicted.

5.2 Future Studies

5.2.1 Examining the impact of *rnfC*-deletion on colorectal cancer tumor formation *in vivo*

Our previous studies demonstrate that loss of *rnfC* negatively impacts human colorectal cancer cell (HCT116) invasion and tumor formation *in vitro*, but we did not investigate the ability for *rnf* mutants to stimulate tumor formation *in vivo*. To address this, we have developed a colorectal cancer xenograft mouse model, in which BALB/c mice are subcutaneously injected with HCT116 cells and tumors allowed to form for 7 days followed by intratumoral infection of normalized parent, Δ*rnfC*, or Δ*fadA* cells twice per week for 3 weeks. Intratumoral injection of PBS will be used as a negative control. Given *rnfC*-deletion severely impacts metabolic signaling leading to a reduction in FadA expression on the fusobacterial cell surface, we hypothesize infection with these mutants will result in a significant attenuation in colorectal cancer tumor size, volume, and weight.

5.2.2 Identification of the fusobacterial CarRS activating signal

As the Rnf complex is central to fusobacterial metabolism, and deletion of *rnfC* results in a global reduction of all seven fusobacterial response regulator transcripts, we hypothesize that disruption of Rnf-mediated amino acid fermentation negatively impacts the production of an unidentified signal required for the activation of fusobacterial two-component systems (TCSs). For these studies we will focus on the CarRS TCS as the response regulator, CarR, strongly regulates pFadA production, and the CarRS regulon has been published (25), allowing us to monitor the system's activation by targeting downstream genes as a readout. It is worth noting that no genes encoding quorum-sensing proteins, such as LuxI (autoinducer-1 synthase) or LuxS (autoinducer-2 synthase), exist in *F. nucleatum* (23), despite previous characterization of autoinducer-2 (AI-2) production in this pathogen, and its stated role in *F. nucleatum* biofilm formation (49, 50) and

colorectal cancer progression (51). AI-2 is produced from methionine degradation into S-adenosyl-L-homocysteine (SAH), which is further detoxified into adenine and the substrate for LuxS-catalyzed AI-2 biosynthesis, S-ribosyl-L-homocysteine (SRH) (52). Intriguingly, previous metabolic screening of Δ*rnfC* mutant cells revealed significantly less methionine, adenine, and SAH intermediates compared to the parent strain (26). It is therefore tempting to speculate *rnfC*-deletion reduces production of AI-2, which in turn may prevent the activation of CarRS, and/or other fusobacterial two-component systems, subsequently impacting LepB production as well as FadA processing.

To test this, we will first conduct an AI-2 bioassay to measure autoinducer production in parent and *rnfC*-deletion cells. This assay relies upon the bioluminescence of *Vibrio harveyi* reporter strains after sensing extracellular autoinducers. *V. harveyi* strains that respond only to AI-1 or AI-2 have been designed and will be used in this assay (53). Normalized fusobacterial cell-free supernatant (CFS) will be incubated with *V. harveyi* reporter strains and bioluminescence measured at regular time intervals using a luminescence spectrophotometer. To examine if these autoinducers serve as signals for CarRS activation, we will measure the transcript expression of *radD* by quantitative reverse transcription polymerase chain reaction (qRT-PCR) in the presence or absence of CFS from parent, Δ*rnfC*, or Δ*carS* cells, as the sensor histidine kinase, CarS, was previously shown positively regulate *radD* expression (25). Addition of the AI-2 precursor, (S)-4,5-dihydroxypentane-2,3-dione (S-DPD), will be included as a positive control. A *carS* mutant with a mutation in the critical histidine (H236A) of the histidine kinase A domain (HisKA) required for the phospho-relay reaction with CarR can also be included in these sets of experiments. Identification of the highly conserved autoinducer synthase genes in *F. nucleatum* is warranted. Using our genome-wide transposon (Tn5) mutagenesis library, future studies may look to subject these mutants to the abovementioned autoinducer bioassay and screen for bioluminescent-defective factors.

5.3 References

1. **Dewhirst FE, et al.** 2010. The human oral microbiome. J Bacteriol 192:5002-17.
2. **Caselli E, et al.** 2020. Defining the oral microbiome by whole-genome sequencing and resistome analysis: the complexity of the healthy picture. BMC Microbiol 20:120.
3. **Baker JL, et al.** 2024. The oral microbiome: diversity, biogeography and human health. Nat Rev Microbiol 22:89-104.
4. **Kolenbrander PE, et al.** 1989. Coaggregation of Fusobacterium nucleatum, Selenomonas flueggei, Selenomonas infelix, Selenomonas noxia, and Selenomonas sputigena with strains from 11 genera of oral bacteria. Infect Immun 57:3194-203.
5. **Lancy P, Jr., et al.** 1983. Corncob formation between Fusobacterium nucleatum and Streptococcus sanguis. Infect Immun 40:303-9.
6. **Coppenhagen-Glazer S, et al.** 2015. Fap2 of Fusobacterium nucleatum is a galactose-inhibitable adhesin involved in coaggregation, cell adhesion, and preterm birth. Infect Immun 83:1104-13.
7. **Wu T, et al.** 2015. Cellular Components Mediating Coadherence of Candida albicans and Fusobacterium nucleatum. J Dent Res 94:1432-8.
8. **Rickard AH, et al.** 2003. Bacterial coaggregation: an integral process in the development of multi-species biofilms. Trends Microbiol 11:94-100.
9. **Kolenbrander PE, Andersen RN.** 1989. Inhibition of coaggregation between Fusobacterium nucleatum and Porphyromonas (Bacteroides) gingivalis by lactose and related sugars. Infect Immun 57:3204-9.
10. **Yamaguchi-Kuroda Y, et al.** 2023. Porphyromonas gingivalis diffusible signaling molecules enhance Fusobacterium nucleatum biofilm formation via gene expression modulation. J Oral Microbiol 15:2165001.

11. **Chen YW, et al.** 2022. Genetic Determinants of Hydrogen Sulfide Biosynthesis in Fusobacterium nucleatum Are Required for Bacterial Fitness, Antibiotic Sensitivity, and Virulence. mBio 13:e0193622.

12. **Kaplan CW, et al.** 2009. The Fusobacterium nucleatum outer membrane protein RadD is an arginine-inhibitable adhesin required for inter-species adherence and the structured architecture of multispecies biofilm. Mol Microbiol 71:35-47.

13. **Xu M, et al.** 2007. FadA from Fusobacterium nucleatum utilizes both secreted and nonsecreted forms for functional oligomerization for attachment and invasion of host cells. J Biol Chem 282:25000-9.

14. **Jensen HB, et al.** 1996. Cloning of the fomA gene, encoding the major outer membrane porin of Fusobacterium nucleatum ATCC10953. Microb Pathog 21:331-42.

15. **Parhi L, et al.** 2020. Breast cancer colonization by Fusobacterium nucleatum accelerates tumor growth and metastatic progression. Nat Commun 11:3259.

16. **Udayasuryan B, et al.** 2022. Fusobacterium nucleatum induces proliferation and migration in pancreatic cancer cells through host autocrine and paracrine signaling. Sci Signal 15:eabn4948.

17. **Rubinstein MR, et al.** 2013. Fusobacterium nucleatum promotes colorectal carcinogenesis by modulating E-cadherin/beta-catenin signaling via its FadA adhesin. Cell Host Microbe 14:195-206.

18. **Engevik MA, et al.** 2021. Fusobacterium nucleatum Secretes Outer Membrane Vesicles and Promotes Intestinal Inflammation. mBio 12.

19. **Boehm ET, et al.** 2020. Fusobacterium nucleatum is associated with worse prognosis in Lauren's diffuse type gastric cancer patients. Sci Rep 10:16240.

20. **Gu X, et al.** 2020. Fusobacterium nucleatum Causes Microbial Dysbiosis and Exacerbates Visceral Hypersensitivity in a Colonization-Independent Manner. Front Microbiol 11:1281.

21. **Han YW, et al.** 2009. Uncultivated bacteria as etiologic agents of intra-amniotic inflammation leading to preterm birth. J Clin Microbiol 47:38-47.

22. **Payne MS, Bayatibojakhi S.** 2014. Exploring preterm birth as a polymicrobial disease: an overview of the uterine microbiome. Front Immunol 5:595.

23. **Kapatral V, et al.** 2002. Genome sequence and analysis of the oral bacterium Fusobacterium nucleatum strain ATCC 25586. J Bacteriol 184:2005-18.

24. **Wu C, et al.** 2018. Forward Genetic Dissection of Biofilm Development by Fusobacterium nucleatum: Novel Functions of Cell Division Proteins FtsX and EnvC. mBio 9.

25. **Wu C, et al.** 2021. Genetic and molecular determinants of polymicrobial interactions in Fusobacterium nucleatum. Proc Natl Acad Sci U S A 118.

26. **Britton TA, et al.** 2024. The respiratory enzyme complex Rnf is vital for metabolic adaptation and virulence in Fusobacterium nucleatum. mBio 15:e0175123.

27. **Schmehl M, et al.** 1993. Identification of a new class of nitrogen fixation genes in Rhodobacter capsulatus: a putative membrane complex involved in electron transport to nitrogenase. Mol Gen Genet 241:602-15.

28. **Desnoues N, et al.** 2003. Nitrogen fixation genetics and regulation in a Pseudomonas stutzeri strain associated with rice. Microbiology (Reading) 149:2251-2262.

29. **Curatti L, et al.** 2005. Genes required for rapid expression of nitrogenase activity in Azotobacter vinelandii. Proc Natl Acad Sci U S A 102:6291-6.

30. **Tremblay PL, et al.** 2012. The Rnf complex of Clostridium ljungdahlii is a proton-translocating ferredoxin:NAD+ oxidoreductase essential for autotrophic growth. mBio 4:e00406-12.

31. **Biegel E, et al.** 2009. Genetic, immunological and biochemical evidence for a Rnf complex in the acetogen Acetobacterium woodii. Environ Microbiol 11:1438-43.

32. **Westphal L, et al.** 2018. The Rnf Complex Is an Energy-Coupled Transhydrogenase Essential To Reversibly Link Cellular NADH and Ferredoxin Pools in the Acetogen Acetobacterium woodii. J Bacteriol 200.

33. **Poehlein A, et al.** 2012. An ancient pathway combining carbon dioxide fixation with the generation and utilization of a sodium ion gradient for ATP synthesis. PLoS One 7:e33439.

34. **Seedorf H, et al.** 2008. The genome of Clostridium kluyveri, a strict anaerobe with unique metabolic features. Proc Natl Acad Sci U S A 105:2128-33.

35. **Neumann-Schaal M, et al.** 2019. Metabolism the Difficile Way: The Key to the Success of the Pathogen Clostridioides difficile. Front Microbiol 10:219.

36. **Bruggemann H, Gottschalk G.** 2004. Insights in metabolism and toxin production from the complete genome sequence of Clostridium tetani. Anaerobe 10:53-68.

37. **Liu Y, et al.** 2022. Clostridium sporogenes uses reductive Stickland metabolism in the gut to generate ATP and produce circulating metabolites. Nat Microbiol 7:695-706.

38. **McInerney MJ, et al.** 2007. The genome of Syntrophus aciditrophicus: life at the thermodynamic limit of microbial growth. Proc Natl Acad Sci U S A 104:7600-5.

39. **Worm P, et al.** 2011. Growth- and substrate-dependent transcription of formate dehydrogenase and hydrogenase coding genes in Syntrophobacter fumaroxidans and Methanospirillum hungatei. Microbiology (Reading) 157:280-289.

40. **Suharti S, et al.** 2014. Characterization of the RnfB and RnfG subunits of the Rnf complex from the archaeon Methanosarcina acetivorans. PLoS One 9:e97966.

41. **Jasso-Chavez R, et al.** 2013. MrpA functions in energy conversion during acetate-dependent growth of Methanosarcina acetivorans. J Bacteriol 195:3987-94.

42. **Meng Q, et al.** 2021. Fusobacterium nucleatum secretes amyloid-like FadA to enhance pathogenicity. EMBO Rep 22:e52891.

43. **Rubinstein MR, et al.** 2019. Fusobacterium nucleatum promotes colorectal cancer by inducing Wnt/beta-catenin modulator Annexin A1. EMBO Rep 20.

44. **To K, et al.** 2024. Visualization of a Cell Wall Hydrolase Inhibitor in Fusobacterium nucleatum by Immunofluorescence Microscopy. Methods Mol Biol 2727:27-33.

45. **Callewaert L, et al.** 2008. A new family of lysozyme inhibitors contributing to lysozyme tolerance in gram-negative bacteria. PLoS Pathog 4:e1000019.

46. **Tokuda H, Matsuyama S.** 2004. Sorting of lipoproteins to the outer membrane in E. coli. Biochim Biophys Acta 1693:5-13.

47. **Narita S, Tokuda H.** 2007. Amino acids at positions 3 and 4 determine the membrane specificity of Pseudomonas aeruginosa lipoproteins. J Biol Chem 282:13372-8.

48. **Hayashi S, Wu HC.** 1990. Lipoproteins in bacteria. J Bioenerg Biomembr 22:451-71.

49. **Jang YJ, et al.** 2013. Autoinducer 2 of Fusobacterium nucleatum as a target molecule to inhibit biofilm formation of periodontopathogens. Arch Oral Biol 58:17-27.

50. **Ryu EJ, et al.** 2016. D-Galactose as an autoinducer 2 inhibitor to control the biofilm formation of periodontopathogens. J Microbiol 54:632-637.

51. **Wu J, et al.** 2019. Autoinducer-2 of Fusobacterium nucleatum promotes macrophage M1 polarization via TNFSF9/IL-1beta signaling. Int Immunopharmacol 74:105724.

52. **Vendeville A, et al.** 2005. Making 'sense' of metabolism: autoinducer-2, LuxS and pathogenic bacteria. Nat Rev Microbiol 3:383-96.

53. **Surette MG, et al.** 1999. Quorum sensing in Escherichia coli, Salmonella typhimurium, and Vibrio harveyi: a new family of genes responsible for autoinducer production. Proc Natl Acad Sci U S A 96:1639-44.